Geothermal Cooling in Arid Regions: An Investigation of the Jordanian Harrat Aquifer System

Dissertation

vom Fachbereich Material- und Geowissenschaften
der Technischen Universität Darmstadt (D17)
genehmigte Dissertation
zur Erlangung des akademischen Grades
Doktor Ingenieur (Dr.-Ing.)

TECHNISCHE UNIVERSITÄT DARMSTADT

vorgelegt von
MSc. Sana'a Al-Zyoud
geboren am 3. September 1981 in Amman, Jordan

Referent:	Prof. Dr. rer. nat. Ingo Sass
Korreferent:	Prof. Dr. rer. nat. Rafael Ferreiro Mählmann
Prüfer:	Prof. Dr.-Ing. Rolf Katzenbach
Prüfer :	Prof. Dr. rer. nat. Ahmad Al-Malabeh

Eingereicht am: 20.11.2012
Tag der mündlichen Prüfung: 16.08.2012

Darmstadt, 2012

Getruckt mit Unterstützung des Deutschen Akademischen Austauschdienstes

Abstract

Besides applications of heating and power generation geothermal energy has also the potential to significantly contribute to the cooling of buildings. A shallow basaltic aquifer system in north east Jordan was studied for its potential as a geothermal resource for cooling utilization. The groundwater here is used as a geothermal medium for cooling purposes. Cold water is pumped from the reservoir using extraction wells. This water is fed into the buildings' circuit and heat exchange occurs between the buildings ambient air and the circulating cold water. The recovered warm water is injected again into the ground using injection wells.

The thermophysical properties, the mineralogical and geochemical composition of the Jordanian Harrat basalt were examined. This is followed by an assessment of the basalt's suitability as a geothermal cooling reservoir. Representative thin sections were analyzed for their mineral components and then the results are compiled in a hydrogeothermal and a petrophysical model. Findings of this study will contribute to a better understanding of the relationship between selected petrophysical characteristics of basalt and its heat conducting abilities. A 10 % increase of opaque and ferromagnetic minerals volume proportion in the studied basalts lead to an increase thermal conductivity by approximately 0.5 W m^{-1} K^{-1}. This may significantly contribute in providing a valuable alternative to direct measurements of the thermal conductivity of basalts in Jordan if sufficient mineralogical data is available. Thus, the prediction of thermal conductivity through modal mineral composition may become a key feature for efficient geothermal system exploration in volcanic and plutonic rocks.

Reservoir thermophysical properties were integrated with the hydrological data to develop the numerical model. A GOCAD® 3D structural model was created. Alongside with the reservoir characteristics, this 3D model was implemented into a numerical flow and heat transport model, created with FEFLOW®. This numerical model is used to predict the performance of the geothermal cooling reservoir. Different possible geothermal installations are studied, using various approaches. The study shows that a geothermal utilization of the respective basaltic reservoir is feasible. It features sufficient hydraulic and thermal properties to be utilized for cooling purposes. The developed model has proven to be robust and flexible. It can be easily extended for analyzing other sites.

Zusammenfassung

Geothermie hat neben der Anwendung im Bereich des Heizens und der Stromerzeugung das Potenzial einen bedeutsamen Beitrag zur Gebäudekühlung zu leisten. Ein oberflächennaher basaltischer Aquifer im Nordosten Jordaniens wurde auf sein Potential zur Nutzung im Rahmen der Gebäudekühlung hin untersucht. Das Grundwasser wird dabei in einem offenen Kreislauf als Wärmesenke genutzt. Das kühle Grundwasser wird über Entnahmebrunnen in die Kühlsysteme der zu kühlenden Gebäude geleitet. Dabei kommt es zu einem Wärmeaustausch zwischen der Raumluft und dem Grundwasser. Das so erwärmte Wasser wird über Schluckbrunnen wieder in denselben Aquifer eingeleitet.

Im Rahmen dieser Arbeit wurden die thermophysikalischen Eigenschaften des Harrat Basalts bestimmt und auf Grundlage dieser Ergebnisse die Eignung des Gesteins für die geothermische Nutzung bewertet. Dünnschliffe repräsentativer Gesteinsproben wurden petrographisch untersucht, und die Ergebnisse in einem hydrogeothermischen Modell und einem petrophysikalischen Modell zusammengestellt. Die Ergebnisse dieser Arbeit können zu einem verbesserten Verständnis der Petrologie von Basalten und ihrer thermophysikalischen Eigenschaften beitragen. Bei den untersuchten Gesteinsproben führt ein um 10 % höherer Modalbestand an opaken und ferromagnetischen Mineralen zu einer um ca. 0,5 $W\ m^{-1}\ K^{-1}$ höheren Wärmeleitfähigkeit. Dieser Zusammenhang könnte eine Alternative zu Methoden direkter Wärmeleitfähigkeitsbestimmung darstellen, wenn entsprechende petrologische Daten vorliegen. Demzufolge könnte die Bestimmung der Wärmeleitfähigkeit anhand des Modalbestandes des Gesteins ein Hauptmerkmal der wirtschaftlichen Exploration geothermaler Systeme in vulkanischen und plutonischen Gesteinen werden.

Ein numerisches Reservoirmodell wurde unter Berücksichtigung der thermophysikalischen Eigenschaften und von hydrogeologischen Daten erstellt. In einem ersten Schritt wurde ein strukturgeologisches 3D-Modell mit dem Softwaresystem GOCAD erstellt. Zusammen mit den Reservoireigenschaften wurde dieses strukturgeologische 3D-Modell in ein numerisches FEFLOW Wärmetransportmodell überführt. Mithilfe dieses Modells werden die Betriebseigenschaften des Reservoirs unter dem Einfluss einer geothermischen Brunnenanlage zur Gebäudekühlung simuliert. Verschiedene Varianten geothermischer Brunnenanlagen wurden unter verschiedenen Ansätzen untersucht. Die Simulationen belegen die Durchführbarkeit einer Nutzung des basaltischen Aquifers zu Kühlungszwecken, aufgrund ausreichender hydraulischen und thermophysikalischen Eigenschaften. Das erstellte Modell hat sich in den Simulationen als robust und flexibel erwiesen und kann verhältnismäßig einfach auf andere Untersuchungsgebiete übertragen werden.

To My Daughters Farah and Joud…..

To My Husband…..

To My Mother…..

I dedicate this work
Sana'a

Acknowledgment

The present research work has been conducted at Chair of Geothermal Science and Technology, *Technische Universität Darmstadt* between October 2008 and August 2012.

First of all I would like to take this opportunity to express my grateful thanks and appreciation to my advisor Prof. Dr. Ingo Sass for his invaluable guidance, encouragement, and patience. The confidence he offered me provided a great opportunity to gain experience in research and experimental work.

I want to thank Prof. Dr. Rafael Ferreiro Mählmann for his assistance during the petrophysical investigations and for his prompt willingness to review this dissertation.

I would like to thank Prof. Dr. Ahmad Al-Malabeh from Hashemite University in Jordan for his help in and suggestions in the field work as well as in the mineralogy, chemistry, geology of the Harrat. I admire his support, fruitful discussions and advice.

I am grateful for Prof. Dr.-Ing. Rolf Katzenbach, Director of the Institute and the Laboratory of Geotechnics, *Technische Universität Darmstadt*, for his contribution during the work.

I would thank Prof. Dr. Stephan Kempe for his support, cooperation and advice within this work.

My heartfelt thanks extend to Dr. Wolfram Rühaak for his support, motivation and illuminating instructions. His significance help, beside his inspiring ideas, developed my modeling skills that definitely helped me to advance my work.

I have to thank Mrs. Dunja Sehn and Mrs. Simone Roß-Krichbaum for their endless moral and emotional support, I was motivated by their strength during 4 years; I appreciate also their arrangement of many administrative matters.

The financial support of *Deutsche Akademische Austauschdienst "DAAD"* through the doctoral research is gratefully acknowledged. I would like also to thank NaturPur for their financial support in the field work.

I would like to thank Dr. Kristian Bär for his illuminating instructions. I owe a special thanks to Ms. Johanna Rüther for her help in well design calculations. I want to thank Mr. Sebastian Homuth for his help and being ready to answer my questions. I would like to thank Mr. Philipp Mikisek for his help in GOCAD modeling. I am more than grateful for Mr. Robert Priebs for the dissertation English revision. Many thanks for Dr. Norbert Laskowski, Mrs. Gabriela Schubert, Mr. Rainer Seehaus, Mr. Holger Scheibner and Mr. Jürgen Krumm for their technical help in experimental work. Many thanks to Ms. Petra Kraft and to other colleagues Yixi Gu, Liang Pei, Achim Aretz and Johannes Stegner for their help.

Grateful thanks to Natural Resources Authority (Amman) staff for their support in experimental work and providing the available literature. Many thanks to the Ministry of Water and Irrigation as well as the Ministry of Energy and Mineral Resources in Jordan for their permission to use the available data bank.

I would like to thank my friends and to everyone supported me throughout my research. Especially the people I have met while in graduate school in Darmstadt, who have become my closest and dearest friends, their support to this work is appreciated, and to all I give my love, respect and thanks.

My heartfelt thanks express to my dearest family. To my husband and my lovely daughters for putting up with my absence during the last 4 years and for their continuous help and support. To my parents, brothers and sisters who have inspired me. I owe them all everything and I wish I could show them just how much I love and appreciate them. I hope that this work make them proud.

Darmstadt, August 2012 Sana'a Al-Zyoud

Contents

List of Figures

List of Tables

List of abbreviations

(see text for explanations)

λ : Thermal conductivity (W · m^{-1}· K^{-1})

λ_R : Thermal conductivity of the reference (W · m^{-1}· K^{-1})

Θ_R : Temperature difference of the reference (K)

Θ : Temperature difference of the sample (K)

U_R : Electrical potential of the reference (V)

U : Electrical potential of the sample (V)

q_i : Volumetric flow rate (m^3·d^{-1})

p_L : Atmospheric pressure (N· m^{-2})

p_i : Injection pressure (N· m^{-2})

M_i : Mass flow rate (m^3·d^{-1})

η : Dynamic viscosity (Pa·s)

r : Adaptor radius (m)

F_G : Geometric factor

k : Permeability (m^2)

n_{ofm}: Opaque and ferromagnesian minerals volume proportion (%)

Q : Cooling load (MW)

$(\rho c)_f$: Volumetric heat capacity of the fluid (kJ· kg^{-1}· K^{-1})

$(\rho c)_g$: Bulk volumetric heat capacity of the rock (kJ· kg^{-1}· K^{-1})

T : Temperature (K)

K_e : Effective thermal conductivity of the saturated rock (W · m^{-1}· K^{-1})

∇ : Laplace operator

H : Heat source

t : Time (s)

$S_{0:}$ Saturation

h : Groundwater head (m)

W: Source (sink) term

T_i : Injection water temperature (°C)

T_o : Extraction water temperature (°C)

q : Volumetric flow rate ($m^3 \cdot d^{-1}$)

K: Hydraulic conductivity ($m \cdot s^{-1}$)

$K_{fr:}$ Fractured hydraulic conductivity ($m \cdot s^{-1}$)

b: Fracture aperture (m)

ρ: Fluid density ($g \cdot cm^3$)

g: Gravity acceleration ($m \cdot s^2$)

S_w : Equilibrium drawdown (m)

r_e : Influence radius of pumping well (m)

r_w : Well radius (m)

q : Pumping rate ($m^3 \cdot d^{-1}$)

T_s : Aquifer transmissivity ($m \cdot s^{-1}$)

r_1 , r_2 : Distance of other two well located in the system (m)

Δl : Tube length (m)

r_p : Effective well pipe radius (m)

Δh : Head difference between the two ends of the tube (m)

ρ_w : Water density ($g \cdot cm^3$)

v_{crit} : Critical velocity of groundwater penetration ($m \cdot s^{-1}$)

q_f : Well intake capacity ($m^3 \cdot d^{-1}$)

r_p : Pipe radius (m)

Th : Aquifer thickness (m)

q_a : Actual well take capacity (m)

Hs: Static head (m)

h_w : Depth of water in the well while pumping (m)

R : Range of Sichardt formula

S_w : the drawdown in the well during pumping (m)

A_o : Open area (m^2)

A : Open area percentage (%)

sl : Slot size (mm)

w : is the wrap-wire face width (mm)

A_T : Total screen area (m^2)

L_s : Screen length (m)

δ : System potential (%)

Q_m: Modeled cooling load (MW)

Q_d: Demand cooling load (MW)

1. Introduction

1.1. Preface

Both governmental and private sectors in Jordan are interested in developing new and environmentally sustainable energy resources, such as geothermal energy. The possible utilization of geothermal energy in Jordan exists for cooling as well as heating purposes. Exploration and application are still in the initiating phase. Due to the hydrocarbon and nuclear energy debate worldwide a more detailed investigation and evaluation of the geothermal potential is required to substantiate the future energy strategies of Jordan.

Due to the very limited use of thermal springs in Jordan, geothermal utilization is still in a juvenile phase of development. Those hot springs are scattered on the eastern shoulder of the Dead Sea rift and are closely related to national heritages sites. However, the geothermal potential of the hot mineral waters of Jordan are under ongoing investigations (i.e. Schäfer & Sass 2012). No further geothermal resources are detected or developed so far.

The demand for cooling of buildings and industrial facilities is increasing. This is mainly due to an increase of maximum summer temperatures especially in arid regions like Jordan (Bani-Domi, 2005). In addition, the proximity of the potential reservoir to prospective consumers makes the cooling applications favorable. Cooling of buildings requires large energy related investments. This increasing cooling demand is mostly served by conventional fossil energy sources.

The utilization of geothermal resources for heating and power generation is well established. However, using the relatively low temperature of the shallow subsurface and of the groundwater for cooling purposes is also a viable geothermal application.

The production horizon discussed in this study is the upper basaltic groundwater reservoir in the Amman Zarqa basin in north east Jordan. The formation is located within the Jordanian Harrat basalt. It is composed of several volcanic flow extrusions of varying thickness ranging from 50 m to 400 m with an average thickness of 250 m (Ibrahim, 1993). An additional potential target layer, below the basalt flows, is a late cretaceous limestone formation with an average thickness of about 250 m (Abu Qudaira, 2004). These formations represent an important shallow aquifer (Al Mahamid, 2005). This is due to a relatively medium porosity (12 %) and high hydraulic conductivity averaging $8 \cdot 10^{-5}$ m s^{-1} (Al Mahamid, 2005), additionally hydraulic conductivity is enhanced by numerous NW-SE and some NE-SW trending faults. As the studied infrastructures in this research are mostly located on the basalts flows, more details were focusing on the basalts rather than other lithological unit in the study area.

The geothermal installations discussed here are intended to provide cooling for different types of buildings. All geothermal cooling installations discussed herein are open loop systems, consisting of two arrays of vertical wells. The first one consists of extraction wells for cold groundwater and the second of injection wells for the heated water. Russo & Civita (2009) conducted a feasibility study for providing heating and cooling for a new large commercial building in Italy. They used an open loop groundwater heat pump system.

In this work, different cooling setups were tested. Depending on the cooling demand, the considered setups may not be sufficient; therefore the additional coupling with night sky cooling (Birtles et al., 1996; Dobson, 2005) during winter is modeled, too.

1.2. Thesis Outline

The thesis consists of 4 chapters; renewable energy and energy policy in Jordan were reviewed in the first chapter. A review of previous studies and investigations on geothermal energy utilization in Jordan, thermophysical properties of rocks, groundwater in the study area and geothermal modeling using FEFLOW® software are also presented in the same chapter.

In chapter 2, the geology, hydrogeology as well as the reservoir rocks petrology and thermophysical properties of the studied basalts are discussed. It includes a description of the field work and of the study area, too.

In chapter 3, the 3D numerical model using GOCAD® and FEFLOW® is presented. The model structure and features are explained in detail. The cooling applications, heat and flow transport model were performed. Well design of the geothermal installation is discussed in this chapter, too. Additionally, the environmental advantages of geothermal cooling systems are illustrated.

Finally, in chapter 4, results of the 3D modeling are presented and discussed. Conclusions are drawn from this and future prospects are outlined.

1.3. Renewable Energy and Energy Policy in Jordan

Renewable Energy Utilization

Most of the energy demand in Jordan is satisfied by imports, due to the limited availability of domestic fossil fuel resources. The energy resources are limited to small gas reserves, oil shale deposits and tar sand. It also has some modest potential in hydropower, wind power, biogas and geothermal energy (Ministry of Energy and Mineral Resources, 2010a).

In 2010 the Jordanian Minister of Energy and Mineral Resources Khalid Tuqan stated that the costs of Jordan's imports of energy in 2010 was estimated to be USD 3.6 billion which is equal 13.5 % from GDP (Akbar Jordan, 2010). In 2010 the energy imports accounted for 96 % from the total energy used in Jordan (Norton Rose, 2010). The Jordanian energy sector master strategy for the future (2007 - 2020) states that the target is to obtain 1.800 MW or 10 % of the country's supply through renewable energy sources (Ministry of Energy and Mineral Resources, 2010b). The strategy involves an increase of electricity generation through wind power to 350 MW until 2012. Five projects scattered throughout the eastern and southern Jordanian desert are expected to increase the capacity to 600 MW by 2015.

In addition, the capacity for electricity generation through photovoltaic contributed 5 MW in 2011. The use of solar thermal energy for domestic water heating for household reached 20 % in 2011 (Ministry of Energy and Mineral Resources, 2010a).

Natural Gas Company (BIO-GAS) which works on the organic waste treatment at Rusaifa Waste Landfill reported that in 2008 the generated electricity from the project was 9178 MWh, while the total generated electricity in the period between 2000 and 2008 was 23.4 GWh (Ministry of Energy and Mineral Resources, 2008).

Geothermal energy is another alternative resource of energy in Jordan, which could be utilized for several purposes. Jordan is blessed with this energy resource in certain parts of the country but the current level of usage is very limited. It is used in spa and aqua farming applications in the western hot springs. A systematic program to explore the geothermal

energy started in 1975 by the Natural Resources Authority (NRA). The project was based on previous work, which was concentrated around the Zarqa Ma'in and Zara hot springs, in order to assess the geothermal resources of the whole country. The British Geological Survey was acting as advisors to the project, which involves co-operation among several scientific disciplines.

Shallow and deep drilling programs were also implemented in central Jordan (Sunna', 2004). The work included geochemical, geological, geophysical, hydrological and a preliminary feasibility studies (Myslil, 1988).

Sunna' (2004) reported: "Thermal springs form the main surface manifestation of geothermal energy in Jordan has temperature ranges between 20 and 62°C. These springs are distributed along the eastern escarpment of the Jordan and Dead Sea graben (200 km long). Known manifestations occur from the Yarmouk River in the north to Wadi Hasa in the south. More than 100 wells drilled for thermal water in the Dead Sea – Rift Valley, in the Area of the Azraq Basin and in Risha (northeast Jordan near Iraqi borders), as well as in the area south of Queen Alia Airport have low to intermediate–temperatures, which can be considered as an excellent potential for direct use. According to the thermal water properties, several economic projects could be developed using the thermal energy of the springs and the wells. Heating greenhouses, fish farming, animal breeding, space heating and agricultural applications, some industrial processing, de-icing and therapeutic spa is the most ideal projects, which might be established within the areas of geothermal potential in Jordan".

National Environment Strategy for Jordan (1991) stated that significant low temperature resources (less than 100 °C) exist in two main areas at the eastern margin of the Dead Sea Rift. It stated that Zarqa Ma'in thermal springs produce a total of around 60 MWh of thermal energy. Some of these springs have been tapped for the spa and hotel complex at Zarqa Ma'in. The most well-known thermal springs in this area locate in the Lisan and the Afra. In Ibn Hammad, near Lisan, an 800 m deep borehole produces water at a temperature of 50 °C (National Environment Strategy for Jordan, 1991). The Ibn Hammad well is an artesian well with an estimated flow rate of about 400 $m^3 \cdot hr^{-1}$. This implies a potential thermal capacity of around 13 MW (National Environment Strategy for Jordan, 1991). According to our knowledge, this well is not used for geothermal purposes yet. It is a very promising geothermal resource considering the costs. The water extraction costs are minimized by the artesian flow of the drilled wells at this site. The second area of proven geothermal resource is on the plateau south of Amman, in the region east of Madaba. Here more than 20 private wells used for irrigation discharge thermal water at temperature of 30 - 40 °C (National Environment Strategy for Jordan, 1991). According to the thermal water properties, several projects could be considered using thermal water in Jordan. Heating for greenhouses, aqua farming, space heating (Sunna', 2004) and cooling (this work). Overall, the geothermal installed thermal capacity in 2001 in Jordan was 153.3 MW and the energy is mainly used for spa applications (Lund, et al., 2010).

Renewable Energy Policies and Laws

Jordan has introduced several regulatory measures in energy sector that form part of its Nationally Appropriate Mitigation Action (NAMA) plan. This plan sets out the policies and actions adopted by developing countries to reduce greenhouse gas emissions. Each developing country reports its NAMA directly to the United Nations Framework Convention on

Climate Change. The NAMA actions concepts recognize that each country must take an individual approach to reduce GHGs emissions.

The Jordanian energy strategy passed a law (Law No. 12 of 2012: Renewable Energy and Energy Efficiency Law) which contains a number of measures to increase the use of renewable energy by encouraging the establishment of renewable energy projects (Norton Rose, 2010). No specifications for geothermal energy installations stated in this law except the customs fees free for all imported equipment.

1.4. Literature Review

Geothermal Utilization in Jordan

Several investigations on geothermal energy utilizations have taken place over the last three decades in Jordan. Most of these studies were conducted by Natural Resources Authority (NRA) incorporated with different institutions and companies. They concluded that Jordan is rich in low enthalpy geothermal resources. In Jordan, there are 108 hot springs discharging about 25 million cubic meters of thermal water into the Dead Sea per year (Kabariti, 2005).

The first study was undertaken by MacDonald and Partners in 1965, they performed a chemical analysis of samples from Zarqa Ma'in thermal water. The same spring was studied and described by Bender (1974) along with other major and minor thermal spring fields. A resistivity survey and drilling was suggested to investigate the area after the revision of the existing hydrochemistry data (McNitt, 1976). The first estimation of the geothermal potential of the east escarpment of the Dead Sea Rift, based on temperature and hydrochemistry, was conducted by Marinelli (1977). He concluded that this area especially the Zarqa – Ma'in area possessed the most favorable geothermal potential.

Truesdell (1979) revealed that the Zarqa Ma'in and Zara Springs are fed by deep circulating waters. They received heat from a normal geothermal gradient. He estimated that these waters exist at a maximum temperature of 110 °C at depth and are cooled during their ascent by mixing with colder groundwater.

In 1980, Abu-Ajamieh reported the major exploration techniques carried out by NRA in the Zarqa Ma'in - Zara thermal area in the period of 1977-1978. An important geothermal reservoir is indicated in the area of the springs in this report. Probably, this reservoir is heated by the Hammamat Umm Hasan basalt plug. In addition, the moderate radioactivity of the waters was also reported.

Hakki and Teimeh, 1981, carried out a detailed geological study of the Zarqa Ma'in -Zara area. Their work connected the hottest springs to the highest intensity of shearing in the area.

In 1981, Di Paola concluded that the temperature of Zarqa Ma'in springs was most probably due to the ascent of deep circulating waters caused by a normal geothermal gradient.

Galanis et al, (1986) estimated and calculated the heat flow values at 18 sites in Jordan. As the first heat flow measurements in Jordan, the presented heat flow data were measured in boreholes drilled specifically for that study. Additional data were obtained from other boreholes used previously for other purposes.

In 1988, Myslil, re-evaluated the heat flow data presented by Galanis (1986), included more recent data and presented a temperature gradient map which identified two favorable zones for future hot water exploration. After this, the Natural Resources Authority (NRA) initiated a

geothermal gradient map for Jordan based on this work (Fig.1) and other reports (Williams, et al., 1990). This marks the early evaluation of the geothermal potential of Jordan.

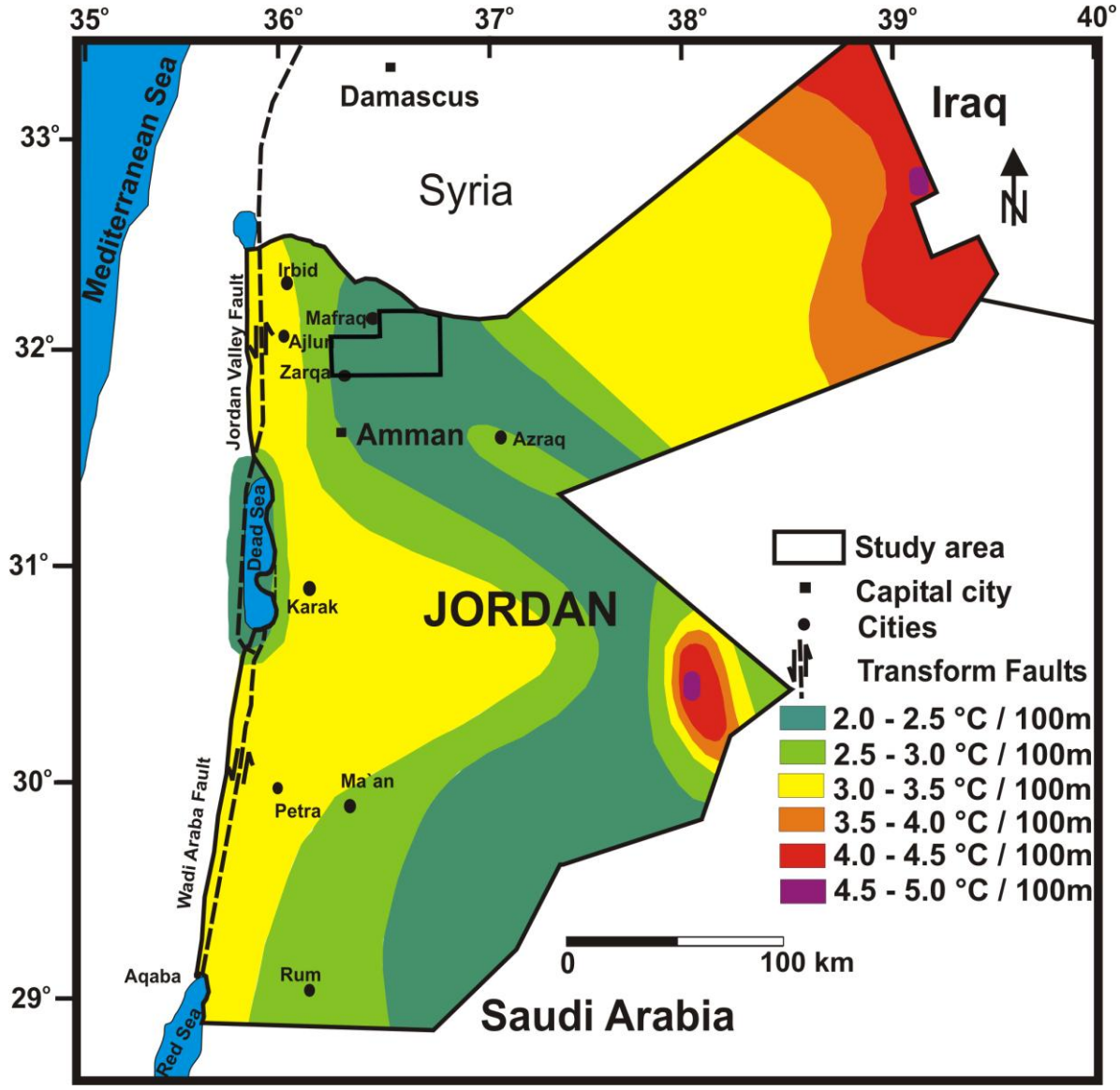

Figure 1: Geothermal Gradient Map of Jordan (modified after Williams, et al., 1990).

Allen, (1988) reviewed and summarized all the previous geothermal investigations and studies in Jordan and introduce proposal for future geothermal studies.

Thermal water near Queen Alia Airport was studied by Swarieh (1990 and 1992). He stated that the presence of the thermal water in the shallow boreholes near Queen Alia Airport is due to the water mixing between the thermal water and cold water of two hydraulically connected aquifers. The temperatures measured exceeded 40 °C (Saudi, 1999).

In central Jordan, Karak and Wadi Ibn Hammad hot spring were studied (Swarieh & Massarweh, 1993). They later also described, in 1995, the Zara & Zarqa Ma'in reservoir and made suggestions as for the optimum use of this source of energy. Two years later, in 1997, they studied the thermal water in Mukhiebeh and Shuneh thermal fields in North Jordan.

Several geo-scientific studies of geothermal waters from central Jordan were conducted. They evaluated the possible use of the geothermal water for desalination. They predicted, using a

mineral saturation index for the reservoir, that the highest water temperature of about 115 °C (Saudi, et al., 2004).

Early in 2004, the World Bank awarded a grant to the Natural Resources Authority to investigate the geothermal energy potential for future uses and to locate the best site for drilling for geothermal water for future exploitation (Saudi & Swarieh, 2005).

In 2005, a joint venture project was carried out by West Japan Engineering Consultants Inc. and GeothermEx Inc., in USA to evaluating the available data related to the thermal water in Jordan. They presented a model which regards the existence of thermal water in shallow wells in central Jordan (Garaibeh, 2008).

In 2006 a Japanese Bank-funded consultancy study reviewed the geothermal energy potential in Jordan. It concluded that exploitation through electricity generation is commercially not feasible in Jordan (Mason, et al., 2009).

Most of the published work focuses on the Dead Sea Rift area where more than 50 hot springs were studied (Swarieh, 2000 ;Sunna', 2004; Schäfer, 2010; Schäfer & Sass, 2012). Thermal water in Jordan has been used directly as curative water; e.g. Zara, Zarqa – Ma'in, Afra and North Shunah hot springs (Al-Dabbas, 2011; Salameh, et al., 1991; International Geothermal Association, 2012). Swarieh (2008) gave an overview on geothermal water in Jordan and suggested a future geothermal utilization for air conditioning and heating of the Queen Alia Airport. Abu-Hamatteh et al., (2011) discussed the possibility of geothermal utilization through electricity generation in Jordan. They concluded that electrical power could be generated using geothermal energy in Jordan.

Thermophysical Properties of Rocks

Several models have previously been developed to determine thermal conductivity based on different rock properties; porosity, rock density, P-wave velocity, uniaxial compressive strength as input parameters (e.g. Wang et al., 2006; Singh et al., 2007; Abdulagatova et al., 2009; El Sayed, 2011). Some experimental studies were performed on the relation between thermal conductivity and permeability for sedimentary rocks and graphite (Zierenberg et al., 2000; Wang et al., 2010). However, the results of some investigations on oceanic basalts (Griffiths et al., 1992; Franzson et al., 2001) could not be applied on the Jordanian continental Harrat flood basalts.

Thermal conductivity and permeability are considered to be the utmost interest to estimate the heat efficiency of a geothermal between thermal conductivity and permeability is only feasible where both parameters are measured for the same sample, so anisotropic factors can be taken into account (Mielke, et al., 2010).

Extensive investigations were reported by Popov et al. (2003) of thermal conductivity and permeability interrelation on both dry and saturated samples. He defined factors which control the effect of permeability on thermal conductivity in sedimentary rocks i.e. minerals crystal size, mineral geometry, vesicle size, internal geometry and vesicle microstructures. Popov et al. (2003) investigated mineral crystal size and microstructure for their effect on thermal conductivity and permeability correlation.

In order to investigate the increase of permeability with thermal conductivity relationship, and determine the factors affecting this correlation, the mineral proportion of the studied basalt is considered. A series of predefined models which focus on the prediction of thermal

conductivity from its mineral proportion were applied. Sass et al. (1971) developed a new geometric model for water saturated basalt fragments correlating thermal conductivity with mineral composition. Numerical as well as empirical models were routinely applied based on physical properties or mathematical formalisms (Pasquale et al., 1997; Hartmann et. al., 2005). The results of the above mentioned studies are limited to a geographic region and geological setting. Jessop (2008) established a numerical model for thermal conductivity in multi-crystalline rocks, dependent on rock mineral components. He concluded that the order of crystallization and crystal size causes differences in the thermal conductivity between 2% to 3%. Pasquale et al. (2011) compared the results of measured thermal properties of rocks from the Po Basin, Italy to re-calculate thermal conductivities predicted by applying Hashin and Schtrikman's (1962) method. Two widely accepted models; the geometric model (Sass et al., 1971) and the non - geometric model (Birch and Clark, 1974) were considered. To predict thermal conductivity from all mineral proportions in the studied basalt these models were applied. The conclusion of applying both models did not lead to any obvious correlation between the total mineral proportion and the thermal conductivity of the instigated basalts. A correlation between each mineral proportions and the thermal conductivity were done. This correlations prove the dependence of basalt's thermal conductivity on the volume proportion for some minerals than others. In addition, a continental basalt in Vogelsberg in eastern upper Hesse - Germany and oceanic basalt from Iceland were investigated to the same relation. The results support the main conclusion of the dependence of basalt's thermal conductivity on some (but not all) mineral proportion. This method could be a prospective approach for predicting thermal conductivity from some mineral phases presented in the basalts. Thermal conductivity is of important in the geothermal reservoir model set up. This importance comes from that the thermophysical initial model, which should integrated with the study area lithology, is the key model for heat transport considering that the basalt is the main heat conductor in the reservoir. The permeability is an important parameter too, for evaluating the mobility of groundwater which acting as the heat convector in the studied geothermal system.

Groundwater in the Study Area

In northern central Jordan the Dead Sea rift valley faulting extended to very deep levels of some parts of the aquifers in this region. This is one of the main reasons for development of a rather complex hydraulic system with considerable differences in flow directions and groundwater head in large parts of northern central Jordan. For practical purposes, the sequence of aquifers and aquitads has been divided into the following hydraulic complexes of regional importance (Margane et al., 2002):

a. The Shallow (Upper) Aquifer System (Alluvium, B4/ B5 (Umm Rijam / Wadi Shallala Formations), basalt).

b. The Upper Cretaceous A7/B2 (Amman / Wadi Sir Formations) Limestone Aquifer

c. The Deep Sandstone Aquifer System (formed by the Paleozoic Ram Group, including the Disi Formation, and the Lower Cretaceous Kurnub Sandstone).

Northern central Amman Zarqa Basin is investigated here into their thermophysical properties for its possible geothermal application. This part of the basin is composed of two aquifers Amman-Wadi Sir Aquifer System (B2/A7) and the upper shallow basaltic aquifer (B7). B2 is Amman silicified formation; the second formation from Belqa group, A7 is Wadi Sir formation; the seventh formation from Ajlun group and B7 is the basaltic extrusion.

Amman-Zarqa Basin is the most important basin in Jordan because this basin is one of the transitional areas between high lands in the west and desert in the east. It receives the highest amount of modern recharge (Al Mahamid, 2005) and isconsidered to be the principal source of fresh water for domestic as well as for irrigated agriculture in the Plateau (Margane et al. 2001, Ministry of Water and Irrigation, 2000).

Amman-Wadi Sir Aquifer System (B2/A7) composed of the uppermost of the Ajlun Group and the lower part of the Belqa group. They are considered as one hydrogeological unit. It consists of the Wadi Sir Limesone Formation (A7) and Amman Silicified Limestone (B2). Geologically its characterized by massive limestone, dolomitic limestone and dolomite with intercalated chalk, marl chert and phosphorite are predominant in the A7/B2 aquifer (Margane et al., 2001, Abu Qudaira, 2004).

The upper shallow aquifer of basalt which extends in the study area along the road from Mafraq to Eastern Al Khalidiyya is quite productive (Margane, et al., 2001) the groundwater quality is good and the aquifer is heavily exploited. However, to the north towards the Syrian border, the groundwater exploitation becomes uneconomic since depth to hydraulic head is very high (about 400 to 460 m) (Ministry of Water and Irrigation, 2000).

Wadi Dhuleil area as a part of the study area is a graben surrounded by two main faults. It is composed of basalt at the top covering the major part of the study area. The outcrop of the horst area is limestone and limestone with chert. Most of the investigated area in this work is located in Wadi Dhuleil where the basalt are extruded over limestone.

Jordan suffers under water scarcity which is probably more serious than in other countries in the Middle East (Al-Weshah, 1992). This shortage is due to many reasons such as low rainfall rates, uneven water distribution, high losses due to evaporation and an increasing demand for drinking and agricultural water caused by population growth (Al-Kharabsheh & Al-Mahamid, 2002). Dottridge & Abu Jaber (1999) reported that the current groundwater abstraction exceeds both average recharge and the safe yield of the Azraq aquifer northeast Jordan. Surface water resources are very limited; therefore groundwater is the main water resource (Al Mahamid, 2005). As a result the groundwater within the Jordanian basins is subjected to extensive extraction through municipal and private wells. Rimawi & Al– Ansari (1997) found that groundwater salinity in the upper aquifer complex in the north-eastern part of the Mafraq area has increased during the last decades. This is due to intensive exploitation of groundwater for irrigation purposes. This exploitation was also shown by El-Naqa et al. (2007) in the Azraq basin (adjacent to the Amman Zarqa basin). They concluded that due to over pumping from the shallow groundwater aquifers, the water level dropped dramatically and signs of salinization and depletion have started to occur (El-Naqa et al., 2007). Salameh (2008) reported drop in groundwater levels, considerable decrease in spring discharges, saltwater intrusions and deteriorating water quality in 6 wells scattered throughout the Jordanian area. A groundwater drawdown in central Amman Zarqa basin was reported to be 1.1 $m \cdot a^{-1}$ (Al-Zyoud, et al., 2012a). Groundwater drawdown as well as the hydraulic head in the studied aquifers are necessary to set up the initial flow transport model (section 3.4) in 3-D modeling of the geothermal reservoir using FEFLOW (Chapter 3). In this model as the groundwater is the heat conducer it is of important to include this parameters. In addition, the measured and resulting drawdown (calculated from the recorded hydraulic head) is very useful for the flow transport model calibration.

Geothermal Cooling Systems and 3-D Modeling Using FEFLOW

Worldwide, geothermal cooling systems have been highlighted and discussed in the literature in recent years. For instance Trombe et al. (1991) pointed out the advantages of using borehole heat exchangers for air cooling. Two basic techniques; air conditioning system and borehole heat exchanger, were evaluated in a series of experiments, as natural cooling technologies by Solani et al. (1998). The cooling performance of a water-to-refrigerant type ground source heat pump system installed in a Korean school building is discussed in Hwang et al. (2009); a similar study was performed by Eicker & Vorschulze (2009). Technical and economic analyses have shown that geothermal heat pump systems offer good potential for heating and cooling utilization within the Mediterranean basin (Kolin et al., 2002; Mertoglu et al., 2000). Despite the lack of discovered high-temperature geothermal resources, Jordan has a shortage of expertise and experiences in geothermal utilizations of all types (National Capacity Self Assessment for Global Environmental Management, 2006). Al-Dabbas (2009) investigated the potential of seasonal heat storage coupled with solar assisted heat pumps. He stated the yearly energy savings with a preliminary evaluation of the system efficiency. Al-Dabbas (2011) designed a ground source heat exchanger that utilizes geothermal energy for heating in the Ma'in area in Jordan. He used the FLUENT software program to calculate the parameters and the potential amount of energy saved (Al-Dabbas, 2011).

In this work, the possible utilization of geothermal energy for the cooling of buildings will be studied, as there is currently very limited experience with the cooling (without heating) performance of ground based systems in arid climate (İnallı & Esen, 2005).

Middle East countries have few studies which investigating the geothermal resources. In Sharqawy et al. (2009) the thermal properties of soils were determined by recording unsteady thermal responses of a borehole heat exchanger; which has been installed for the first time in Saudi Arabia. In Jordan, a 3-D numerical investigation of a geothermal standing column well (SCW) for heating simulations was presented by Abu-Nada et al. (2008). Before this study, there exists no previous practical experience with geothermal cooling in Jordan. The initial numerical model for a prospective cooling system in northeastern Jordan was presented by Al-Zyoud et al., (2012b).

Computer modeling of geothermal systems has become a widely recognized approach to investigate and evaluate natural geothermal systems. O'Sullivan et al. (2001) reviewed the state-of-practice in geothermal reservoir simulation models from early 1960 to 2001. Recently, different simulators were used in geothermal modeling; e.g. FlexPDE (Florides et al., 2012) and SHEMAT (Mottaghy et al., 2011).

FEFLOW® is modeling shallow geothermal systems (Diersch, 2005). FEFLOW® (Finite Element Subsurface Flow and Transport) is professional software for fluid flow modeling and transport of dissolved constituents and/or heat transport processes in the subsurface. It contains pre- and post-processing functionality and an efficient simulation engine (DHI-WASY, 2012). Nam & Ooka (2010) conducted a 3-D numerical heat-fluid transfer simulation of ground source heat pump systems using FEFLOW®. The results were compared with the experimental results and confirmed the simulation validity. It is widely used for geothermal (flow and heat transport) systems (Blöcher et al., 2010; Magri et al., 2010; Nam & Ooka, 2011). It's also suitable for other geothermal applications e.g. mine water use (Renz et al., 2009). Diersch et al. (2011a,b) implemented a new finite-element algorithm for modeling the

geothermal heat exchanger in shallow aquifer systems using FEFLOW®. Rühaak et al. (2008) presented three modeling approaches with FEFLOW®. These models include deep geothermal systems, heating through mine drainage water and calculation the model efficiency for shallow geothermal installations utilizing groundwater through extraction / injection (heat exchangers) arrays.

2. Analysis of the Geothermal Situation in the Jordanian Harrat Region

2.1. Study Area

2.1.1. Location of the study area

The Hashemite Kingdom of Jordan is located in the northwest of the Arabian Peninsula covering an area of about 90,000 km^2 (Department of Statistics, 2010). The Jordanian desert is a widespread ecosystem in Jordan, covering over 80 % of the country (Rawajfih et al., 2005). More than 82 % of the Jordanian territory is classified as an arid region according to United Nations Environment Program (UNEP) Classification of Arid Lands and others (UNEP, 1997; Fardous et al., 2004; Freiwan & Kadioglu, 2007).

The study area is located about 28 km northeast of Zarqa city (Fig. 2); the second largest city in Jordan. Many industrial infrastructures are situated on this basalt such as Jordan Petroleum Refinery, the Jordanian Free Zone Areas and Al Hussein Thermal Power Station, Jordan's main power station.

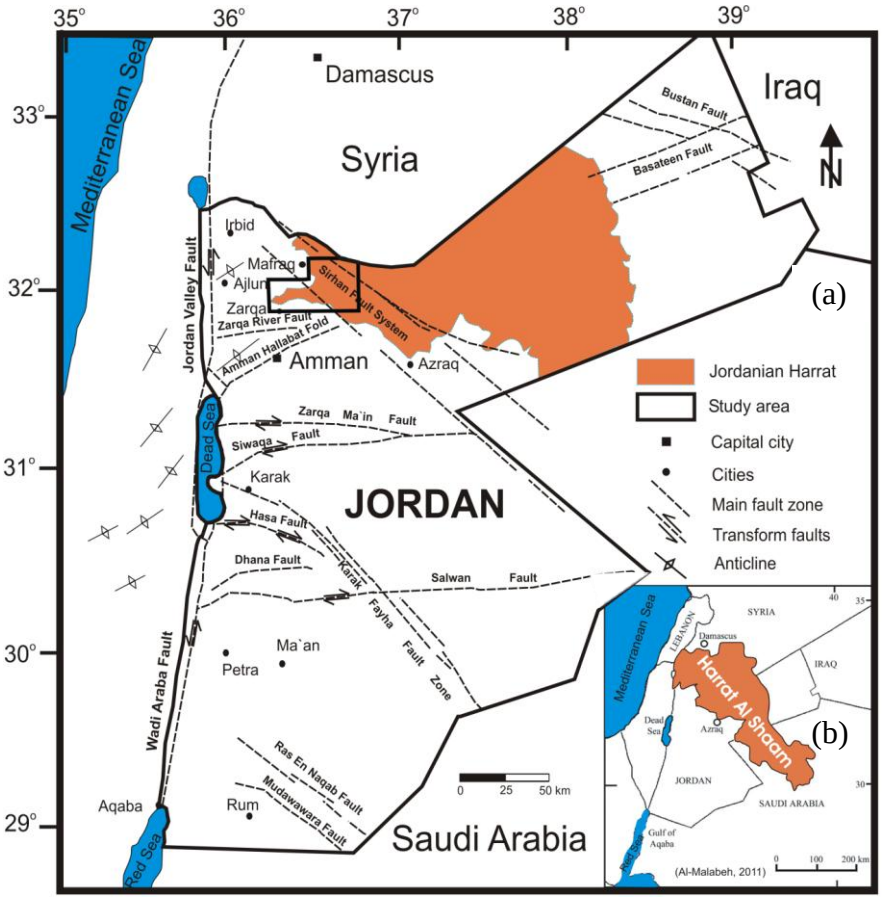

Figure 2: (a) Location and structural map of Jordan includes the study area (modified after Diabat and Masri, 2002). (b) Jordanian Harrat and Harrat AlShaam are modified after Al-Malabeh, (2011).

The study area is a part of the north-eastern plateau within the Jordanian Harrat (Fig. 2), covering parts of the Zarqa and Mafraq governorates. The basalts cover an area of about 1,360 km^2 of the total 1,780 km^2 of the study area (75%) from the study area. Limestone and recent sediments cover the remaining 780 km^2. The study area is defined by the coordinates

of latitude: 32° 1' - 32° 22' and longitude: 36° 01' - 36° 30' in UTM - coordinate system (3546262 – 3586480 and 784931 – 829344 in UTM meter coordination system of WGS84 - Zone - 36N).

The Jordanian Harrat basalt is part of large Intra-continental flood basalt (Bender, 1974). These basalt flows cover with gentle slopes the northern Jordanian desert, with a mean elevation of about 750 m above sea level (Al-Mashagbah, 2010). The highest elevation of the study area is about 1040 m a.s.l. near the Syrian – Jordanian border in the northeastern corner of the study area. On the contrary, the lowest elevation of about 480 m a.s.l, is located along Wadi Az Zarqa (Seil Az Zarqa). Together with the underlying limestone, basalts represent the shallow groundwater aquifer of the Amman Zarqa basin (Al-Kharabsheh & Al-Malabeh, 2002). These basalt flows are highly fractured vesicular extrusive rocks. Some clay intercalations appear within the basaltic flows.

2.1.2. Climate of the study area

The Jordanian climate is classified as Mediterranean. This climate is characterized by a high-temperature dry season in summer (May to September) and a low–temperature rainy season in winter (April to October). A wide range of air temperature is recorded in this area due to this climate. Some winter nights are characterized by freezing temperatures (bellow -1 °C). Normally, precipitation begins in October and reaches its maximum in January and ends in May. The rainfall recorded in the study area varies from 47.6 to 292 mm a^{-1} (records from 2005 to 2011). The average rainfall (between 2005 and 2011) is about 115 mm a^{-1} (Jordan Meteorological Department, 2011). The mean monthly temperature measured between 1999 and 2010 in the study area ranges from 7.5 °C in January to 34 °C in July. Minimum temperatures in winter can reach 2 °C, while the maximum temperature is typically around 18 °C. In summer the minimum temperature does not fall below 15 °C, while the maximum temperature may reach 43 °C (Al-Mashagbah, 2010; Jordan Meteorological Department, 2011).

The mean daily air temperature in summer is 24 °C and in winter is 17 °C. The temperature difference between day and night was recorded to be 17 °C and 10 °C in summer and winter respectively (Jordan Meteorological Department, 2011). The warmest months of the year are July and August and the coldest are January and February. The mean relative humidity of the study area is 70 % in winter and 45 % in summer (Al-Mashagbah, 2010).

2.2. Field work and sampling

In this work, two representative sites of the studied basalt flows are addressed after consideration of several determining criteria such as location, outcrops, structural aspects and basalt freshness. These are the Az-Za`atri lower flow and the Al-Ajib upper flow. In these wadies the basaltic rocks are lithologically well distinguished and structurally well developed (Fig.3).

The studied flows could be subdivided into three successive sub-flows (A1-A3 and Z1-Z3) by petrographic criteria. The upper Al Ajib flow eruption took place at 700 m a.s.l. And the lower Az Za`atri flow erupted at 600 m a.s.l. These sub-flows are separated from each other by zones of highly vesicular basalt at the top of each flow. The Al Ajib basalt flow, 31 m total thickness, is divided to A1, A2 and A3 sub-flows from bottom to top. The Az Za`atri basalt flow, 34 m total thickness, is divided to Z1, Z2 and Z3 sub flows from bottom to top. A3 and Z3 are characterized by hummocky (lumpy or in small uneven knolls) structure of Pāhoehoe

lava flow and the existed orthogonal cooling fissures are generated along with crystallization process. A blocky structure (of small blocks < 50 cm in diameter) is exhibited by the middle flows A2 and Z2 which presents a transitional stage between lower ‘a‘ā lava flow and Pāhoehoe higher lava flow . The lower part of both flows consists of the largest irregularly shaped blocks of massive basalt. These blocks exceed 1 m in diameter and are present within the A1 and Z1 sub-flows. These blocks indicating the ‘a‘ā lava flow type. The middle and lower sub-flow in each flow is characterized by tectonic brittle fractures.

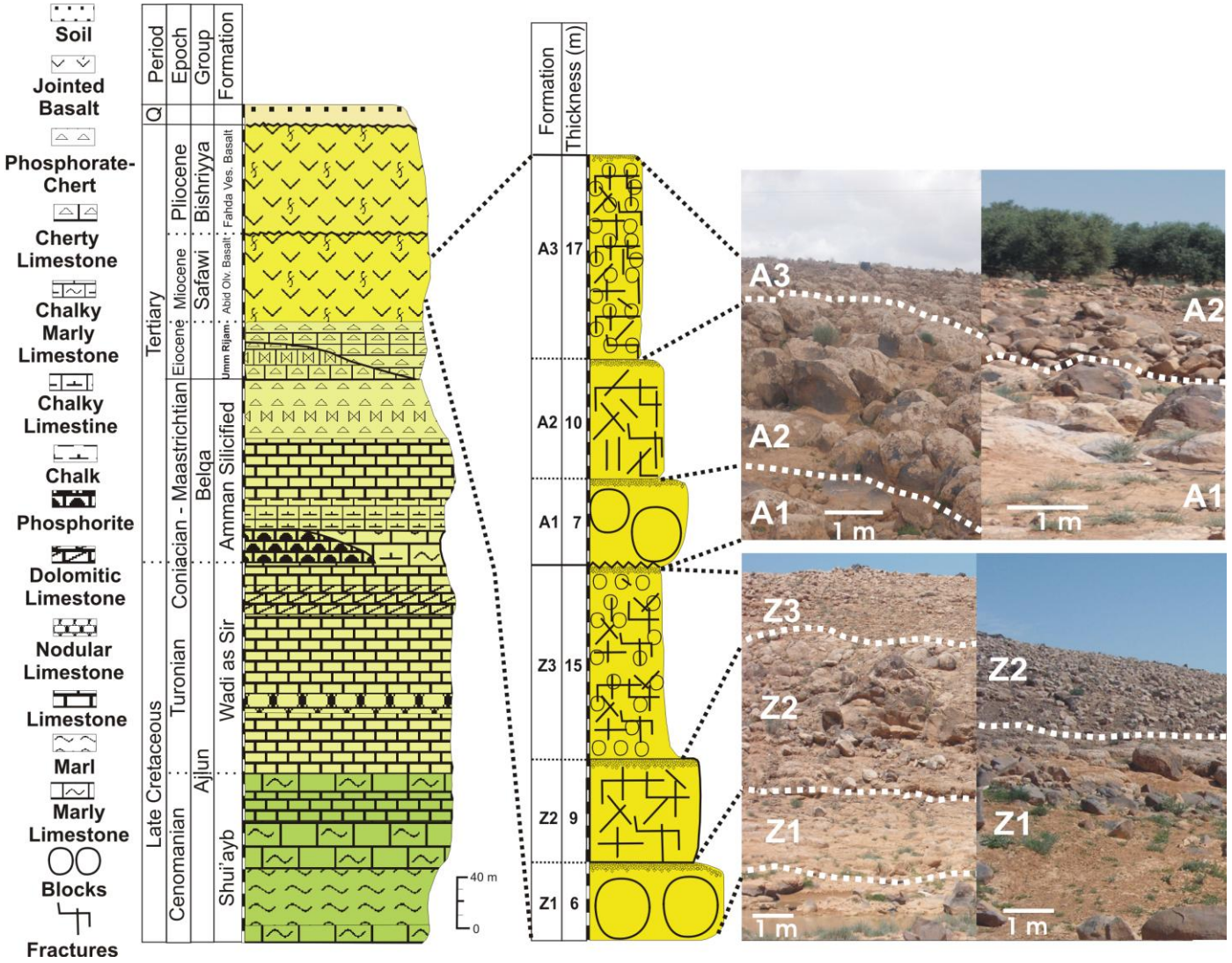

Figure 3: Lithological section with images showing typical occurrences in Wadi Al Ajib (A1 to A3) and Wadi Az Za`atri (Z1 to Z3) (cross section modified after Abu Qudaira, 2004).

Rock Sampling

72 core samples from the studied sub-flows were drilled with core drilling equipment. The core diameter is 64 mm and the length of the core varies from 18 to 33 cm depending on the fracture fabric. The cores were either taken parallel or perpendicular to the flow direction depending on outcrop accessibility (Fig. 4).

(a) (b)

(c) (d)

Figure 4: (a and b) Rock core samples (length: 30 cm, diameter: 6.4 cm), (c and d) different sampling orientations and coring angles.

2.3. Geology and Tectonic Settings

The magmatic activity within the Arabian plate occurred from the Miocene to sub-recent time and produced several basaltic plateaus. The Jordanian Harrat basalts are part of the Cenozoic continental basaltic rocks known as Harrat Al-Shaam (Fig. 5) covering an area of approximately 12,000 km^2 (Al-Malabeh, 2011). Van den Boom & Sawwan (1966) concluded that the basalts of Jordanian Harrat resulted from six major basalt flows (named B1-B6) and one eruption of tephra (assigned as B't). Basaltic flows B1-B3 are not exposed in Jordan, but are known from borehole data (Hunting Technical Services, 1965). This classification is

renamed by Ibrahim (1993) as the following groups: Wisad, Safawi, Asfar, Rimah (Tephra) and Bishriyya (from oldest to youngest, respectively). Absolute ages are given by Barberi et al. (1979), based on K-Ar dating, range from 10.53 Ma to 9.37 Ma, while Moffat (1988), using the same method, obtained ages between 13.7 and 0.5 Ma for the exposed basalts. Moreover, Ilani et al. (2001) suggested a new classification based on more detailed K-Ar dating. They subdivided the volcanics into three major episodes: Oligocene to early Miocene (26 Ma – 22 Ma), middle to late Miocene (13 Ma - 8 Ma), and late Miocene to Pleistocene (7 Ma to < 0.1 Ma). Finally, Al- Malabeh (2009) studied the Jordanian Harrat and distinguished three major volcanic fields in the area namely Remah, Ashaq and Al- Dhirwa.

The volcanic activities within the Arabian plate are closely related to the tectonic framework of the major regional structures of the area. The Harrat basalts flow parallel to the Wadi Sirhan fault system extending NW – SE (Fig.5). Basalts of about 400 m thickness of successive flows are found in the NE part of the study area, while less than 100 m is found in the southern parts of the study area (Hunting Technical Services, 1965).

Basalts in the study area belong to youngest eruption phase with an age of 3.7 Ma - 0.1 Ma (Ilani, et al., 2001). These basalts cover about 60 % of the studied basalt outcrops. While the basalt of Late Miocene age of 9.30 Ma – 8.45 Ma (Ilani, et al., 2001) occupies about 40 % of the studied outcrops. This basalt is exposed along the selected wadies Wadi Al Za`atri, and Wadi Al Ajib (Fig.5).

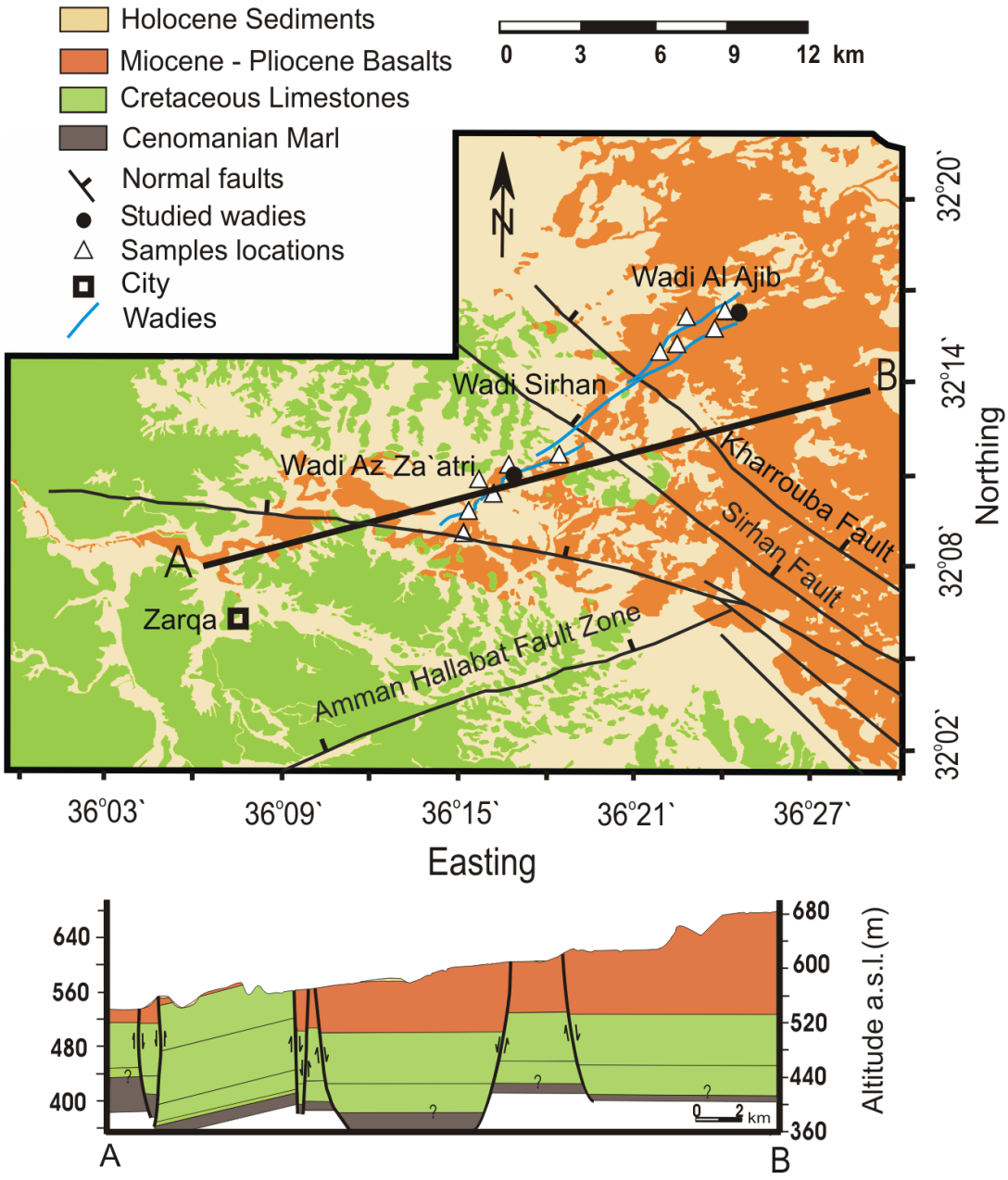

Figure 5: Geological map modified after Abu Qudaira, (2004) shows the aquifer lithology.

Both Al Ajib and Az Za`atri flows were studied with respect to their lithology and structure. Together with the underlying limestone, the studied basalt represents the shallow groundwater aquifer of the Amman Zarqa basin (Al-Kharabsheh & Al-Malabeh, 2002). The underlying limestone formation is a creamy yellowish, massive dolomitic limestone in intercalation with the Coquina limestone (Smadi, 2000) and cherty bearing limestone (Abu Qudaira, 2004). An aquitard layer of 35- 60 m marl underlain this aquifer (Abu Qudaira, 2004).

A hydrogeological model of this basalt-limestone aquifer, with predominantly fracture porosity, was created (Al-Zyoud et al., 2012b) as a prerequisite for the subsequent calculation of its performance as a geothermal reservoir.

2.4. Petrography and Mineralogy

2.4.1. Methodology of Mineral Analysis

Mineralogical analysis under a polarized light microscope and point analysis was conducted. Modal proportions were determined by point counting on thin sections. For every slide approximately 500 points covering phenocrysts and groundmass were counted. Whereas, the minerals point analysis was performed in Tübingen University laboratories. Selected samples were analyzed using the JEOL 8900 electron microprobe. The analytical conditions were 1·10-8 mA, 25 - 50 nA specimen current potential, 20 kV acceleration potential and 10 sec. integration time. Analytical accuracy is in the order of +/-1% (relative), detection limits are typically >50 ppm . The SPI mineral standards were used for calibration process. This electron microprobe lab has 68 mineral standards (SPI mounts 02758-AB, 02753-AB). Computerized Bence Albee matrix was used to perform an On-line-Data reduction and integration time of 10 sec.

2.4.2. Modal Analysis

Modal analysis is now common practice to determine the percentages of a rock's constituent minerals (the "mode") by a point-counting method, in which the identity of the mineral underlying each of a series of equally-spaced points on a grid is determined. Many systems of igneous rock nomenclature, such as those of Nockolds (1954), Chayes (1957), and Streckeisen (1967), use modal analysis as a classificatory criterion. Thus, for the ith mineral, found at x, points out of a total of N points counted, the best estimate of its percentage in a rock is : 100x / N. Of critical importance there is an error associated with this estimation.

Point counting, which is the usual procedure for carry out modal analysis, depends on two factors only one of them can be controlled from the operator (Neilson and Brockman, 1977). The mechanics of point-counting are such that the grid distance maybe selected. The grid distance is the distance between successive points on a grid. With respect to the grain size one of the two conditions are existing: weather is the grid distance exceeds the grain size or not. The second factor is the rock texture under microscope in related to the nature of this rock. In the investigated basalt both cases are found because of the inter-granular texture of this rock. Of the many rock properties that may affect a point-counting, such like texture, the most important is the distribution of the constituent crystals. Here, two possibilities exist: crystals are stochastically independent, or the composition of any crystal is related to the compositions of adjacent crystals just like the investigated basalt in this work. Modal analysis of the Jordanian Harrat basalt, which carried out on more than 500 points, is illustrated in the table below with the estimated error for each mineral. Modal analyses show that basalt flows of each studied site have a small variation in modal proportions (Table 1). The results are represented in Pie chart next in Figure 6.

Table 1: Average values with standard deviation of modal analyses of the mineral composition. Each flow is represented by 12 samples.

Sub-flow	Modal analyses (Vol. %)						
	Plagioclase	Pyroxene	Olivine	Opaque Minerals	K-Felspar	Nepheline	Vesicles
A3	58.68 ±0.48	25.71 ±0.26	4.34 ±0.36	3.26 ±0.17	0.90 ±0.10	0.19 ±0.03	9.86 ±0.13
A2	54.18 ±2.58	27.14 ±1.00	4.22 ±0.30	4.39 ±0.12	0.57 ±0.03	0.10 ±0.01	10.03 ±0.13
A1	54.58 ±1.01	26.39 ±0.86	2.46 ±0.75	2.33 ±0.32	0.61 ±0.01	0	10.82 ±0.19
Z3	56.29 ±0.85	28.46 ±0.74	4.71 ±0.32	4.32 ±0.35	0.51 ±0.04	0.37 ±.01	6.88 ±0.41
Z2	54.81 ±1.49	29.85 ±1.27	4.14 ±0.12	4.02 ±0.21	0.63 ±0.02	0	6.67 ±0.17
Z1	46.52 ±2.19	27.88 ±1.75	4.81 ±0.68	4.82 ±0.23	0.9 ±0.04	0.48 ±0.03	10.65 ±0.14

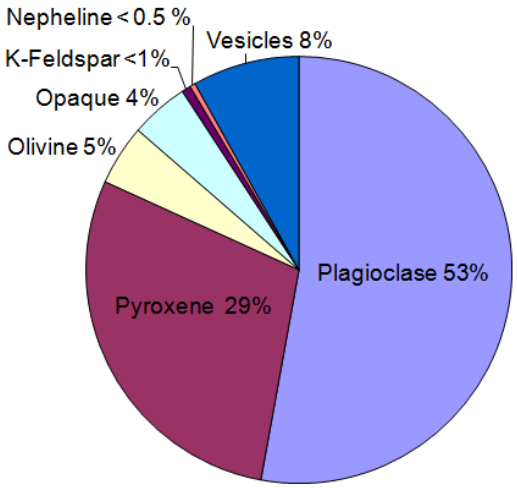

Figure 6: Modal proportions for the studied flows in Al Ajib and Az Za'atri, showing the average mineral volume proportions for the six sub-flows. The minerals volume proportions were analyzed using polarized microscope.

The results of modal analysis are plotted on the APF triangle (Fig. 7) of Streckeisen (1979), it indicates the basalt to foid- bearing basalt composition. Based on modal analyses (Fig. 6), the studied basalts are classified as plagioclase, pyroxene, olivine – phyric vesicular basalt (Al-Malabeh, 1993).

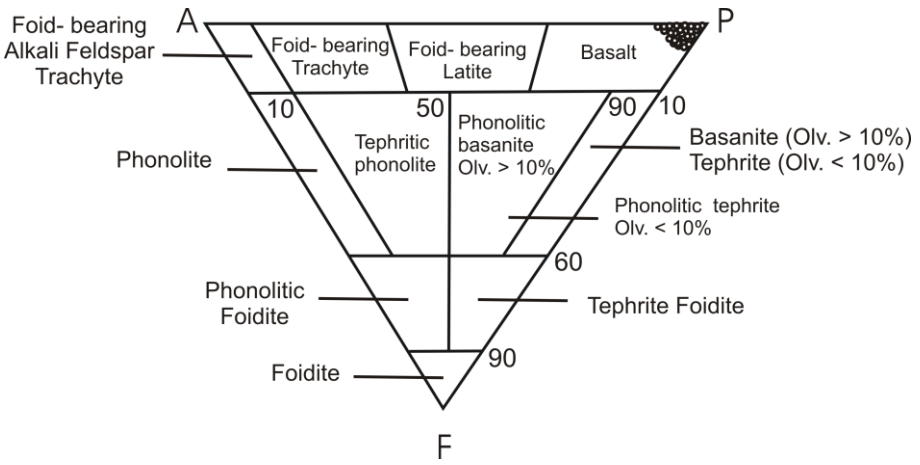

Figure 7: Classification and nomenclature of the studied basalts according to their modal mineral contents using the APF silica under saturated diagram. (Streckeisen, 1979).

2.4.3. Minerals Description

The studied basalts are relatively uniform in their mineralogical composition. They are characterized by plagioclase, pyroxene, olivine and rare nepheline and K-feldspar. This may indicate magma differentiation at early stages of crystallization and continental contamination. Generally, most thin sections exhibit micro-doleritic texture which identifies the crystal size of about 1 mm (Raymond, 2002).

Crystals rarely exceed 3 mm in length. Furthermore, most flows exhibit fine porphyritic texture with fairly uniform petrographic features; e.g. glomerocrysts of intergrowth subhedral to euhedral clinopyroxene. As the texture of the basalt is micro-doleritic, the analysis through point counting is sufficient to distinguish all mineral phases and thus a modal rock determination (normative chemical study is not required).

Plagioclase and K-feldspar

Plagioclase is the most abundant mineral phase in the studied samples. It occurs as phynocrysts, in clusters and in groundmass (Fig. 8). The phynocrysts are mainly hypdiomorphic, but idiomorphic crystals are also abundant. They are usually lath-like, but some of them occur as euhedral tabular crystals, particularly in the samples from A2 and Z3. Some of them show good cleavage in two directions and are often fractured.

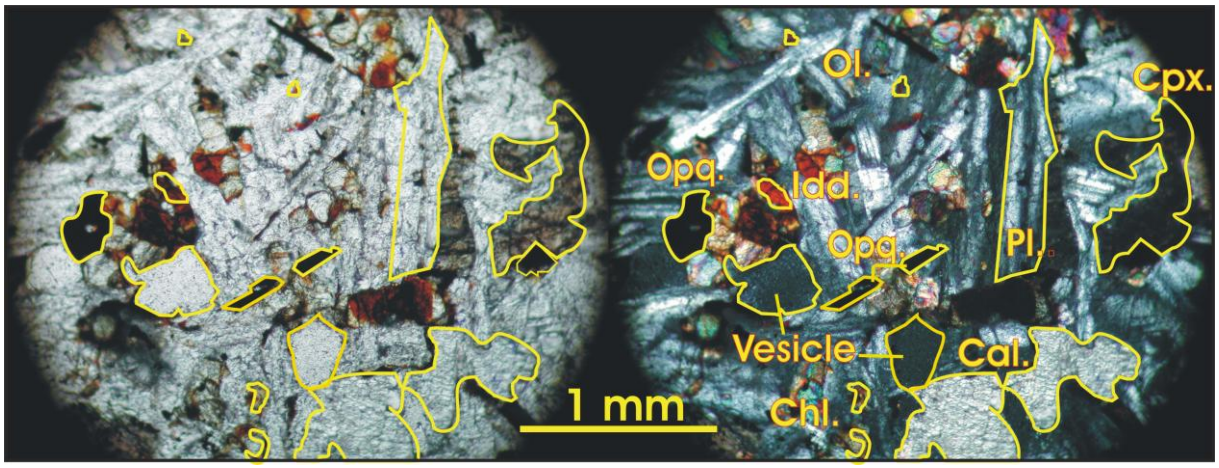

(a) **(b)**

Figure 8: Mineral components phynocrysts of Jordanian Harrat Basalt from one representative sub-flow A2 :(a) plane PL, (b) CN. Ol.: Olivine; Idd.: Iddingsite; Pl.: Plagioclase; Cal.: Calcite; Mag.: Magnetite; Cpx.: Pyroxene and Chl.: Chlorite.

Zoning is not visible optically. The laths are randomly oriented and individually distributed (Fig. 9), but clusters are also observed. Glomeropophyritic clusters of up to 6 crystals are recorded. The crystals show multiple or polysynthetic twinning on the albite law which characterizes plagioclase. The multiple twining is wide, straight and parallel. Simple twinning is also recorded, in which twin lamellae are uniformly developed and follow Carlsbad law.

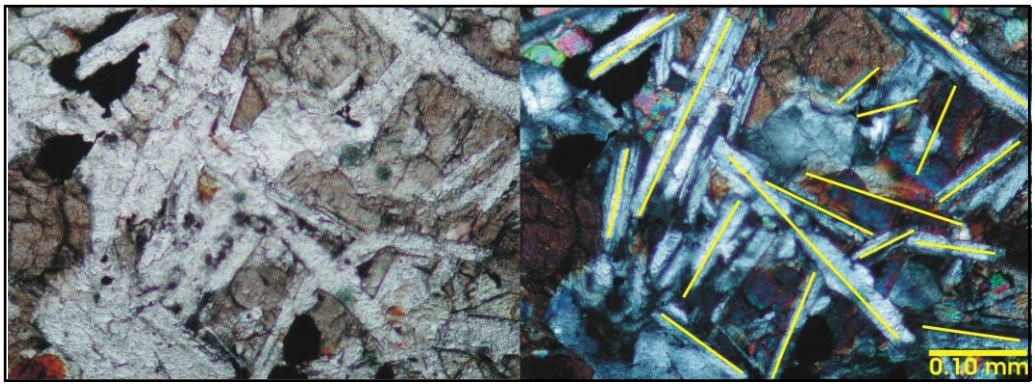

(a) **(b)**

Figure 9: Randomly crystallized plagioclase laths, yellow arrows are the crystals axes. (a) PPL. (b) CN.

Plagioclase laths were found to have an extinction angle between 33° to 38°, indicating a labradorite (An_{59} – An_{68}) composition (Kerr, 1977). Grain sizes define a limited distribution and range in length from 0.5 to 2 mm, but some crystals up to 3 mm. They have generally 2:1 and 3:1 length-to-width ratio. Groundmass plagioclase occurs as skeletal-like microlites. The microlites have a grain size range from 0.04 to 0.12 mm and randomly oriented. The phenocrysts are little higher in An than the micro-lath plagioclase in the matrix.

High temperature K-feldspar porphyric phenocrysts indicate together with some chemical shifts (Al_2O_3 and Na_2O) a slight contamination of the ultramafic source. Karlsbad twinning and parallel extinction are diagnostic. Due to the low K_2O content, K-feldspar of orthoclase composition is to be expected (Table 2). Selected point analyses were carried out on some laths and microlites using X-ray microanalyser. The analysis (Table 2) show relatively uniform composition. The analyses of plagioclase from the studied samples assign the plagioclase to the labradorite range of composition (An_{50-70}) and indicate normal, albite limited, zoning.

Table 2: Analyses of plagioclase in the investigated basalts.

	Al Aqib Basaltic Flow			*Az Za'atri Basaltic Flow*		
	A1	A2	A3	Z1	Z2	Z3
SiO_2	55.64	52.11	51.18	52.77	51.12	52.01
Al_2O_3	28.47	29.79	31.83	28.64	30.1	29.89
FeO	0.89	0.67	0.52	0.91	0.81	0.6
CaO	10.71	12.63	12.83	12.7	14.15	12.7
Na_2O_3	3.81	4.37	3.21	4.65	3.61	4.37
K_2O	0.48	0.43	0.43	0.33	0.21	0.43
Total	100.00	100.00	100.00	100.00	100.00	100.00
Number of the ions on the basis of 8 oxygens						
Si	2.503	2.38	2.324	2.42	2.338	2.376
Al	1.509	1.53	1.703	1.529	1.622	1.601
Ca	0.516	0.615	0.624	0.615	0.693	0.617
Fe^{2+}	0.033	0.03	0.02	0.035	0.031	0.026
Na	0.332	0.314	0.283	0.414	0.32	0.386
K	0.028	0.022	0.025	0.018	0.012	0.025
Total	4.921	4.891	4.979	5.031	5.016	5.031
Si+Al	4.013	3.87	4.027	3.349	3.96	3.976
Na+Ca+K	0.876	1.03	0.932	1.048	1.026	1.028
An (Si/Al)	48.73	65.04	66.65	54.75	64.04	60.03
Ab (Si/Al)	48.12	34.72	30.68	43.52	34.77	37.54
Diff.:	10.12%	2.9%	0.31%	3.76%	3.52%	0.95%
An (Na/Ca)	58.85	67.94	66.96	58.51	67.56	60.98
Ab (Na/Ca)	38.03	30.31	30.47	39.67	31.42	36.64
Or	3.12	1.75	2.57	1.82	1.02	2.38

Clinopyroxene

Clinopyroxene is only recorded in the investigated basalt. It occurs as hypidiomorphic. Resorption embayment are common. The crystals displays two sets of good cleavage intersecting at approximately 90°. The dominant mineral component of clinopyroxene is augite and rarely diopside. Crystals appear as one generation (phenocrysts) ranging in size from 0.25 to 1.0 mm. Clinopyroxene crystals have an inclined extinction angle between 35° – 48°, which indicates an augite mineral composition. The crystals also bear the effects of alteration processes which are visible as green pleochroitic Fe-Mg-chlorite on the fractures, crystal rims, and on the cleavage sets. This alteration has an influence on thermal conductivity of pyroxenes.

Chemical analysis as point analysis on selected clinopyroxene crystals from each subflow were carried out (Table 3). The composition of the pyroxene is closed to augite (Fig.10), according to classification of Morimoto et al., (1988). They characterized by their high contents of Aluminum (~ 5 wt.%) and TiO_2 (~ 2 wt.%), similar to pyroxene from basic alkaline rocks (Coombs, 1963).

Table 3: Analyses of pyroxene in the investigated basalts.

	Al Aqib Basaltic Flow		***Az Za'atri Basaltic Flow***	
	A1	A3	Z1	Z2
SiO_2	55.86	54.74	53.39	56.78
TiO_2	1.49	1.49	1.45	1.27
Al_2O_3	4.37	4.3	4.27	3.41
FeO	5.7	6.4	6.88	5.65
MgO	13.25	13.33	14.41	13.42
MnO	0	0	0.15	0.02
CaO	18.65	19.02	18.89	18.76
Na_2O_3	0.31	0.38	0.15	0.43
K_2O	0.05	0.07	0.07	0.06
Cr_2O_5	0.28	0.27	0.28	0.2
Total	99.96	100	99.94	100
	Number of ions on the basis of 6 oxygens			
Si	2.035	1.898	1.930	1.908
Ti	0.035	0.049	0.040	0.040

Al	0.148	0.203	0.183	0.192
Fe^{2+}	0.171	0.196	0.179	0.174
Mg	0.707	0.784	0.830	0.754
Mn	0.00	0.00	0.005	0.001
Ca	0.682	0.795	0.757	0.790
Na	0.035	0.027	0.011	0.138
K	0.002	0.003	0.00	0.039
Cr	0.004	0.008	0.007	0.006
		Chemical formula		
Z				
Si	2.035	1.048	1.930	1.908
Al	0.00	0.102	0.07	0.092
Sum	2.035	2.00	2.00	2.00
Y				
Al	0.184	0.101	0.113	0.100
Cr	0.004	0.008	0.007	0.006
Ti	0.035	0.049	0.040	0.040
Mg	0.707	0.784	0.830	0.754
Fe^{2+}	0.070	0.059	0.010	0.100
Mn	0.00	0.00	0.00	0.00
Sum	1.00	1.00	1.00	1.00
X				
Mg	0.00	0.00	0.00	0.00
Fe^{2+}	0.101	0.138	0.168	0.074
Mn	0.00	0.00	0.005	0.001
Ca	0.682	0.795	0.757	0.790
Na	0.035	0.27	0.011	0.138
K	0.002	0.003	0.00	0.039
Sum	0.821	0.963	0.940	1.042

	End members			
En	45.52	44.26	46.59	43.78
Wo	43.51	44.74	43.16	45.28
Fs	10.96	11	10.12	10.72

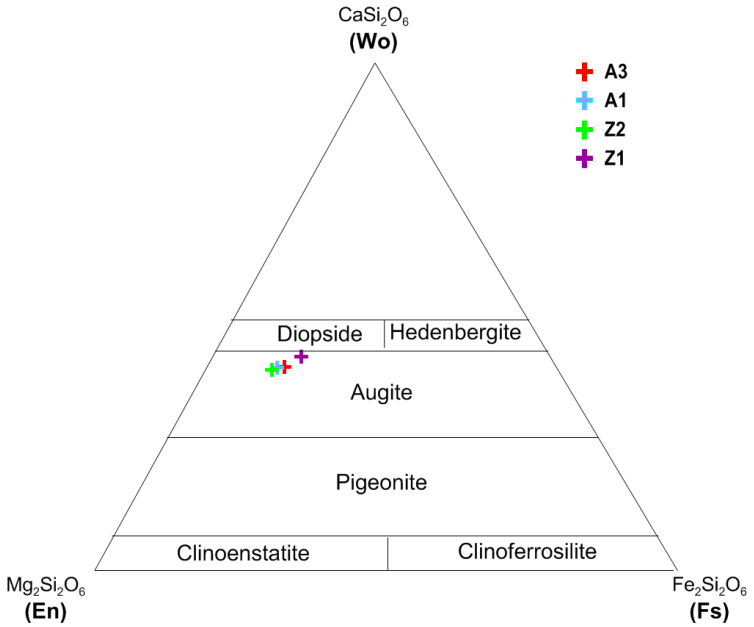

Figure 10: Wo-En-Fs plot (Morimoto et al., 1988) for the pyroxene from the studied basalts.

Olivine

Olivine is characterized by early crystallized, isometric phase with resorbtion and erosion features in the groundmass. It commonly occurs in all the studied samples. It dominantly occurs in two generations, as phenocrysts and as small crystals and needles in the groundmass. The phenocrysts are mainly hypidiomorphic; some are allotriomorphic or idiomorphic: six-sided euhedral shapes, rounded forms as well as equidimensional crystals are abundant. They occur usually as individual crystals, however, glomeroporphyritic aggregates of as many as four to eight crystals are occasionally observed. Most of the larger olivine crystals are broken and fractured. The large crystals commonly include euhedral to subhedral grains of opaques. The grain size reflects seriate texture. The crystals range in size from 0.05 mm to about 0.5 mm. However, all basalt flows show some corroded olivine crystals. The shape of resorbed olivine is noted through bands of iddingsite that form along embayment rims. Chemical composition of selected olivine crystals was carried out. Analysis were carried out on phenocrysts and groundmass olivine. The results are listed in Table 4. The analysis show a limited variation with compositional ranges. The crystals magnesia rich olivines with limited iron content have a chrysolite range of composition (Fo_{70-90}) except A3 sample that have a composition of forsterite to chrysolite.

Table 4: Analyses of olivine in the investigated basalts.

	Al Aqib Basaltic Flow		*Az Za'atri Basaltic Flow*	
	A2	A3	Z1	Z3
SiO_2	41.65	41.38	41.03	41.12
FeO	13.16	8.61	11	10.1
MnO^+	0.00	0.00	0.00	0.00
MgO	44.67	49.45	47.09	48.16
CaO	0.15	0.14	0.31	0.15
NiO	0.36	0.35	0.55	0.35
Total	99.99	100	99.19	100
Number of ions on the basis of 4 oxygens				
Si	1.034	1.018	1.022	1.009
Fe^{2+}	0.262	0.143	0.222	0.207
Mn	0.00	0.00	0.00	0.00
Mg	1.646	1.825	1.717	1.764
Ca	0.005	0.005	0.009	0.005
Ni	0.006	0.006	0.01	0.006
Sum	2.965	2.955	2.98	2.991
End members				
Fo	84.666	91.652	88.02	89.68
Fa	15.334	8.348	11.98	10.32

Opaque Minerals

Opaque minerals are common. They occur in very few percent and most commonly as inclusions within olivine crystals. The majority are idiomorphic, and occurs as equal crystals as square or polygonal in thin sections suggesting magnetite. Opaques range in size from 0.01 mm to 0.08 mm. Much smaller fine lath and bipyramidal crystals are evident in the groundmass. These minerals are too small for a precise identification. The chemical composition of some crystals from the studied basalts (Table 5) shows them to be

titanomagnetite, with TiO_2 contents ranges between 24.32 and 26.85 wt%. The total iron (FeO) contents range from 69.8 and 72.64 wt% and Al_2O_3 contents from 1.00 to 2.18 wt%.

Table 5: Analyses of opaque minerals in the investigated basalts.

	Al Aqib Basaltic Flow		***Az Za'atri Basaltic Flow***	
	A2	A3	Z1	Z3
SiO_2	0.12	0.03	0.03	0.14
TiO_2	25.82	25.64	26.85	24.32
Al_2O_3	1.46	2.18	1.01	1.00
FeO	70.39	69.8	70.39	72.64
MnO	0.76	0.49	0.35	0.78
NiO	0.00	0.00	0.00	0.00
MgO	1.37	1.7	1.32	0.98
CaO	0.08	0.16	0.05	0.14
Total	100	100	100	100
	Number of ions on the basis of 4 oxygens			
Si	0.003	0.001	0.001	0.006
Ti	0.732	0.756	0.785	0.738
Al	0.06	0.099	0.02	0.016
Fe^{2+}	2.321	0.00	2.31	20418
Mn	0.021	0.016	0.019	0.024
Ni	0.00	0.00	0.00	0.00
Mg	0.073	0.097	0.075	0.05
Ca	0.003	0.005	0.002	0.00

Nepheline and Apatite

Nepheline is observed in all subflows except A1 and Z2 basalt subflows. The hexagonal crystals are colorless under plane polarized light and their proportion is less than 1 vol. %. The crystals are euhedral to subhedral in shape and exhibit two sets of cleavage that intersect at 90°. This is an important phase and indication of the SiO_2 under- saturated source magma, but in contrast to the bulk chemical high SiO_2, Al_2O_3 and Na_2O content.

Apatite exists in both basalt flows as an accessory mineral of less than 1 vol. %. It exhibits a micro needle like shape (typical *1-100*, *10-10*, *01-10* faces) scattered without preferred orientation, thus some typical hexagonal (*0001*) head are found.

Secondary Minerals

Several secondary (authogenic) minerals formed due to the hydration and oxidation of the pyrogenic minerals. These alteration processes include albitisation and seritisation of labradorite (Al-Malabeh and Kempe, 2009), iddingsitisation of olivine and chloritization of pyroxene. The studied samples experienced a low to moderate degree of chloritization on clinopyroxenes like augite. Two types of calcite can be distinguished. The first type is uniquely comprised of spot-like patches of calcite as interstitial crystals occurring at a higher proportion in the Al Ajib flow. The other form of calcite was precipitated in vesicles. Due to post-eruption alteration processes, this calcite presents an amygdaloidal texture with palisade calcite. This type is typical for late fluid migration and precipitation. It appears in the same volume proportion in both studied basalts.

Vesicles

The vesicles volume proportion of the studied basalts averages 9 % and ranges from 6 to 11 vol.% in both studied flows; Al Ajib and Az Za'atri flows, most vesicles are partly filled with calcite. The porosity ranges from 6 to 12 %. The difference between the porosity measured in thin sections (vesicularity) and the porosity measured in the laboratory is expected; the variation is explained through the larger size limit of vesicle diameter which is distinguishable under the microscope. Petrographically, this limit is assumed to be 30 µm in diameter which is equal to the thin section thickness. Whereas the porosity measured in the lab detects all vesicles, including micro-pores smaller than 30 µm, leading to this discrepancy (Franzson et al., 2001).

2.5. Geochemistry

2.5.1. Analytical methods

Chemical analysis was carried out on the investigated basalt using wavelength dispersive X-ray fluorescence spectrometry at the Group of Technical Petrology (TUD). The wavelength dispersive X-ray fluorescence spectrometer Tiger S8, Bruker AXS at the Group of Technical Petrology (TUD) is equipped with a 4 kW Rh X-ray tube working at maximum 60 kV and 170 mA. Samples are powder grounded in a WC mortar down to <63 µm grain size. A mixture was prepared with Hoechst Wachs C 2 g added as a binder to 8 g of sample powder and as next pressed in an Al-cup with 160 kN. Then the test results were analyzed using the GEOS software, based on calibration with international geological rock standards. The contents of the major oxides of Si, Ti, Al, Fe, Mg, Mn, Ca, Na, K and the trace elements were analyzed.

2.5.2. Chemical analysis results

The contents of major elements (with 0.58 % standard deviation) and trace elements (with 2 ppm standard deviation) were used to classify the basalts (Table 6 and 7) together with the modal mineral composition. Several diagrams were constructed to determine the trends of the elements and the chemical character of the basalt. Chemical contents are expressed in these diagrams in wt% for the major elements and in ppm. for the trace elements. Moreover, some binary diagrams of inter-elemental relationships, particularly for trace elements, were also constructed.

Table 6: Bulk chemical analyses in wt. % for the studied basalts carried out with x-ray fluorescence spectrometer.

Basalt Flow	SiO_2	TiO_2	Al_2O_3	Fe_2O_3	FeO	MnO	MgO	CaO	Na_2O	K_2O	P_2O_5	L.O.I	Total
A3	46.9	1.66	17.3	2.49	7.61	0.17	4.3	11.5	3.74	0.73	0.32	1.54	98.09
A2	48.5	1.65	17	2.48	8.62	0.17	5.3	9.7	3.77	0.71	0.34	1.8	99.87
A1	47.5	1.63	17.9	2.45	8.65	0.17	4.5	9.8	3.77	0.72	0.35	2.26	99.53
Z3	49.3	1.82	17.4	2.73	8.77	0.16	4.6	9	3.07	0.76	0.48	1.7	99.63
Z2	48.8	2.12	17.9	3.18	7.92	0.15	3.9	10.4	3.86	0.93	0.43	1.01	100.45
Z1	46.5	1.78	17.1	2.67	9.03	0.16	4.5	11.5	3.48	0.92	0.53	2.31	100.32

Table 7: Trace elements in ppm for the studied basalts carried out with x-ray fluorescence spectrometer.

Basalt Flow	Rb	Pb	V	Cr	Ni	Co	Zn	Cu	Sr	Ba	Nb	Zr	Ce	La	S	Y
A3	10	7	197	269	112	47	79	59	400	170	14	122	61	14	217	17
A2	10	7	201	293	118	50	82	59	403	127	14	121	64	14	390	17
A1	11	7	192	312	125	52	79	61	377	124	13	120	63	11	394	17
Z3	11	7	186	232	89	49	89	46	498	191	17	117	70	23	3	16
Z2	11	7	181	199	90	48	82	48	518	169	20	133	77	16	0	17
Z1	10	7	176	180	91	48	84	56	571	210	19	134	77	14	79	17

The chemical analysis of the Jordanian Harrat is compared with other basaltic rocks worldwide indicating a similar chemical composition of continental alkaline basalts (Table 8).

Table 8: The average chemical analysis of different alkali basalts comparing to Jordanian Harrat basalt.

	JORDAN				ARBIAN PLATE		WORLD WIDE		
	Northern Jordan Umm Al-Qutein(1)	Within Rift (2)	Central Jordan (3)	Jordanian Harrat(4) This study	Al – Madina(5)	Rahat(6)	Syria(7)	Romania(8)	Spain(9)
SiO_2%	45.68	43.36	45.13	47.92	47.12	47.12	47.052	47.4	44.9975
TiO_2%	2.36	2.847	2.281	1.78	2.62	2.48	2.361	1.59	2.695
Al_2O_3%	14.3	13.93	12.83	17.43	16.22	16.08	15.266	16.08	11.9875
Fe_2O_3%	12.33	13.29	12.45	2.67	12.32	11.45	3.725	9.12	4.125
FeO%				8.43			8.146		7.1575
MnO%	0.18	0.174	0.16	0.16	0.19	0.19	0.188	0.15	0.17
MgO%	8.21	8.92	9.64	4.52	7.35	7.67	7.443	8.64	11.4525
CaO%	9.12	9.35	10.89	10.32	9.6	9.78	9.536	9.45	11.3375
Na_2O%	3.78	4.41	3.32	3.62	3.64	3.59	3.312	3.69	2.7025
K_2O%	1.64	1.04	1.2	0.80	0.8	0.8	1.144	1.61	1.15
P_2O_5%	1.57	0.64	0.45	0.41	0.52	0.5	0.512	0.46	0.67
Rb (ppm)	n.d.	24	19	10.5	6.8	7.4	n.d.	29.57	31.25
V (ppm)	230.86	195	223	188.8	233.3	228.3	n.d.	336.33	230
Cr (ppm)	n.d.	163	347	247.5	180.6	215.1	n.d.	n.d.	407.25
Ni (ppm)	n.d.	157	261	104.17	101.6	122	152.2	200.33	234
Co (ppm)	164.57	57	65	49	n.d.	n.d.	n.d.	160.33	38
Zn (ppm)	44.86	125	103	83	86.7	85.6	n.d.	40	101.25
Sr (ppm)	n.d.	924	620	461	539.1	550.2	211.9	850	821
Ba (ppm)	605.57	381	350	165	95.3	108.2	n.d.	877.33	702.25
Nb (ppm)	n.d.	63	37	16	22.4	23.3	n.d.	78	55
Zr (ppm)	30.14	214	161	125	202.1	197	195.3	41.13	254.5
Ce (ppm)	n.d.	59	55	69	50.5	49.5	n.d.	93.67	92.125
La (ppm)	n.d.	34	25	15.3	17.6	17.2	n.d.	45.33	46.925
Y (ppm)	172.29	15	17	181	539.1	25	24.8	179.67	28.75
Ga (ppm)	246.71	n.d.	n.d.	n.d.	18.8	18.3	n.d.	n.d.	n.d.

Where:

* n.d. : Not Determined

(1) Average basalt analysis of seven samples, Al-Malabeh el al. (2002).

(2) and (3) Average basalt analysis of four samples, Saffarinii et al. (1985)

(4) Basalt analysis of six samples from the Jordanian Harrat (This study).

(5) and (6) Average basalt analysis of 48,64 samples from Al-madina and Rahat basalt, respectively, Camp and Robool, (1989).

(7) Average basalt analysis of nine samples, Mouty et. al. (1992).

(8) Average basalt analysis of three samples, Downes et. al, (1995).

(9) Average basalt analysis of four samples, Cebria and Lopez-Ruinz , (1995).

2.5.3. Rock Classification and nomenclature

Rock nomenclature

The total alkali versus silica diagram, which Le Maitre et al., (2002) called TAS offers a simple and direct use of the analytical data. It is one of the most frequently used, to chemically classify igneous rocks, as well as assign the rock name. Plotting the analyses of the investigated samples on the diagram (Fig. 11) modified and recommended by Le Maitre et al., (2002) gives a cluster of data points in the basalt field.

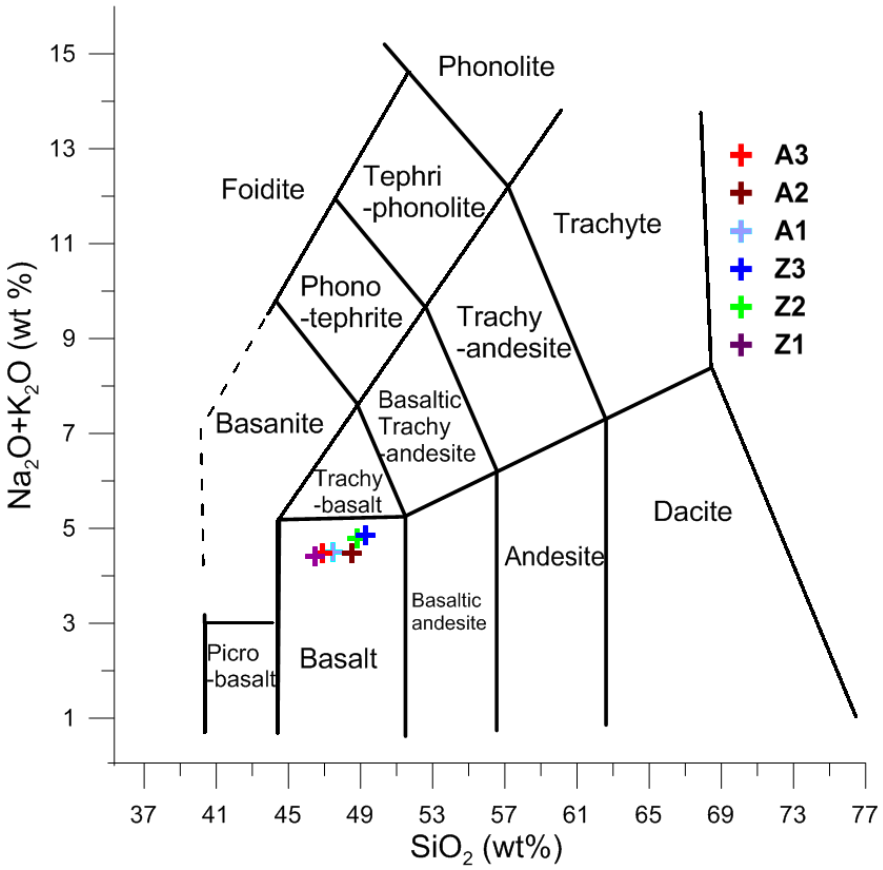

Figure 11: Total Alkali Silica or TAS - Diagram (Le Maitre et al., 2002) for the studied basalts, each cross present one sub-flow sample.

The alkaline affinity of the studied basalt

Results are shown on the Zr / TiO_2 versus Nb / Y diagram (Wichester & Floyd, 1977). On this diagram, the analyses from the studied basalts plot on the alkali basalt field (Fig. 12).

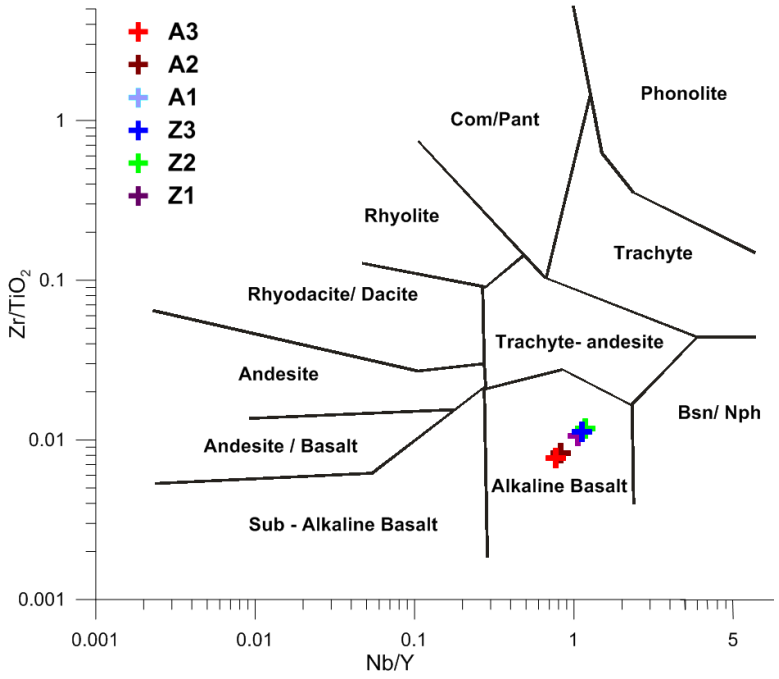

Figure 12: Zr / TiO_2 – Nb / Y diagram (Winchester & Floyd, 1977) for the basaltic rocks from the studied sub-flows.

The alkali character of the studied basalts is reflected by their low silica content, relatively high total alkalis, low Y / Nb, low Zr / Nb, and in the concentration of major, trace and rare earth elements. The partial projection Cpx-Ol-Opx of the clinopyroxene – olivine – orthopyroxene diagram, is used to distinguish between alkaline and subalkaline basic volcanic rocks. This diagram is an output of Chayes' study in 1956, in which he determined two lines to be used as a discriminate functions. The straight line is for the linear plus quadratic function (Irvine & Bargar, 1971). The weight percent of Cpx-Ol-Opx is plotted on this diagram. The plot obviously shows that the analyses of the studied rocks fall in the area of alkaline basalt (Fig. 13).

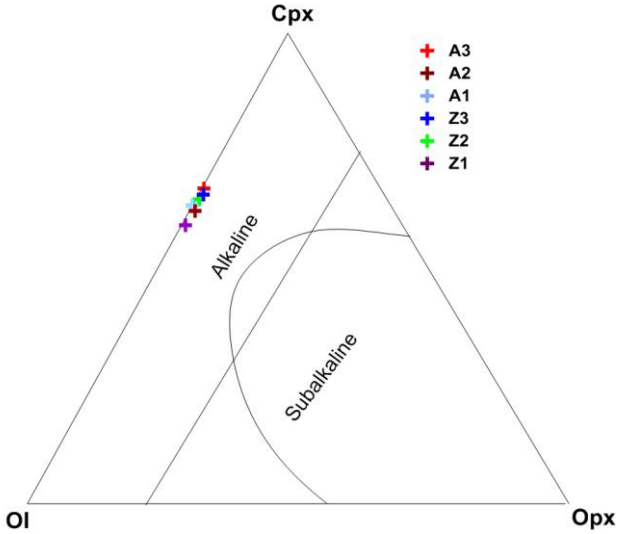

Figure 13: Cpx-Ol-Opx projection (Irvine & Bargar, (1971) in weight percent, of the investigated basalts.

Sodic series

On a ternary plot of normative An-Ab'-Or proposed by Irvine & Bargar (1971) and used to discriminate between sodic and potassic series, An and Or are in norm weight percent, and Ab' is calculated as sum of Ab + 5/3 Ne. On this diagram (Fig. 14) all analyzed samples are plotted in the sodic series.

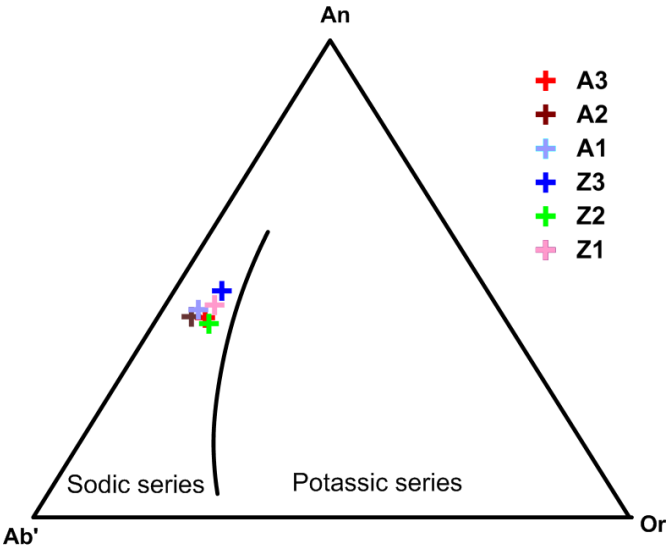

Figure 14: An-Ab'-Or (Irvine & Bargar, 1971) from the basalts of the studied flows; Ab'= Ab+5/3Ne, An and Or in weight percent.

The alkaline affinity of the studied basalt is cleared by the discrimination diagrams. The total alkali –silica diagram, which discriminate between basalts of tholeiitic and various degrees of alkaline affinities has derived by Irvine & Bargar, (1971). On this diagram, the studied basalt samples are mildly alkaline (Fig. 15). In addition, Zr/P_2O_5 versus TiO_2 (Winchester and Floyd, 1977), variation diagram shows alkali basalt affinity (Fig. 16). The studied samples have Na_2O/K_2O ratios greater than one, reflecting their Na-enriched nature.

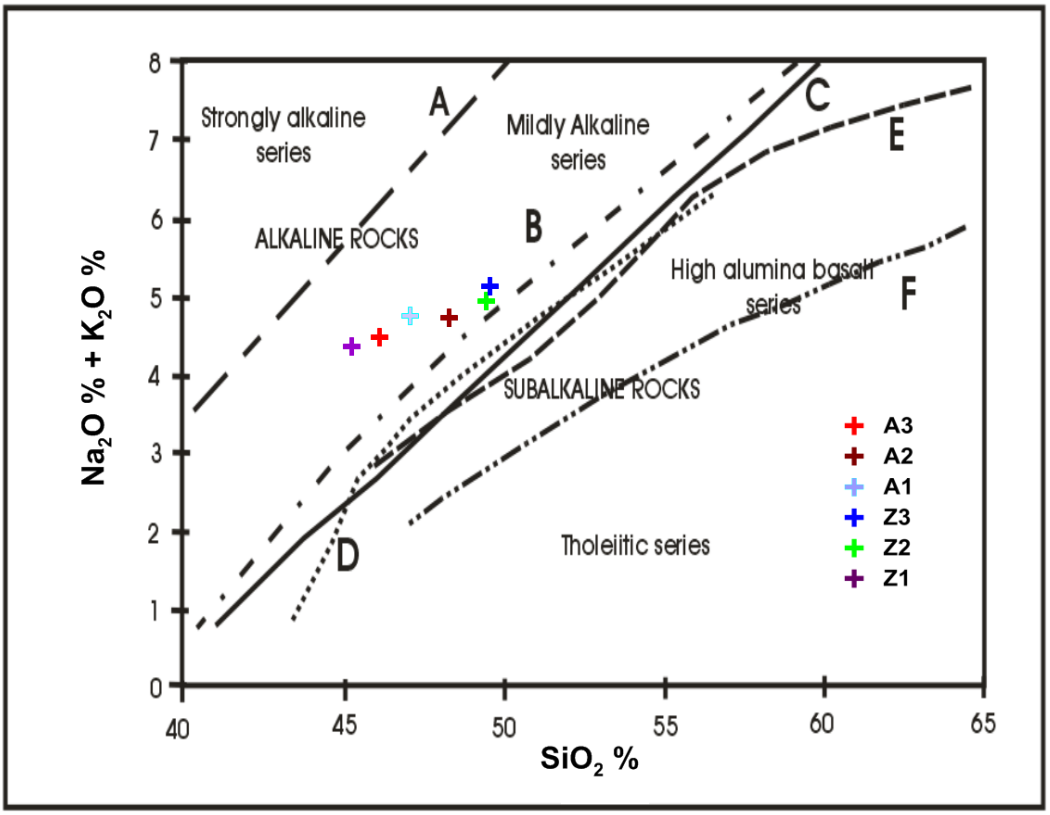

Figure 15: Alkaline-silica diagram from studied basaltic rocks. Dividers are A: Saggerson & Williams (1964), B: Irvine & Bargar (1971); C: Macdonald & Katsura (1964); D,E,F: Schwarzer & Rogers (1974).

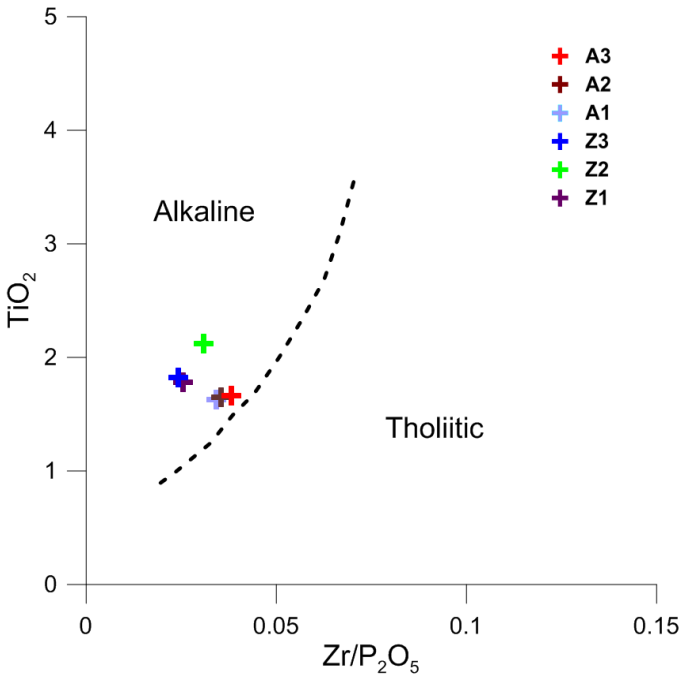

Figure 16: Zr/P_2O_5 versus TiO_2 (Winchester and Floyd, 1977), variation diagram showing alkali basalt affinity of the Jordanian Harrat basalts

Within– Plate environment of eruption

The basalt occurrences of the Jordanian Harrat were emplaced in (within-plate) environment. This interpretation is supported by the chemical composition of the studied rocks. The logarithmic binary plot of TiO_2 versus Zr (Pearce, 1980) is used it distinguish three different basalt environments: within-plate lava, arc lava and MORB basalt. Moreover, a simple two-fold division into basic and evolved lavas is also suggested on the diagram. On this diagram, analyses of the Jordanian Harrat samples fall in the within-plate and MORB field. Moreover, all the analyses plot in the basic field (Fig.17). Consistent results are given by the TiO_2-Y/Nb plot, which Floyd and Winchester (1975) intended to discriminate between continental alkali basalt (CAB), continental tholeiitic basalt (CTB), oceanic alkali basalts (OAB) and oceanic tholeiitic basalts (OTB). On this diagram, the analyses of the studied rocks plot partly in the CAB field and, partly in the area of overlap between CAB and CTB fields (Fig. 18).

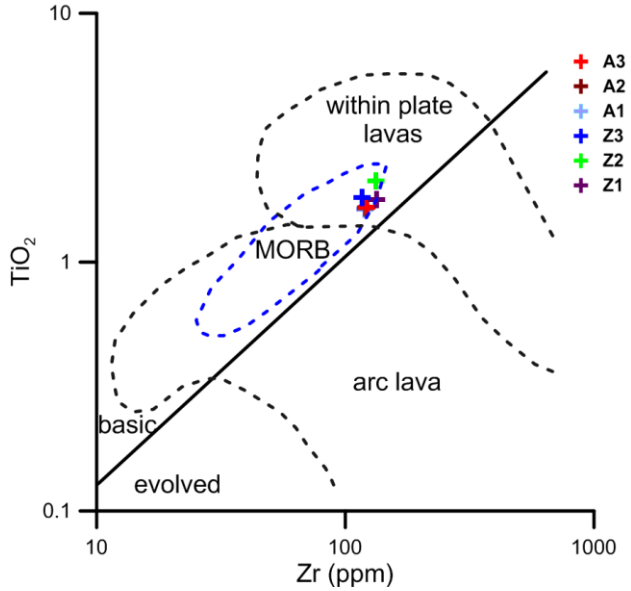

Figure 17: TiO_2-Zr diagram (Pearce, 1980), showing the typical (within-plate) character of the pyroclasstic rocks from the studied volcanoes.

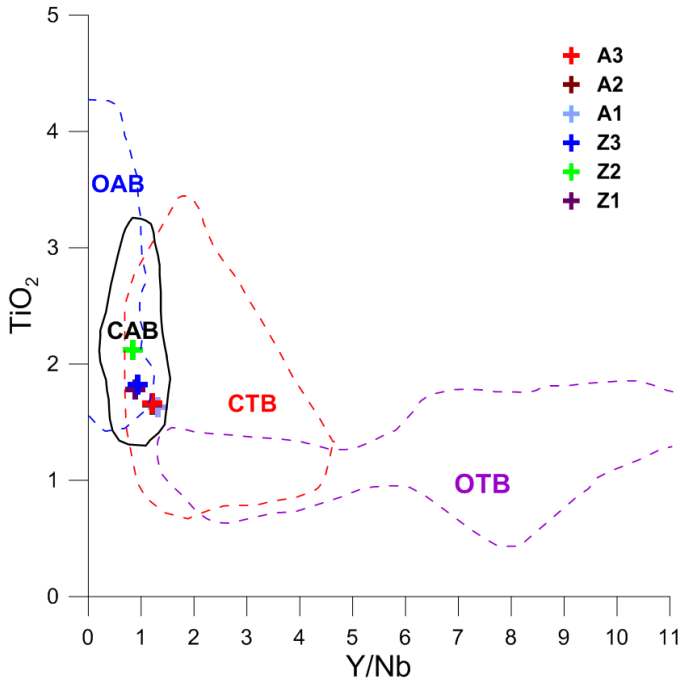

Figure 18: TiO_2-Y/Nb diagram (Floyed & Winchester, 1975) for the pyroclastic rocks from the studied volcanoes. C: Continental, A: Alkali, T: Tholiitic and B: Basalt.
The analyses plot almost entirely in the CAB-field.

Magma characteristics

The volcanic rocks are of SiO_2 mafic composition with a high Al_2O_3, TiO_2, CaO, Na_2O and low MgO content. The amount of the other oxides are typical basaltic. The difference in major elements shows a mafic-ultramafic source (also Cr, Co, Ni) with K-poor continental contamination (deduced also from the Rb/Sr relation and Ba content) and early differentiation. The slight variations in concentrations of Major oxides e.g., SiO_2, MgO, Na_2O, K_2O, FeO may suggest the source is homogeneous (Raymond, 2002). This conclusion is further supported by the limited variation of the Y value and the similar trace element patterns. It may suggest that the basaltic suite is resulted of limited degree of partial melting Shaw (1970). In the Sr-Zr diagram (Camp & Roobol, 1989) the analyzed basalt samples are fall in the partial melting (Fig. 19) showing limited plagioclase fractionation. Moreover, the limited variation in the ratios of incompatible elements such as Ba/Rb, Zr/Nb and Y/Zr, support this conclusion. Depending on the constancy of Y concentration, the high Zr/Y and the low Zr/Nb ratios may indicate that the inferred source of the studied rocks is of asthenospheric parts of the garnet lehrzolite mantle zone (Al-Malabeh, 1993). This basalt appears to present relatively highly alkaline primitive magma composition. Therefore, this basalt is unlikely to have assimilated a significant amount of crustal material. This leads to the conclusion that the basalts are of the chemical alkaline type (alkali-olivine basalts with a shift to the sodic series (Irvine & Barger, 1971).

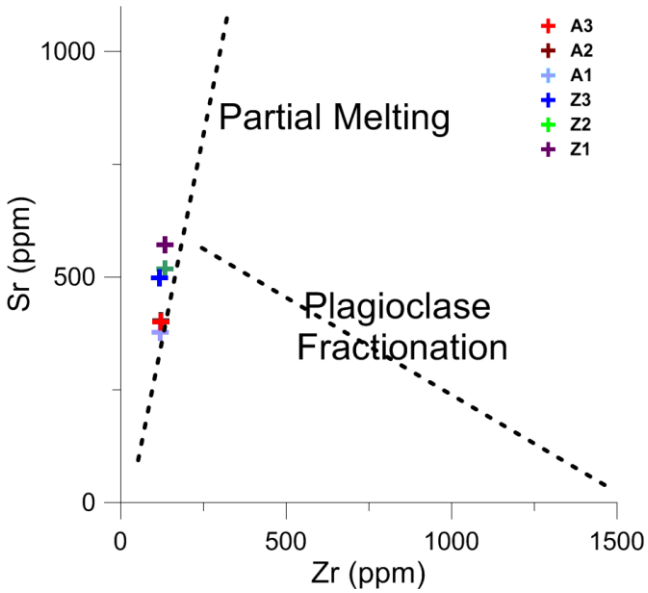

Figure 19: Plot analyzed samples on the Sr-Zr diagram (Camp & Roobol, 1989), showing the limited plagioclase fractionation.

2.6. Thermophysical Properties

2.6.1. Methodology

Thermal conductivity, permeability and porosity measurements were conducted under standard laboratory conditions on oven dried core samples. 72 samples were analyzed using thermal conductivity scanner, minipermeameter and pycnometer (Fig. 20 a, b and c) for their thermal conductivity, permeability and porosity respectively.

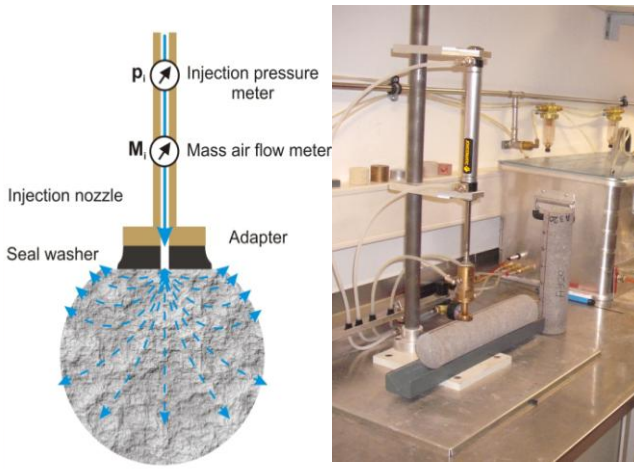

(a)

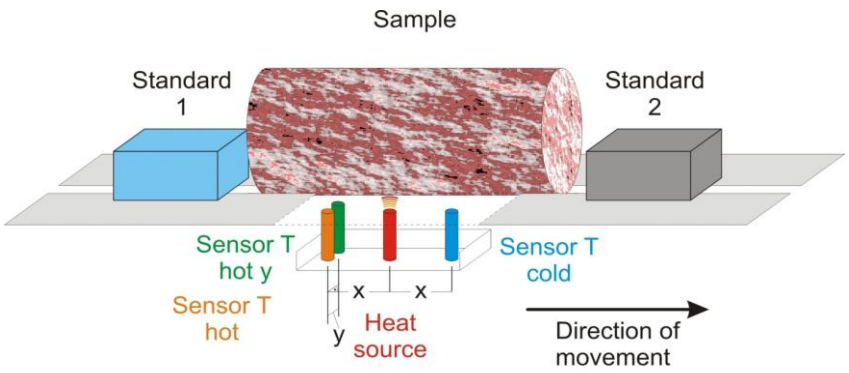

(b)

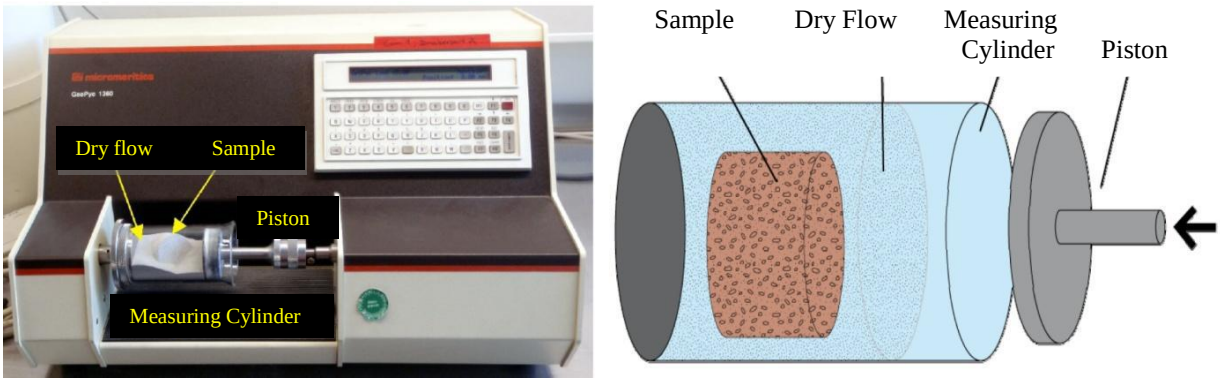

(c)

Figure 20: (a) Thermal Conductivity Scanner, the left part after Mielke, 2009 and Bär, 2008, (b) Minipermeameter the lower part after Mielke, 2009. (c) Pycnometer modified after Bär, 2012.

Thermal conductivities were measured using the Optical Scanning Method (Popov, et al., 1999). This method is based on scanning a sample surface with a mobile, focused, and continuously operated constant heat source in combination with a temperature sensor. It allows relatively quick measurements of different samples' quality and a detailed study of the anisotropy of their thermal conductivity (Mielke, et al., 2010). The heat source is moving and heating the sample surface during this passing. No contact is made with the sample (Fig.20a). The size of the heating spot is 1 mm in diameter. The temperature sensor and the heat source move together with a constant speed and to a fixed separation distance to each other (Mielke, et al, 2010). Thermal conductivity of the 4°C heated surface is determined as an arithmetic mean of local conductivities along the entire scanning line after the temperature is measured prior and after heating (Popov, et al., 1999).

The comparison between the induced temperature differences of the standards (with known thermal conductivity λs) and the sample of unknown thermal conductivity deduce the sample thermal conductivity λ (Eq. 1).

The ratio of Θ_R and Θ is proportional to the measured electrical potential U_R and U is described as follows (Mielke, et al., 2010):

$$\lambda = \lambda_R \left[\frac{\Theta_R}{\Theta} \right] = \lambda_R \left[\frac{U_R}{U} \right] \quad (1)$$

Different shapes can be measured with this scanner; prismatic and cylindrical. The standards used in the measuring device are made from a material has a similar thermal conductivity of the tested samples. Measurements can be done using oven-dry and moist samples with an accuracy of 3% (Popov, et al., 1999).

Permeability measurements were performed using a gas pressure minipermeameter (Mielke, et al., 2010). A gas pressure permeameter permits an infinite number of measurements, this can be assigned to individual layers of a rock sample. The device is a pressure air driven gas-permeameter, which measures the rock permeability precisely on rock surface. A smooth curved or plane samples' surface is used to measure the rock permeability. The measurements are non destructive. A probe attached to an adjustable pneumatic ram and

pressed perpendicular to the samples' surface. Pressured air is injected through a nozzle; with a circular adapter which has a seal washer to avoid leakage, initiating a particular flow-through (Fig. 20b). The exchangeable adapter has an inner diameter of 4 mm and an outer of 25 mm, in addition these adapter were designed in different shapes to accommodate the best fitting on the samples' surface. The seal washer of neoprene is fixed between the stamp and the sample to avoid leakages. A quasi- stationary volumetric flow rate built up. This can be happened after pressured air is injected into the sample through the central opening of the adapter and its seal then a particular flow-through is initiating. Alongside with dynamic viscosity and adaptor radius, the resulted volumetric flow rate (Eq. 2) is used to calculate the permeability (Eq. 3) (Goggin et al., 1988).

$$q_i = \frac{p_l}{pi} \; M_i \tag{2}$$

Where q_i is the volumetric flow rate, p_L is the atmospheric pressure, p_i is the injection pressure and M_i is the mass flow rate.

The permeability (k) is calculated then as follow

$$k = \frac{q_i \eta p_i}{r({p_i}^2 - {p_L}^2) F_G} \tag{3}$$

Where η is the dynamic viscosity, r is the adapter radius and F_G is a geometric factor.

Samples are oven-dry measured to enable comparability. Measuring oven-dry samples improves the measurements accuracy as moist samples may not be measured within the desired error limit (Mielke, et al., 2010). Mielke et al., 2010 stated that the error is limited to a maximum deviation of 5%.

Porosity was measured using the GeoPyc 1360 Pycnometer (Fig. 20c). The AccuPyc completes analyses by using volumes between 0.1 to 350 cm^3. With a known envelope volume, bulk density and the particle density, the porosity can be measured using this device. It computes both density values by measuring the displacement generated by the volume of the whole sample including pore volume. The device consists of a cylindrical measurement cell with an expandable ram. Simply, the cylinder is filled with the unknown powder volume of graphitized glass spheres. The ram is pushed into the cylinder and compacts the powder while start measuring the distance needed to reach a predefined pressure. The procedure is repeated with the existence of the sample where the ram reaches the predefined pressure in shorter distance. The volume is calculated and by incorporating the oven dry weight of the sample the particle density is calculated. Then the porosity can be calculated. The measurements accuracy is 0.03% (Micromeritics, 2012).

2.6.2. Results

The results are given in Table 9 analog with other calculated parameters. Most of the values result from measurements performed for this study. The resulting bulk values of thermal conductivity and specific heat capacity are calculated as linear average with respect to the

porosity, using either the standard properties of water or, in the upper unsaturated part of the model, the respective values for air (Diersch, et al., 2011a). In this part of the model thermal conductivity of air which averages 0.025 $W \cdot m^{-1} \cdot K^{-1}$ were used in the this part of the model instead of water. Here an assumption was used stated that all pores in this zone were filled by air. Despite that the solid material in this zone (soil and rocks) is the main heat conductor, the air play an important role in the reservoir thermal characterization (model setup illustrated in section 3.3). In addition, basalts properties for each sub-flow were measured individually in detail (Fig. 21) and the results were implemented in the model. As the reservoir is composed of four lithologic units each unit thermophysical properties has to be included in order to characterize the whole reservoir in the FEFLOW model.

Table 9: Lithology, hydraulic and thermophysical properties of the modeled units.

Unit	Stratigraphic Unit	Lithology	Thermal Conductivity ($W \cdot m^{-1} \cdot K^{-1}$)	Specific Heat Capacity ($J \cdot kg^{-1} \cdot K^{-1}$)	Porosity (-)	Density ($kg \cdot m^{-3}$)	Hydraulic Conductivity ($m \cdot s^{-1}$)
1	Quaternary	Sediments (Silt, Sand & Gravel)	0.58±0.21	800±120	0.35 ±0.02	1,420 ±230	$*5.8 \cdot 10^{-7}$
2	Tertiary	Basalt	1.65±0.19	860±100	0.10 ±0.01	2,777 ±670	$4.0 \cdot 10^{-4}$
3	Late Cretaceous	Limestone	2.36±0.32	840±250	0.10 ±0.10	2,550 ±552	$*8.1 \cdot 10^{-5}$
4	Late Cretaceous	Marl	2.25±0.48	840±200	0.02 ±0.21	2,740 ±610	$*1.0 \cdot 10^{-9}$

*Al-Mahamid, 2005

The interrelation between measured; thermal conductivity, porosity, permeability and density (or calculated: thermal diffusivity and specific heat capacity) properties for the studied basalts flows are illustrated in Fig. 21 . Here, it is evident that there is no obvious correlation between thermal conductivity and porosity while a clear correlation was found between thermal conductivity and permeability for the investigated basalt sub-flows. In order to characterize this basalt from thermophysical point of view this interrelation will be discussed in details later in this research.

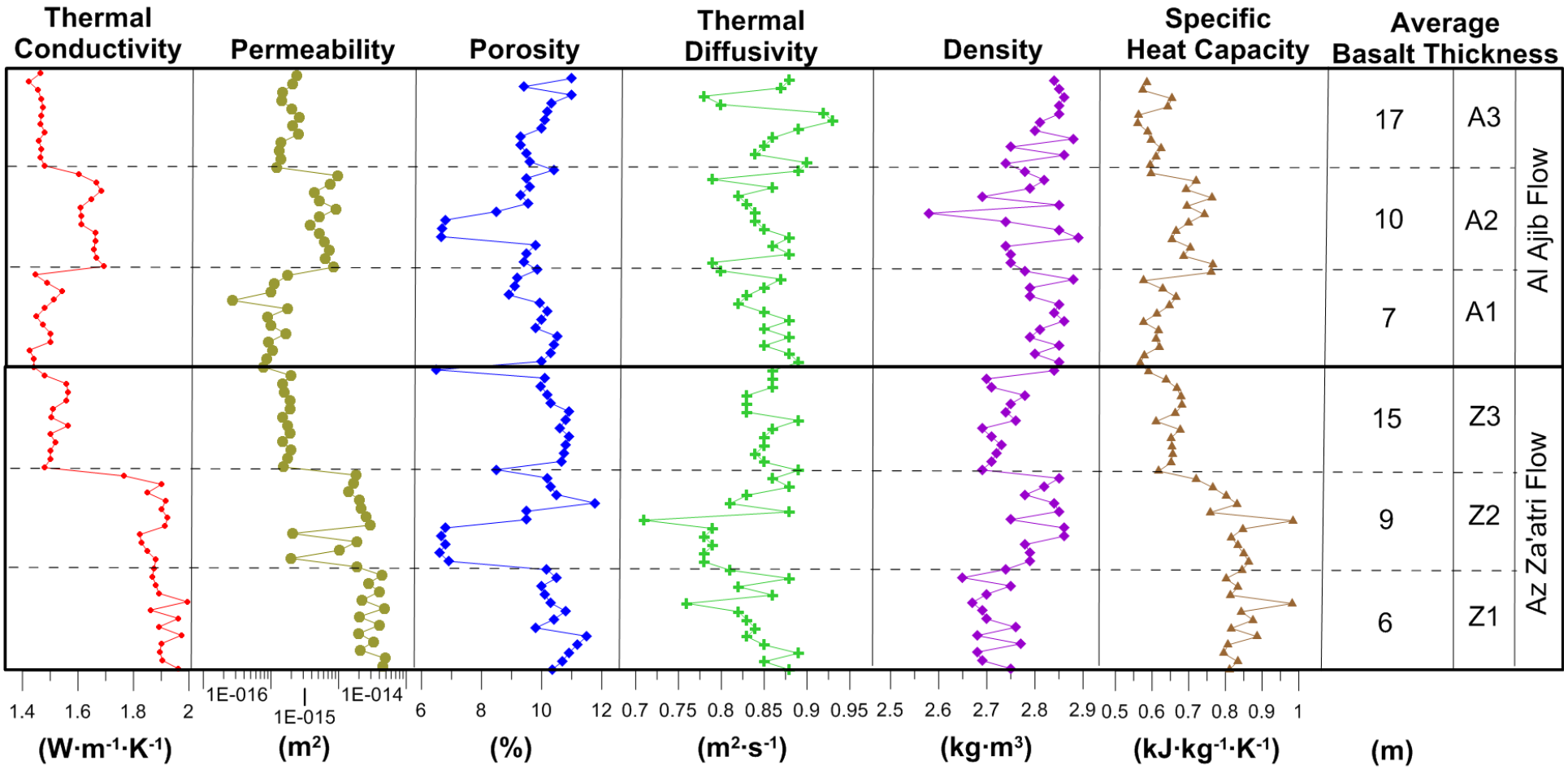

Figure 21: Thermophysical properties of studied basalt flows, n = 12 for each subflow.

The average thermophysical property values which illustrated in Figure 21 above with the calculated (cubic law – Snow, 1965) hydraulic conductivity for Al Ajib (A1 – A3) and Az Za`tri (Z1 – Z3) sub-flows are listed below (Table 10). Z1 is the bottommost and A3 is the topmost flow.

The statistical analysis for the results was performed. Figure 22 shows the box-and-whisker diagram for the results. It is presented the graphically depicting groups of numerical data through their five-number summaries: the smallest observation (sample minimum), lower quartile (Q1), median (Q2), upper quartile (Q3), and largest observation (sample maximum) for each property measurements.

Table 10: Average thermophysical properties of basalts sub-flows (from bottom Z1 to top A3).

Basalt Flow	N	Thermal Conductivity ($W \cdot m^{-1} \cdot K^{-1}$)	Permeability (m^2)	Porosity (%)	Thermal Diffusivity ($m^2 \cdot s^{-1}$)	Density ($kg \cdot m^3$)	Specific Heat Capacity ($kJ \cdot kg^{-1} \cdot K^{-1}$)	Hydraulic Conductivity ($m \cdot s^{-1}$)
A3	12	1.46±0.02	$1.84 \cdot 10^{-15}$	10.4±0.6	0.86±0.04	2.82±0.05	0.60±0.03	$6.75 \cdot 10^{-4}$
A2	12	1.65±0.03	$6.52 \cdot 10^{-15}$	8.7±1.3	0.84±0.03	2.77±0.09	0.71±0.04	$2.39 \cdot 10^{-3}$
A1	12	1.48±0.04	$1.09 \cdot 10^{-15}$	10.3±1.1	0.85±0.02	2.83±0.03	0.61±0.03	$4.00 \cdot 10^{-4}$
Z3	12	1.52±0.03	$1.73 \cdot 10^{-15}$	10.8±0.7	0.85±0.02	2.72±0.03	0.66±0.02	$6.35 \cdot 10^{-4}$
Z2	12	1.87±0.05	$1.64 \cdot 10^{-14}$	9.5±1.9	0.81±0.05	2.81±0.04	0.82±0.07	$6.02 \cdot 10^{-3}$
Z1	12	1.92±0.04	$3.40 \cdot 10^{-14}$	10.7±0.5	0.84±0.04	2.71±0.04	0.85±0.05	$1.25 \cdot 10^{-2}$

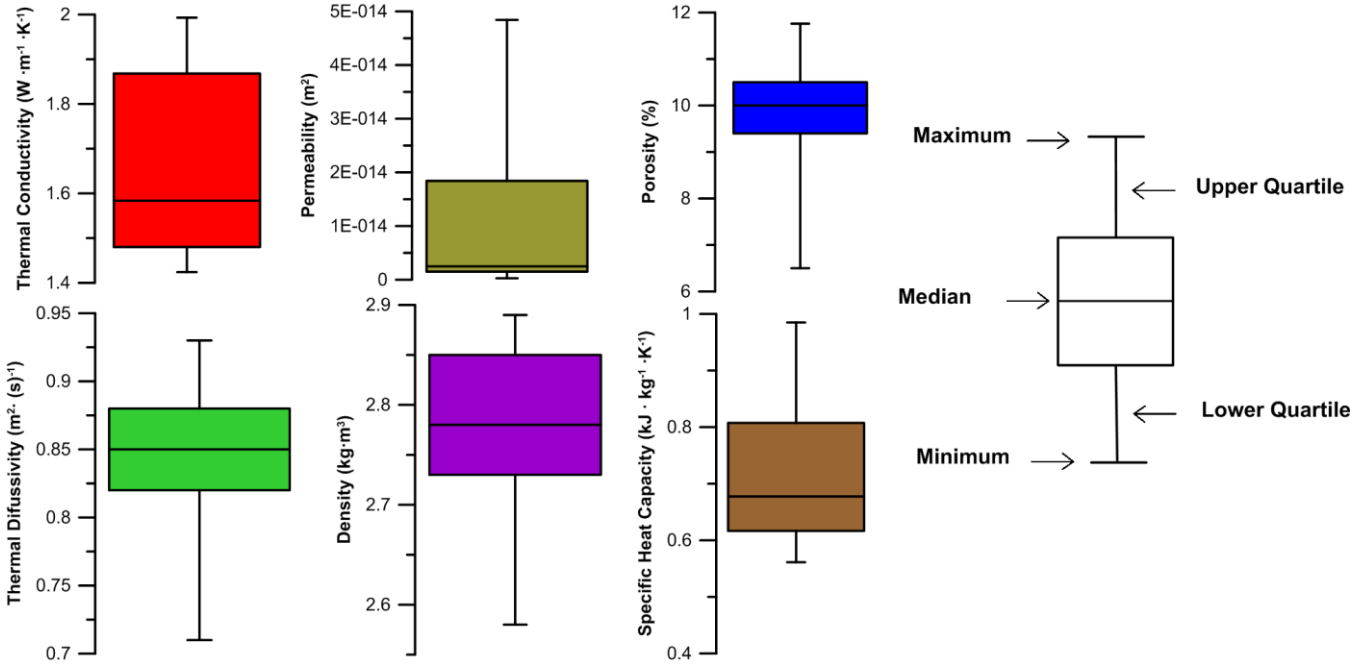

Figure 22: Box-and-whisker diagram for thermophysical properties of basalts.

2.6.3. Thermophysical Properties Interrelations of the studied basalts

Preface

This study introduces a new conceptual framework to predict the thermal conductivity of basalts based on their mineral composition. The developed arithmetic formula is applied to data from ongoing field and laboratory studies to verify whether it is a reliable method to predict geothermal reservoir thermal conductivity from mineral volume proportions. This formula can be applied during early exploration stages of the development of potential geothermal systems. The development of underground geothermal cooling systems is considered to be the most effective utilization strategy of geothermal energy in Jordan. Jordan has a strong interest in applying new and environmentally sustainable energy systems such as geothermal energy. Knowledge of thermal conductivity is an absolute necessity for the calculation of heat flow models (Sass et al., 1971). Permeability and thermal conductivity are the key parameters for characterizing any geothermal reservoir (Tester et al., 2005).

Yet, thermophysical properties and mineral-controlled parameters have not been investigated in the Jordanian Harrat basalts. Al-Malabeh et al. (2002) investigated the magnetization of the Jordanian Harrat basalts. He concluded that the magnetization of the evaluated basalts is directly controlled by the ferromagnetic minerals volume proportions.

The scientific motivation for this part of the study arises from the fact that the thermophysical properties should be determined in one comprehensible approach. A new geothermal petrophysical model, where parameters are dependent on mineral composition, may represent such an approach. In the early stages of exploration, where thermal conductivity data is not yet available, modal mineral composition analysis enables the determination of thermophysical rock properties through the presented correlation. If preliminary studies include detailed mineralogical analysis, the geothermal exploration concept becomes more precise and reliable. Investigations to predict thermal conductivity may offer cost-effective opportunities to gain data transferrable to geothermal systems of homogenous basalts at greater depths.

Correlation between thermal conductivity and permeability

Permeability and thermal conductivity are positively correlated over all investigated basaltic sub-flows (A1 – A3, Z1 – Z3) (Fig. 15). The core permeability which exceeds the average values in A1 and Z2 is probably caused by micro cracks. The porosity is presented in the correlation profile (Fig. 11) in order to evaluate its influence on thermal conductivity as well as on permeability. Thermal conductivity averages $1.65 \pm 0.03\ W \cdot m^{-1} \cdot K^{-1}$ and ranges from $1.43\ W \cdot m^{-1} \cdot K^{-1}$ to $1.98\ W \cdot m^{-1} \cdot K^{-1}$. Permeability averages $1.03 \cdot 10^{-14}\ m^2$ with minimum value of $6.52 \cdot 10^{-15}\ m^2$ and maximum value of $4.89 \cdot 10^{-14}\ m^2$. Porosity averages 10.2 % and rages from 6.6 – 12 %. No correlation was found between porosity and permeability or porosity and thermal conductivity. Figure 22 shows the box-and-whisker diagram for the results.

Permeability correlates log linear with the thermal conductivity (Fig. 23). Due to fractures in sub-flows A2 and Z1, the two sites exhibit the highest permeability of each flow. Similar to permeability, the thermal conductivity is also higher in both these sub-flows. Thermal conductivity values decrease in the Az Za`atri flow from bottom to top (Z1 > Z2 > Z3) and in Al Ajib (A2 > A1 > A3). A similar arrangement is defined by permeability which decreases from Z1, Z2 to Z3 and from A2, A3 to A1.

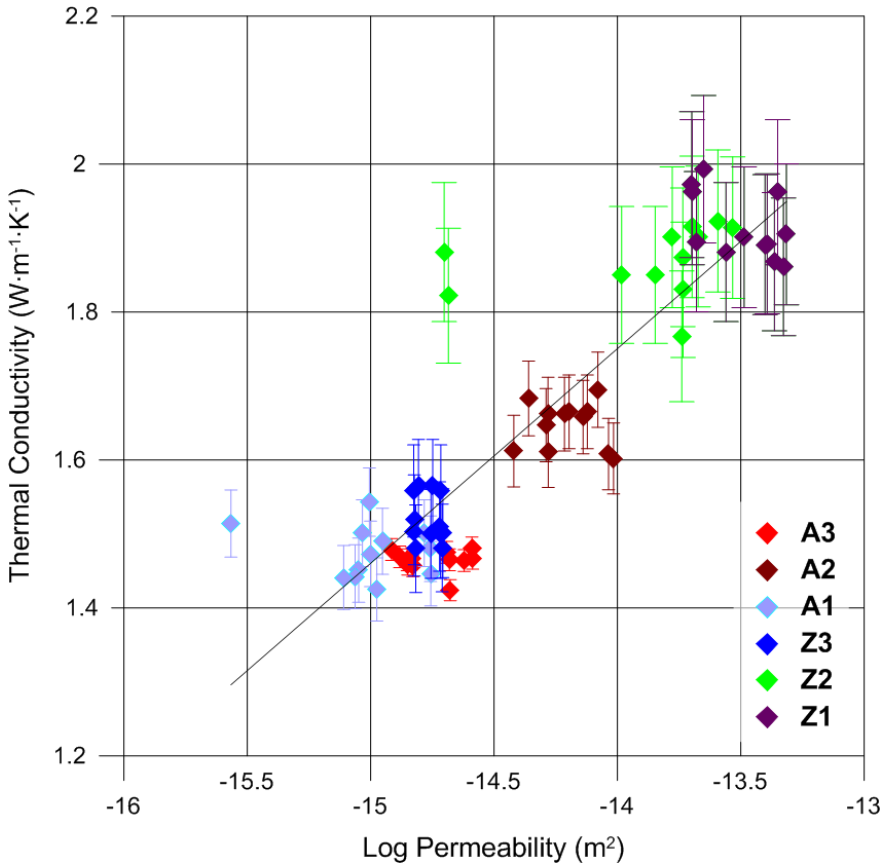

Figure 23: Thermal conductivity and permeability correlation showing the logarithm relationship expressed in Eq. 4

As shown in Fig. 23 a good correlation (correlation coefficient R^2 is 0.80) can be observed between thermal conductivity and logarithm of permeability. An arithmetic equation was developed expressing this correlation (Eq. 4). Where the ordinate is 5.8 (W m^{-1} K^{-1}) and the slope is 0.3.

$$\lambda = 0.3 \log k + 5.8 \quad (4)$$

Where;

λ : Thermal Conductivity, k : Permeability

Correlation between thermal conductivity and mineral volume proportions

Two widely accepted models; the geometric model (Sass et al., 1971) and the non - geometric model (Birch and Clark, 1940) were considered to predict thermal conductivity from all mineral proportions in the studied basalt.

Sass et al., (1971) model predicts thermal conductivity from all mineral institutions in the rock. This model assumes crystals orientation with respect to the heat flow direction during thermal conductivity measurement. This may be the most suitable model for basaltic flows if the crystals have their defined orientation in the texture. In contrast, Birch and Clark, (1940) non – geometric model is dealing with predicting thermal conductivity from those minerals which are randomly oriented in the rock. Neither the geometric model nor the non – geometric model could predict the thermal conductivity value from minerals constituents of the investigated basalts (Fig. 24).

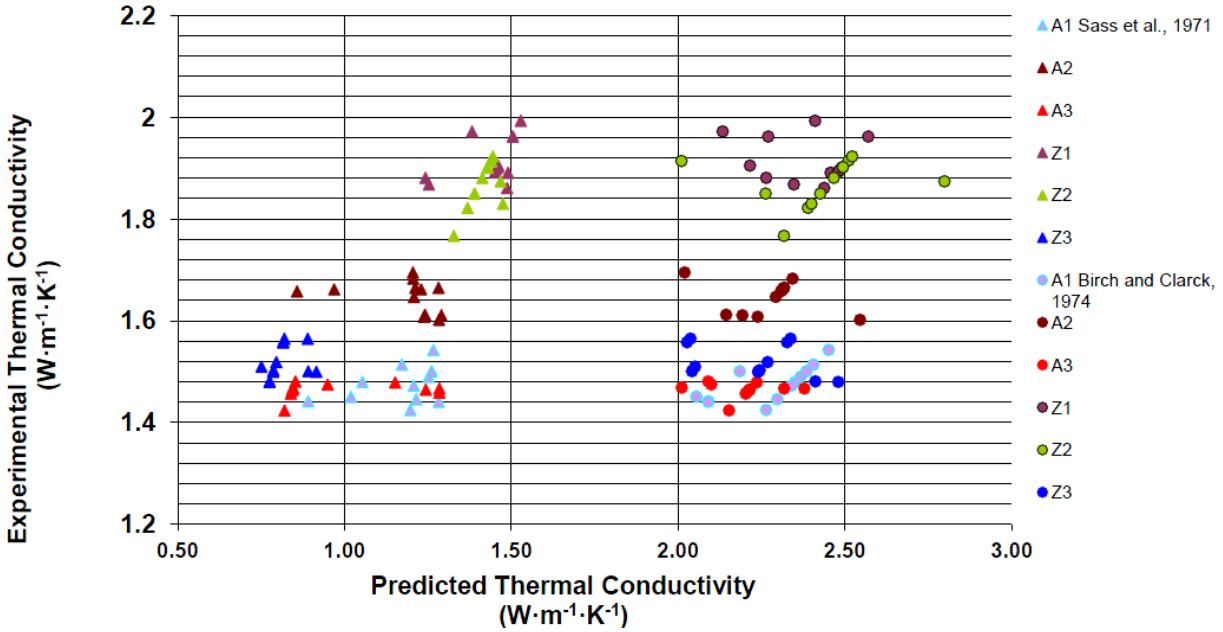

Figure 24: Experimental thermal conductivity versus predicted thermal conductivity using geometric and non- geometric models.

Here, more detailed investigation is needed. In the following, each mineral proportion is examined regarding its possible influence on thermal conductivity of the studied basalts. The results show only two main results; the most abundant mineral: plagioclase and the most influenced minerals; ferromagnetic and opaque minerals.

The correlation between plagioclase, (the most abundant mineral), and thermal conductivity of the studied basalts is poor (Fig. 25). The coefficient of determination (R^2) is 0.03.

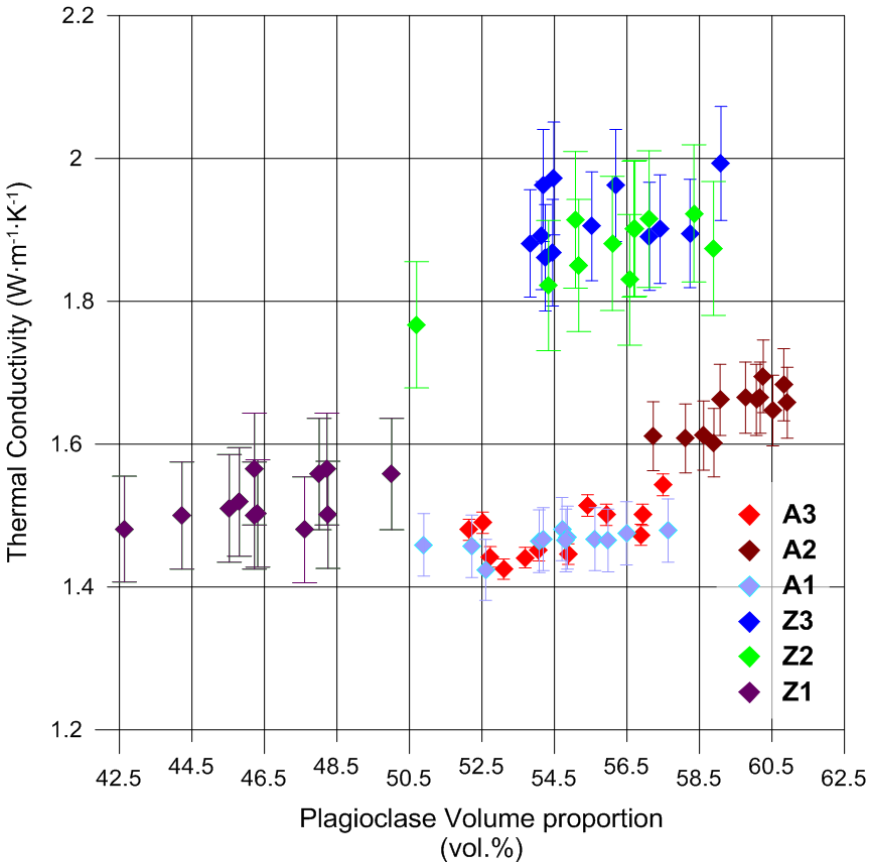

Figure 25: Correlation between thermal conductivity and plagioclase volume proportion.

Thermal conductivity and opaques with ferromagnetic minerals are positively correlated over all investigated basalts sub-flows (A1 – A3 and Z1 – Z3) (Fig. 26). It can be proved that the abundance of ferromagnetic minerals (olivine; $Fo_{85\text{-}90}$, pyroxene; enstatite, augite Fe, Mg- rich (ferroaugite) and opaque minerals mainly magnetite (Fe_3O_4)) directly controls thermal conductivity.

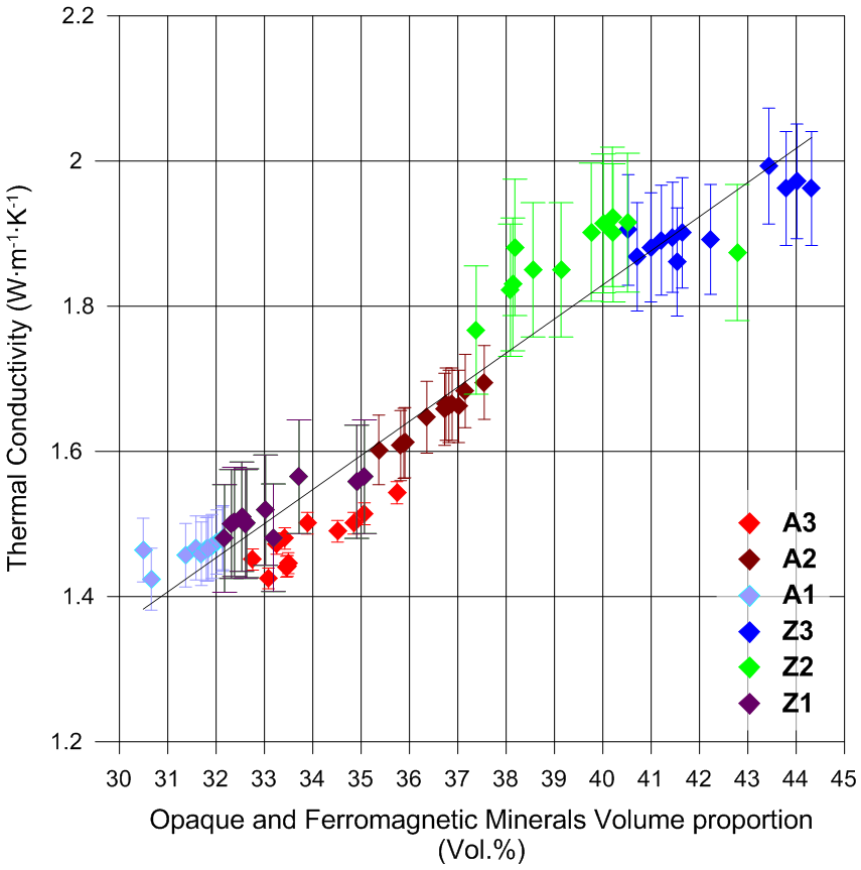

Figure 26: Correlation between thermal conductivity with opaque and ferromagnetic minerals.

This study derived an arithmetic function representing this interrelation (Eq. 5). This function is applicable for the Alkali flood basalts. The total opaques and ferromagnetic minerals in alkali basalts are >10% (Hughes, 1982). This function shows an acceptable coefficient of determination (R^2) of 0.92.

$$\lambda = 0.05 n_{OFM} - 0.06 \quad (5)$$

Where;

λ : Thermal conductivity and n_{OFM} : opaque and ferromagnetic minerals volume proportion.

This equation incorporates the proportion of minerals of iron and magnesium composition, whereas other rock-forming minerals are not included. This interrelation was previously presented by Al-Zyoud and Sass (2010). This is in accord with Robertson and Peck (1974), who found that the increase of the olivine mineral volume proportion in Hawaiian basaltic rocks leads to an increase of thermal conductivity.

In addition, thermal conductivity of continental basalt from Vogelsberg in eastern upper Hesse - Germany and oceanic basalt from Iceland were investigated into their influenced by mineral proportions. The results support (Fig. 27) the main conclusion of depending basalt's thermal conductivity on opaque and ferromagnetic mineral proportion. This is proven by the following functions correlate thermal conductivity with opaque and ferromagnetic mineral volume proportions under predefined uncertainties. The coefficient of determination (R^2) is 0.40 and 0.63 for German and Icelandic basalts respectively.

$$\lambda_G = 0.01 n_{OFM} - 0.88 \quad (6)$$

Where;

λ_G: Thermal conductivity of the German basalts and n_{OFM}: opaque and ferromagnetic minerals volume proportion.

$$\lambda_I = 0.03 n_{OFM} - 0.63 \quad (7)$$

Where;

λ_I: Thermal conductivity of the Icelandic basalt and n_{OFM}: opaque and ferromagnetic minerals volume proportion.

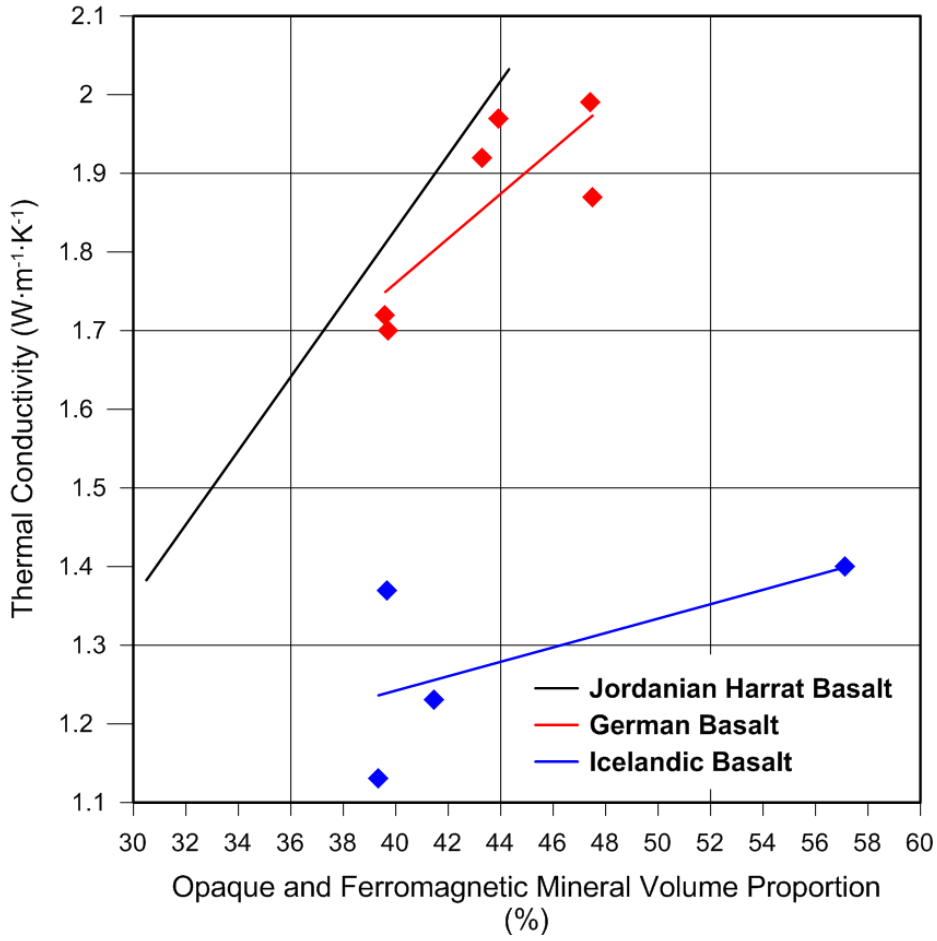

Figure 27: Correlation between thermal conductivity with opaque and ferromagnetic minerals for German, Icelandic and Jordanian basalts.

In Figure 27 a general trend of the continental basalt i.e.: the Jordanian Harrat and the German basalt can be observed. On the other hand, the other type of basalt which represents the oceanic genesis has another trend in a different zone in this chart. This method could be a prospective approach for predicting thermal conductivity from some mineral phases presented in the basalts parallel with the rock genesis.

Porosity, permeability and thermal conductivity relationships

The permeability of the basalts as crystalline rock is largely fracture-controlled (Clauser, 1992). Thermal conductivity of the crystalline rocks depends on the crystal type, crystal geometry and size (Jessop, 2008).

Thermal conductivity it is independent of porosity (for vesicular basalt), if the porosity is less than 35 % (Petrunin et al., 2001). It can be seen obviously that there is no correlation between porosity and thermal conductivity as well as porosity with permeability (Fig. 21) for the studied basalts.

The reported basalt values for thermal conductivity and permeability are within the range typical for basalts (Clauser, 1992; Pasquale et al., 1997; Iturrino et al., 2000; Petrunin et al., 2001). The correlated measurements of thermal conductivity and permeability, which results the logarithmic proportionality of the two properties (Eq. 4), are grouped according to their petrographic characteristics as in Fig. 28. This helps to interpret the relationship between thermal conductivity and permeability as well as the mineral composition. Micro-fractures, crystals size, crystal alteration as well as crystal shape control both permeability and thermal conductivity. The studied basaltic mineral composition is microscopically isotropic and homogeneous (Table 1 & Fig. 6). Thus, the variability of the permeability cannot be related to the mineralogical properties, but must be caused by structural heterogeneities of the samples. In addition to the factors mentioned above, crystal imperfections significantly decrease the thermal conductivity of the materials; minerals themselves have unique thermal conductivity, they make-up the material that then has a conductivity dependent upon mineral properties (Clauser and Huenges, 1995).

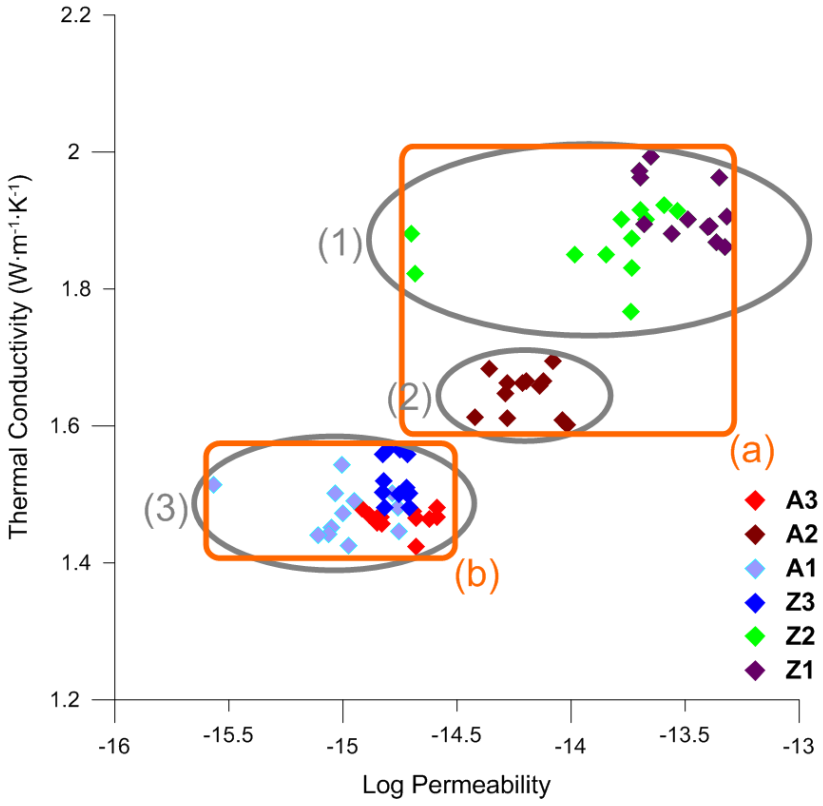

Figure 28: Classification of basalts according to the crystals size (1, 2 and 3) and micro-fractures (a and b). Error bars are in Fig.6.

The highest values of permeability and thermal conductivity occur in flow Z1 and Z2 (group 1 in Fig. 28) which contain some large pyroxene crystals (>3 mm) with a high proportion of olivine in the groundmass. While the lowest permeability and thermal conductivity occurs in A1, A3 and Z3 (group 3) where the grain size of pyroxene is the smallest (<1 mm) and olivine proportion in the groundmass is the lowest. A2 exhibits moderate values for permeability and thermal conductivity with pyroxene crystal size ranging between 1 and 3 mm. In addition, the size of plagioclase crystals ranges from ground mass size (0.1 – 0.5 mm) in A2, Z1 and Z2 (group a in Fig. 28) to large phenocrysts (> 1 mm) in the other flows (group b). In order to determine the influence of crystal size distribution on thermal conductivity more precisely, further research will be necessary (Jessob, 2008).
The basalts of flow A2 (group 2) are the most recent and contain the highest percentage of euhedral pyroxene and olivine crystals. Most opaque minerals in this flow show a rod or quadratic euhedral shape. Z1 and Z2 are the second most recent (least altered) with holocrystalline porphyritic texture; a porphyritic rock texture with a holocrystalline groundmass consisting entirely a crystallized minerals group. While the third group comprising A1, A3 and Z3 show high proportion of secondary (alteration) minerals. This crystals freshness increases the influence on thermal conductivity (Clauser and Huenges, 1995).

Slight differences were observed regarding fracture microstructure and vesicle shape within the same group. The flows grouped by fracture density: (a) Z1, Z2 and A2 show relatively highly fractured pyroxene and olivine, and group (b) A1, A3 and Z3 show slight to moderate fractures in pyroxene crystals (Fig. 8). Horai (1991) stated that randomly oriented micro-cracks increase the sample's anisotropic thermal conductivity. Even if few micro-cracks exist, they can have an insulating effect. Due to the effects of all these factors, thermal conductivity cannot be precisely calculated from permeability without considering these factors.

Here, a more reliable prediction method was developed. It can be concluded that the thermal conductivity is directly proportional to opaque and ferromagnetic mineral volume proportions (Fig. 26 & Eq. 5). Thus, this equation supports the assumption that thermal conductivity of basalt dependence on mineral composition particularly with respect to the proportion of opaque and ferromagnetic minerals. This can be proved by the previous classification of the studied flows into three groups (1), (2) and (3) (Fig. 28) according to pyroxene and olivine abundance.

Other parameters such as crystal boundaries, spacing and contact type should also be taken into account. Undoubtedly, these parameters play an important role in controlling thermal conductivity of the basalts (Petrunin et al., 2001; Jessop, 2008). However, at this stage, the evaluation of the influence of these parameters cannot be performed precisely, and therefore presents a need for further investigation.

Outlook

Thermal conductivity prediction from mineral proportions has become an additional tool for reservoir exploration methods that produces conservative results. The presented data (thermal conductivity, permeability and mineral composition) allows us to propose a concept for predicting thermal conductivity. The reservoir thermophysical parameters are strongly influenced by the opaque and ferromagnetic minerals volume proportion and thus, define the performance of geothermal cooling reservoir storage. Ultimately, the reservoir mineralogy influences geothermal field development and applied technology. Ongoing investigations

include efforts to characterize mineral parageneses based on crystal boundaries, contacts and spacing and resulting influence on the thermophysical reservoir properties. First results indicate that the type of crystal contacts, seem to be of similar importance as mineral proportion.

2.7. Hydrogeology

Amman Zarqa basin is the most exploited watershed in Jordan. The three main aquifers in the Amman Zarqa Basin are formed by (1) a basaltic eruption at the top of (2) a fractured and karstified limestone aquifer in the middle and (3) a sandstone aquifer at the bottom. The Jordanian part of the Amman Zarqa Basin covers an area of 3,918 km^2; 431 km^2 lie in Syria (Al Mahamid, 2005). This basin represents a transitional area between the western hills and the eastern desert. The climatological conditions change from humid to arid leading to different land use patterns. The western hilly areas are relatively densely populated whereas the southeastern areas are deserts and almost without population. More than 60 % of the population of Jordan lives inside the basin (Department of Statistics, 2010). In the areas of upper Zarqa, Baqa`a, Dhulail and Jerash the groundwater is mainly utilized for irrigation (Al-Mashagbah, 2010).

Groundwater from the Amman recharge mound flows in four directions. A flow component is directed north-eastwards down the Amman-Zarqa Syncline to discharge into the upper Wadi Zarqa Valley. The second component is directed westwards and gives rise to Wadi Sir springs. The third component is directed southwards to contribute to the base flow of Wadi Mujib and Wadi Zarqa Ma'in. The fourth component is directed eastwards into the Azraq Basin. In the Qihati fault, the maximum displacement is about 300 meters, which places the impermeable Muwaqqar aquitard against the B2/A7 aquifer. This forms a groundwater barrier, which separates water discharging to the upper Wadi Zarqa Valley from groundwater flowing to the Azraq Basin. (Ministry of Water and Irrigation, 2000).

The main layers of the studied reservoir are represented by the basaltic eruption on top of the fractured limestone succession. Limestone and basalts are hydraulically connected, representing a fractured aquifer (Fig. 5). They are underlain by a marl formation. The mean hydraulic conductivity of the limestone, based on pumping tests, is $8.1 \cdot 10^{-5}$ $m \cdot s^{-1}$ (Al Mahamid, 2005). The limestone formation, called Amman – Wadi As Sir (local nomenclature is B2/A7), is the most important aquifer in the basin. It has a large and continuous extend together with high hydraulic conductivity. It is considered as the main source of groundwater for domestic use as well as for irrigation. The high hydraulic conductivity of the studied reservoir is a result of the basalt's lithology; 12% porosity along with the structural patterns of micro- and macro-fractures. The uppermost basaltic aquifer is formed by highly vesicular and fractured lava flows. The mean hydraulic conductivity of the basalts is good and ranges around $4 \cdot 10^{-4}$ $m\ s^{-1}$. The drainage system is affected by morphological rises and lava flows depressions. It is of moderate relief (Al-Mashagbah, 2010). The wadies drain south and southwest. The most western wadis in the study area which are used as discharge of groundwater have been straightened for drainage purposes (Al-Mashagbah, 2010).

Based on pumping tests, transmissivity values obtained through pumping tests range from $5.0 \cdot 10^{-5}$ to $3.4 \cdot 10^{-1}$ $m^2 \cdot s^{-1}$, with an average of about $8 \cdot 10^{-2}$ $m^2\ s^{-1}$, corresponding to a mean hydraulic conductivity of $2.3 \cdot 10^{-4}$ $m \cdot s^{-1}$. The transmissivity of the limestone aquifer (B2/A7) aquifer varies between $5.4 \cdot 10^{-5}$ and $2.5 \cdot 10^{-2}$ $m^2 \cdot s^{-1}$, where the average is about $5 \cdot 10^{-3} \cdot m^2 \cdot s^{-1}$, corresponding to a mean hydraulic conductivity of $8.1 \cdot 10^{-5}$ $m \cdot s^{-1}$ (Al Mahamid, 2005).

In general the water level is declining in almost all wells in the basin. Ministry of Water and Irrigation (2000) reported that the decline in water level of the limestone aquifer, the local name of this formation is Belqa 2 / Ajloun 7 (B2/A7), ranges between 0.67 m and 2.0 m per

year. Al Mahamid (2005) predicted that the maximum accumulative drawdown will reach more than 70 m by the year 2025. He predicts that some wells between Al Khalidiyya and Umm Al Jimal - located in the center of the basin - will completely dry out. Margane et al. (2002) reported too, that the exploitation of the limestone aquifer (A7/B2) has increased over the past decade, so that water levels are rapidly declining at about 2 m a^{-1}. The results presented in this study are in good agreement with previously published data (Margane, et al., 2002; Al Mahamid, 2005; El-Naqa, et al., 2007; Salameh, 2008; Al-Zyoud, et al., 2012a).

In the present study recent data shows that groundwater levels are continuously declining in the upper basaltic aquifer of the Amman Zarqa basin. More than 1000 groundwater wells were in operation by the end of 2010 in the study area (Ministry of Water and Irrigation, 2010). Excessive groundwater extraction was developed during the last decades. Very limited data of relevant monitoring wells is available. Eight monitoring wells which have a complete water level record (Ministry of Water and Irrigation, 2010) of the last decades (Table 11) were selected (Figure 29).

Table 11: Groundwater drawdown in the studied wells

Well Name	Total Cumulative Drawdown (m)	Well Observation Time Span	Total Time (a)	Mean Annual Drawdown From 2001 Till 2011 (m)
AL 1041	35.60	09.1968 – 01.2008	40.02	0.89
AL 1040	21.42	05.1968 – 04.2010	42.03	0.51
AL 1043	23.52	06.1968 – 04.2010	42.03	0.56
AL 1926	36.24	08.1986 – 04.2010	24.01	1.51
AL 2698	18.05	01.1991 – 04.2010	19.02	0.95
AL 3384	11.44	06.1997 – 04.2010	13.00	0.88
AL 1022	5.10	02.1998 – 09.2004	06.02	0.85
AL 3387	4.32	06.2001 – 04.2010	09.00	0.48

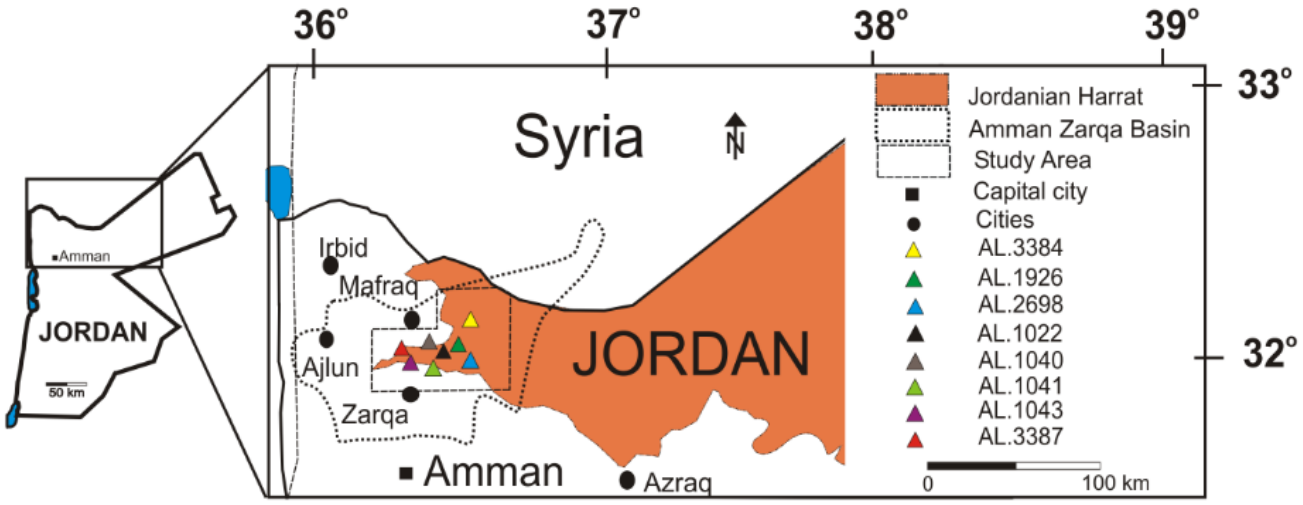

Figure 29: A simplified location map of Jordan showing the studied wells (colored triangles).

Six wells scattered through the Jordanian area previously studied into their groundwater overexploitation (Salameh, 2008). He reported the same decreasing trend in these selected

wells outside the study area. Figure 30 shows the hydrographs for each of the eight monitoring wells records adopted by this study for drawdown analysis.

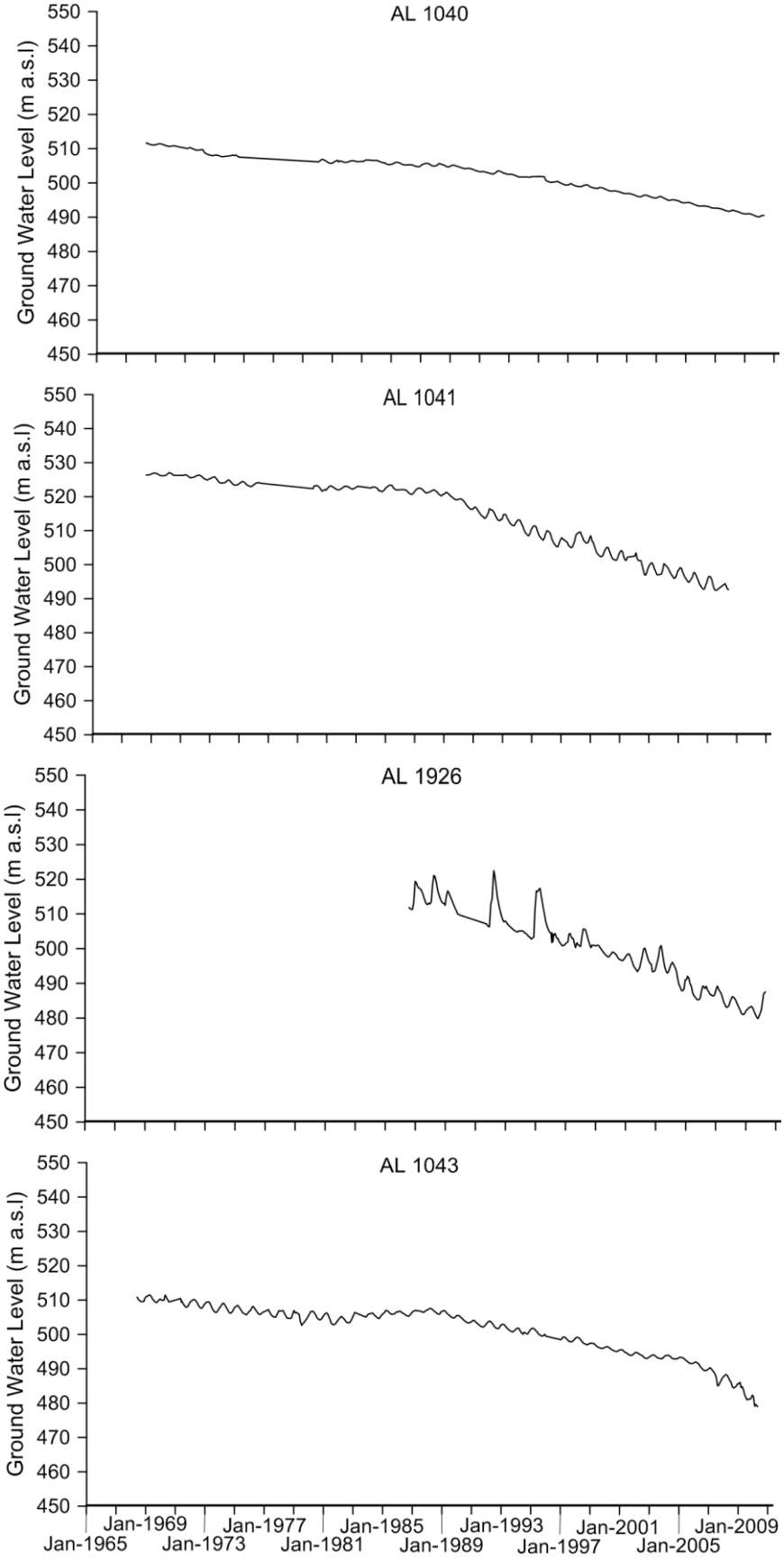

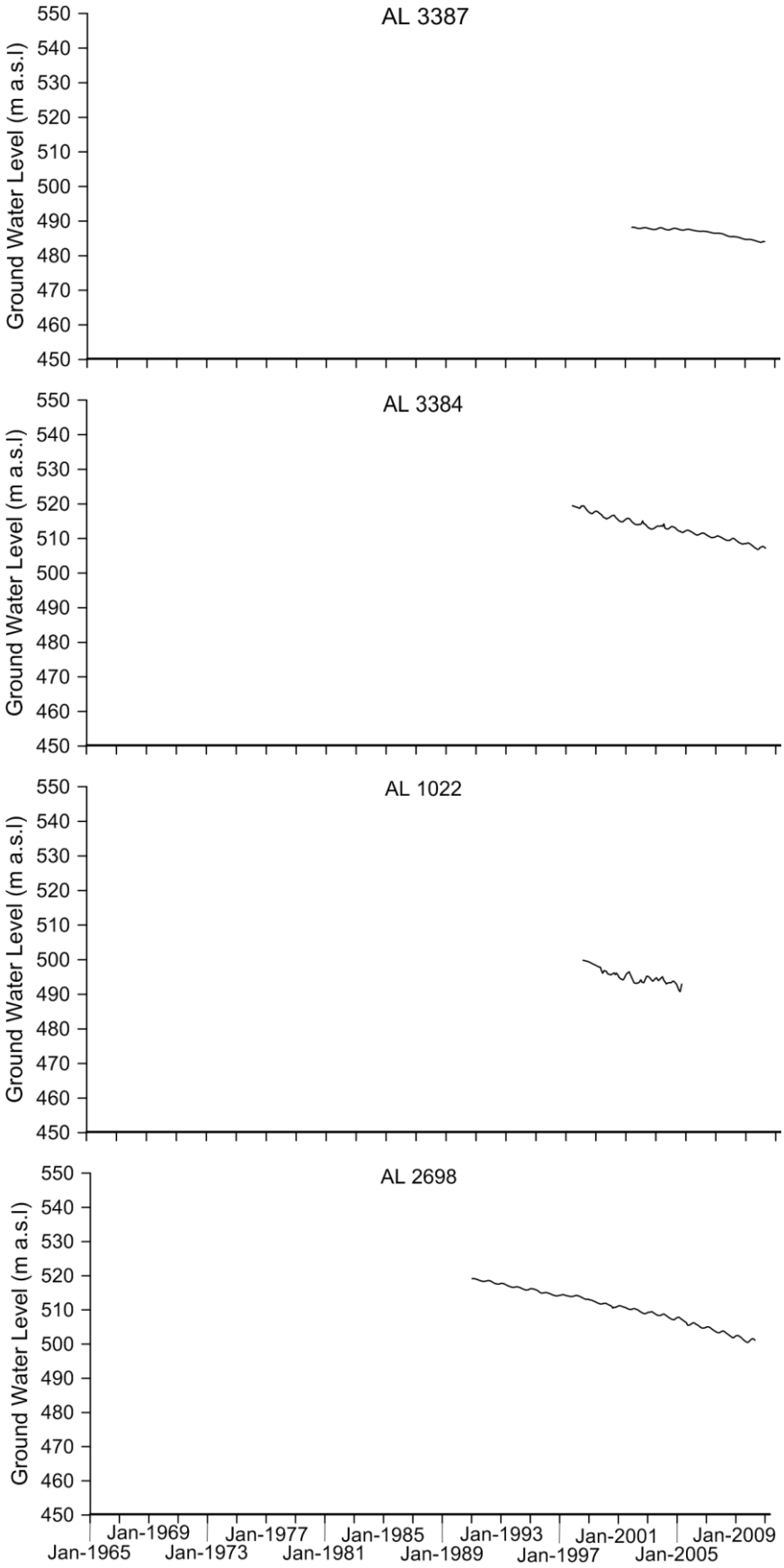

Figure 30: Groundwater level drawdown in the studied. Wells locations are indicated in Fig.19.

The ground water level decline begins at the time where extraction commences until recent years or up to the present. The average drawdown was calculated to be 1.10 $m \cdot a^{-1}$ in the last 10 years (Fig. 31).

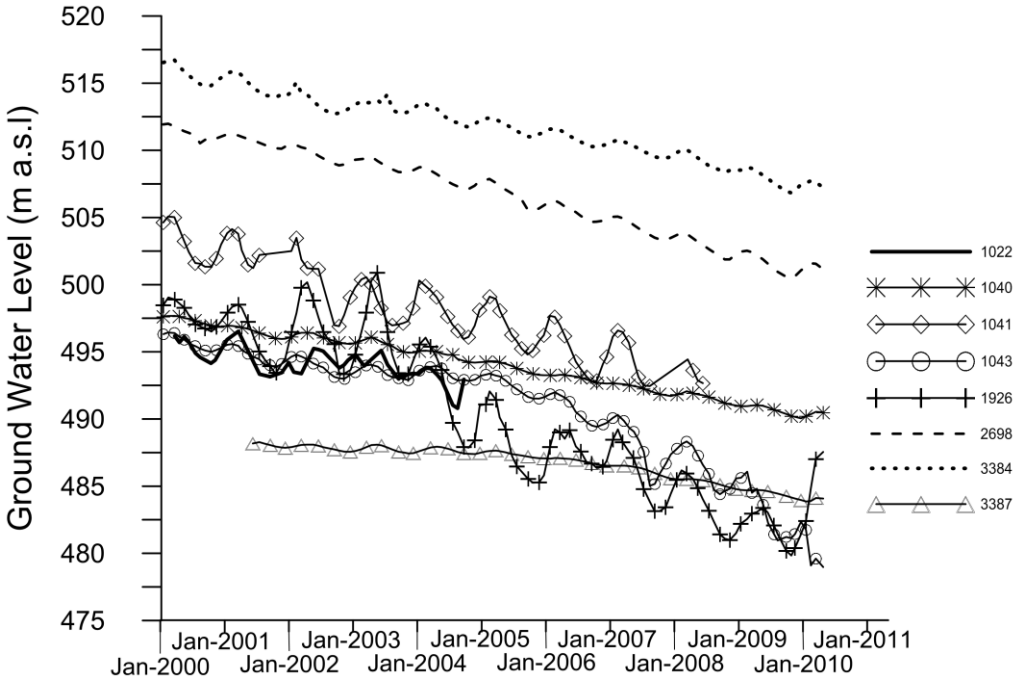

Figure 31: Groundwater drawdown in all studied wells during the last 10 years until April 2010.

In the report by the Ministry of Water and Irrigation (Ministry of Water and Irrigation, 2000) it is shown that since the early 1960s the groundwater levels in the basin are declining. Each well shown in Figure 29 shows a distinct water level decline.

According to (Al Mahamid, 2005) recharge from rainfall is approximately $45 \cdot 10^6$ m^3 a^{-1} and approximately $62 \cdot 10^6$ m^3 a^{-1} from lateral subsurface inflow. Accordingly the outflow is in the order of 66 • 10^6 m^3 a^{-1} into Azraq Basin and 3.4·106 m^3 a^{-1} into Yarmouk Basin. The leakage into the lower aquifer is about $12 \cdot 10^6$ $m^3 \cdot a^{-1}$. In the Mafraq and Dhuleil – Hallabat area in of the Amman Zarqa basin it was proven that the groundwater flows laterally and vertically from the basalts to the lower Amman Wadi Sir limestone (Abu Sharar & Rimawi, 1993). In addition there is an amount of $27 \cdot 10^6$ m^3 a^{-1} flowing towards the Zarqa River (Al Mahamid, 2005).

The average drawdown observed at the studied wells of 1.10 m a^{-1} over the last 10 years should not be considered as the representative trend for all of the Amman Zarqa Basin, because they are concentrated in the central basin (Fig. 29). Furthermore the hydrogeological setting within the Amman Zarqa Basin is complex due to numerous large fault and fold systems. Therefore, this trend may be considered as local drawdown around the studied wells and not regional representative to the whole basin.

According to Al-Mashagbah, (2010) the groundwater is suitable for drinking and agriculture. He proved that the majority of the groundwater sources in the study area belong to Ca-Mg-Na-Cl hydrochemical type. According to Schöller diagrams is the presence of (Mg^{+2} – Ca^{+2} – Cl^{-1}) water type, where the lines combining the anions and cations are approximately parallel

which indicates the same water origin. A Piper diagram (Fig. 32) characterizes the same groundwater hydrochemistry.

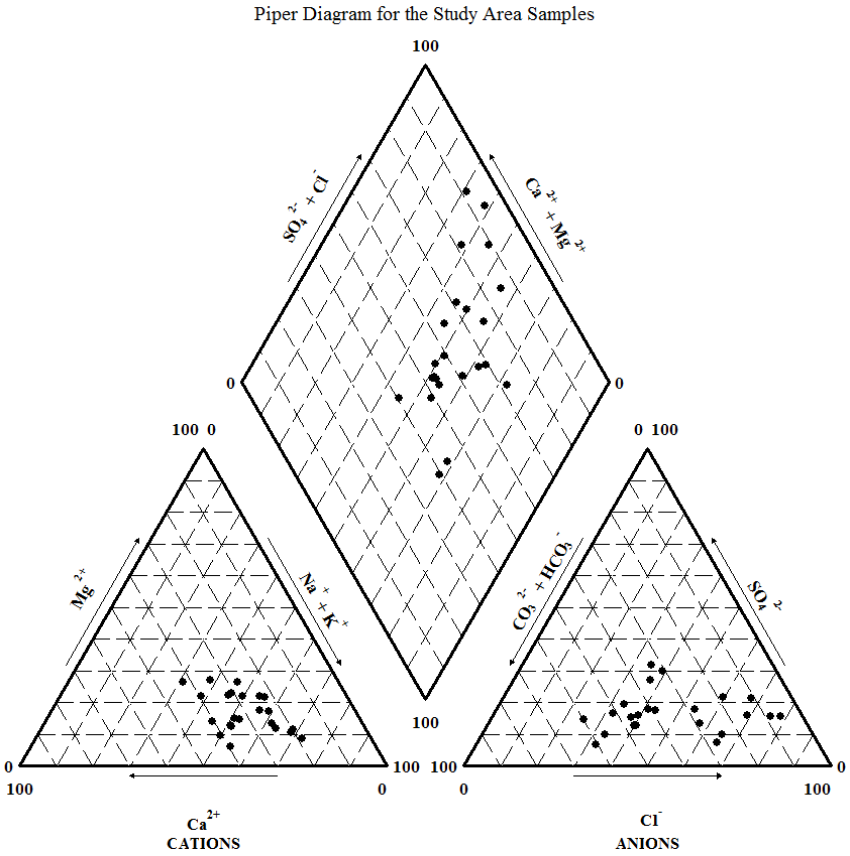

Figure 32: Piper Diagram after Al-Mashagbah (2010).

In addition, Salameh (2008) stated that the major Jordan basins may have become beyond repair. In any case groundwater extraction should be limited to yield the remaining groundwater resources of the basin. Measures have to be taken to guarantee the future generations access to enough water resources.

This reservoir will be used as a geothermal cooling storage. Due to heat sink negative effects on the groundwater is expected. These effects which caused by warming, e.g. chemical and microbiological changes are not discussed in this work. The groundwater is subjected to temperature and pressure changes which may modify its physicochemical properties and microbiological characteristics. These changes could lead to reactions which are not desirable in a geothermal reservoir. However, these parameters have to be examined thoroughly before starting such a geothermal application in order to avoid negative impacts on this most important resource.

The ongoing groundwater extraction, predominantly for irrigation, may also lead to conflicts with possible energy applications in this aquifer system. Groundwater management in the Amman Zarqa Basin presents a challenge for the water managers and experts at the responsible authorities. To preserve the groundwater resource for future generations all factors contributing to groundwater depletion have to be studied carefully. The urgency to implement mitigating measures is again proven by this study which should be understood as a part within a framework of national and international investigations.

3. 3D - Numerical Model for the Prospective Geothermal Reservoir and Geothermal System Design

To evaluate the applicability and effectiveness of a geothermal cooling system using different well array configurations, a numerical computation of the long term heat-transport in the subsurface is necessary.

3.1. Cooling Applications

Four different cooling applications are discussed in the following chapter. They are intended to provide cooling for the Al Hussein Thermal Power Station, the Hashemite University, 100 residential houses in Al Hashimiyya City and the Jordan Petroleum Refinery (Fig. 33). The 100 residential houses were chosen as a representative sample of 170,000 homes dispersed in six conurbation areas in the western part of the Jordanian Harrat basalts.

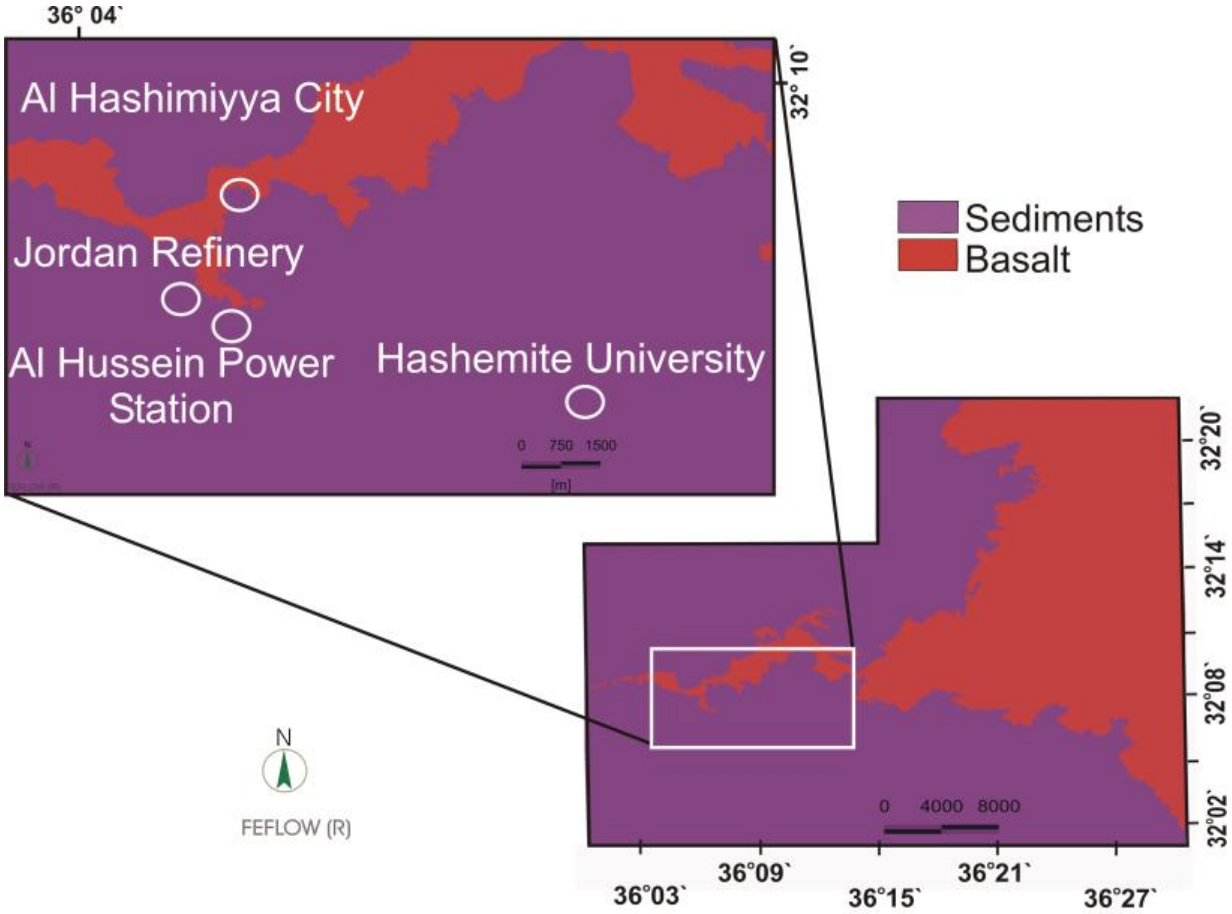

Figure 33: Location of the four scenarios within the model domain.

The amount of water necessary for cooling was calculated based on an approximated temperature spread between extraction and injection (Table 12).

Table 12: Cooling scenarios characteristics.

Nr.	Scenario	Temperature Difference (K)	Cooling Load (MW)	Groundwater Discharge ($m^3\ d^{-1}$)
(1)	Al Hussein Thermal Power Station	8	0.93	2,400
(2)	Hashemite University	9	2.50	1,900
(3)	Al Hashimiyya City (100 houses)	9	2.20	1,700
(4)	Jordan Petroleum Refinery	Dynamic (within 10)	Summer 1.745 Winter (a) 0.8725, (b) 0.582	Summer 3,600 / Winter 1,800

The resulting cooling load is calculated (Eq. 8) according to (Fuchs, 2010):

$$Q = (\rho c)_f \cdot (T_i - T_o) \cdot q \tag{8}$$

Where Q is the cooling load, $(\rho c)_f$ is the volumetric heat capacity of the extracted water, T_i is the injection water temperature – a constant boundary condition, T_o is the computed extraction water temperature and q is the pumping rate. Each scenario is computed for a time-span of 10 years.

3.2. Structural Model

Based on the lithological and additional structural geologic data from a borehole database (Ibrahim, 1993; Smadi, 2000; Abu Qudaira, 2004; Ministry of Water and Irrigation, 2010), including major faults, a structural 3D model was created with GOCAD® (Diersch, 2005). The model covers an area of about 1700 km^2. The generalized geological units are defined in Table 9 and Fig. 34.

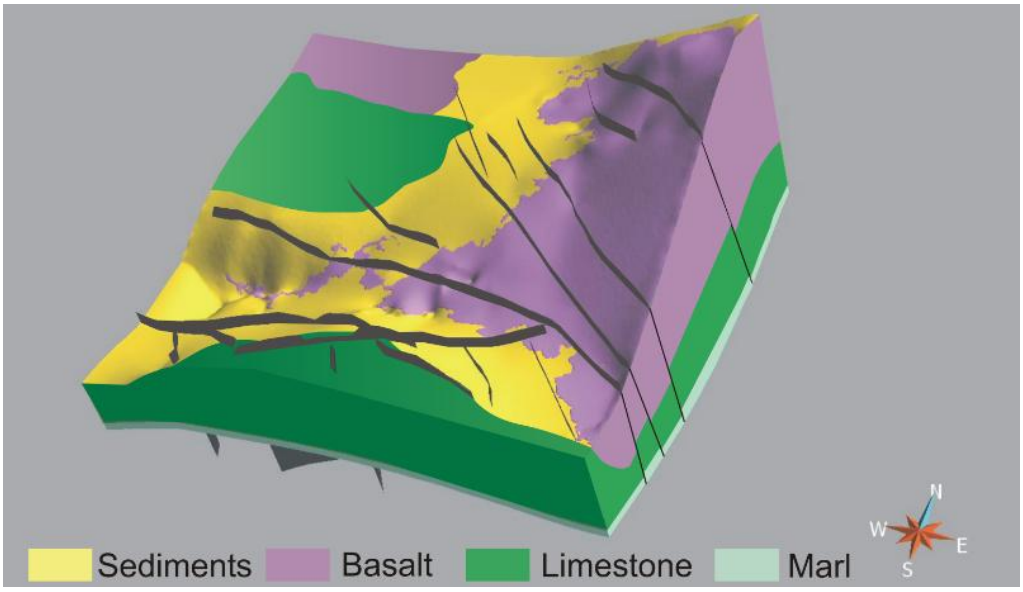

Figure 34: Structural 3D model created with GOCAD

3.3. Heat Transport Model

Based on the structural GOCAD® model a FEFLOW® 3D groundwater flow and heat transport model was created. It is composed of a set of 31 slices and around 1,000,000 nodes (Fig. 35).

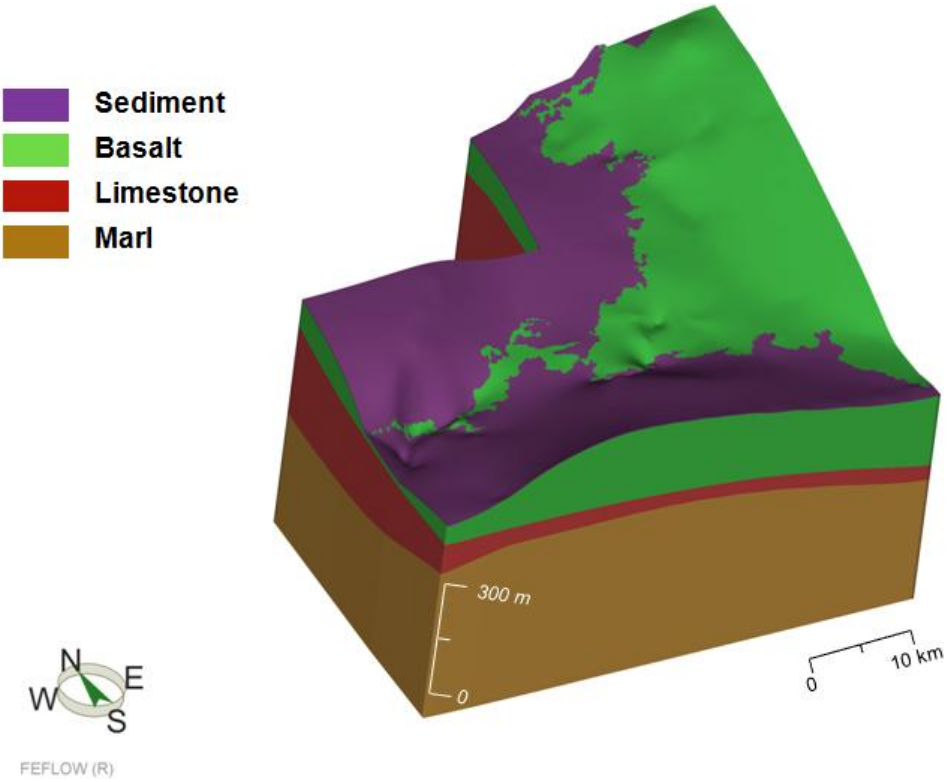

Figure 35: 3D GOCAD® model after implementation into FEFLOW®.

The calculation of the heat-transport in a porous media requires the solution of a set of continuity equations. The three-dimensional heat transport equation can be written as (Anderson, 2005);

$$(\rho c)_g \frac{\partial T}{\partial t} = \nabla \cdot \left(\mathrm{K}_e \nabla T - (\rho c)_f \, qT \right) + H \tag{9}$$

Where T is temperature, t is time (s), $(\rho c)_g$ is the bulk volumetric heat capacity of the rock; q is the seepage velocity (specific discharge vector), K_e is a term that includes the effective thermal conductivity of the saturated rock, ∇ is the Laplace operator, H summarizes heat sources.

In the following (Eq. 10) q is the specific discharge vector, given by Darcy's law

$$\mathbf{q} = -\mathbf{K}(\nabla h) \tag{10}$$

and the continuity equation in a saturated porous media (Bear, 1972);

$$S_0 \cdot \frac{\partial h}{\partial t} = \nabla \cdot \left(\mathbf{K} \nabla h \right) + W \tag{11}$$

Where S_0 is the saturation; h is the groundwater head; K is the hydraulic conductivity tensor; W is a source (sink) term. The equation for saturated porous media is adopted here to assess the vesicular effects which characterize the basaltic rocks. The fractures occurring in basaltic and limestone rocks are included in the model, by calculating the fractured hydraulic conductivity as follows (Snow, 1965):

$$K_{fr} = \frac{(2b)^2 \cdot \rho \cdot g}{12\mu} \tag{12}$$

Where K_{fr} is the fractured hydraulic conductivity, b is the aperture half width, ρ is the fluid density, g is the gravity acceleration and μ is the flow viscosity.

Temperature dependence of the fluid density and viscosity are neglected in this study. It must be noted that the temperature effects cause changes in hydraulic conductivity, $K\,(=k \cdot g \cdot \rho_w \cdot \mu_w^{-1})$ since density, ρ_w, and viscosity, μ_w, of water are temperature dependent. For example, the groundwater viscosity in winter is relatively high and the hydraulic conductivity is relatively low, this is evident by the cone of depression caused by pumping which is larger during winter months (Winslow, 1962). Consequently, Rorabaugh (1956) stated that the rates of infiltration may be comparable in winter and summer even though the gradients between the river and the aquifer are higher in winter. Diurnal fluctuating infiltration from a pond was observed by Jaynes (1990) with maximum infiltration occurring during the day and minimum infiltration occurring during the night.

The numerical model has the same geometry as the GOCAD® model. The uppermost sedimentary layer is laterally not continuous and exists only in some parts of the model region. However, FEFLOW® requires slices to be continuous. To meet this requirement the non-continuous slices are continued with a minimum thickness of 0.1 m while the assigned parameters are set according to the underlying unit.

3.4. Flow - Initial and Boundary Conditions

The availability of high quality hydrological data is limited (Ministry of Water and Irrigation, 2010). The data is extremely fluctuating over time due to the intense but also variable groundwater extraction. Therefore it is difficult to derive a realistic areal groundwater head distribution. Data sets beginning from the year 1965 were evaluated. For this study the data-set of the year 1998 was used as reference data, mainly because the highest number of measurements is available in 1998. In a first step the head values were gridded to the model area using the local polynomial filtering and interpolating approach of the software Surfer®. The resulting hydraulic head distribution (Fig. 36) is used in a FEFLOW® steady state flow model as initial and 1st kind boundary condition of the modeling area. The equilibrium head distribution achieved this way is then used for a transient model. Here, also average values of all known pumping activities are assigned to the specific nodes in the model area. This run was computed for a simulation period of 12 years, ending December 31, 2010.

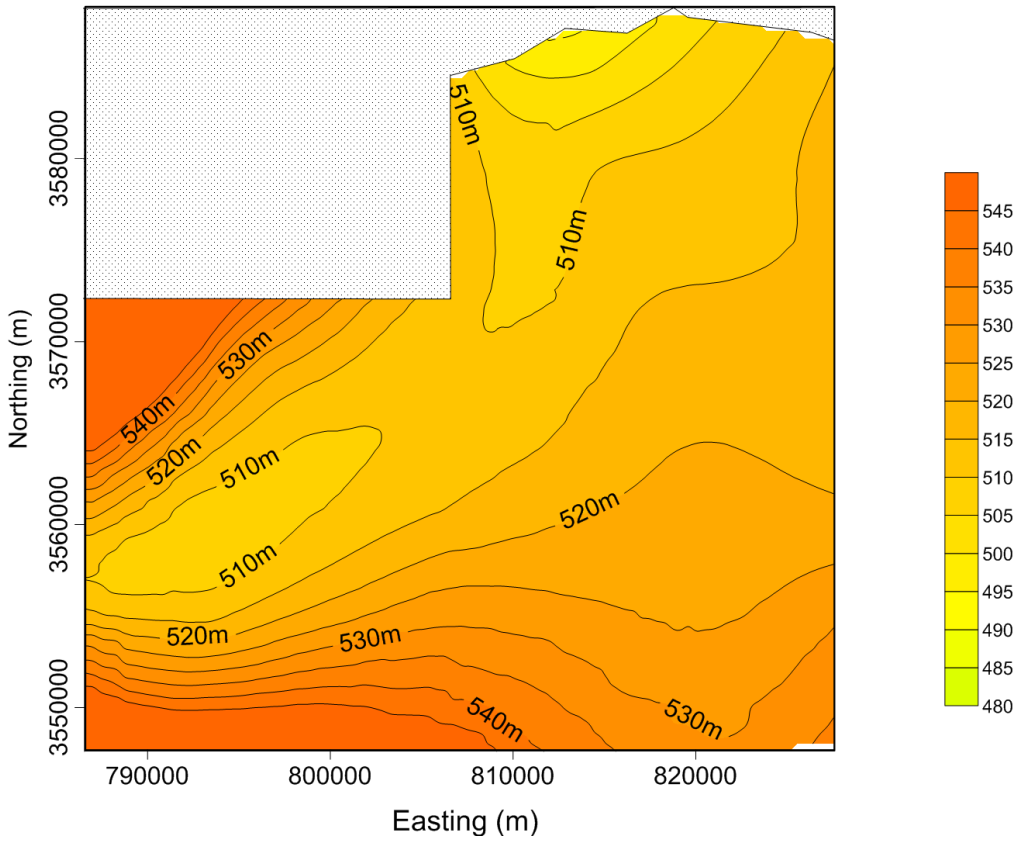

Figure 36: Hydraulic head distribution in the model area, used as initial condition and as boundary condition at the outer margins of the study area in the FEFLOW model. (Coordinates are given in UTM).

Eight monitoring wells with continuous records were selected to calibrate the model (Fig. 37). The model reflects the previously mentioned average drawdown rate of 1.1 m a^{-1} well, with acceptable differences between actual measured drawdown and the modeled drawdown (Table 13).

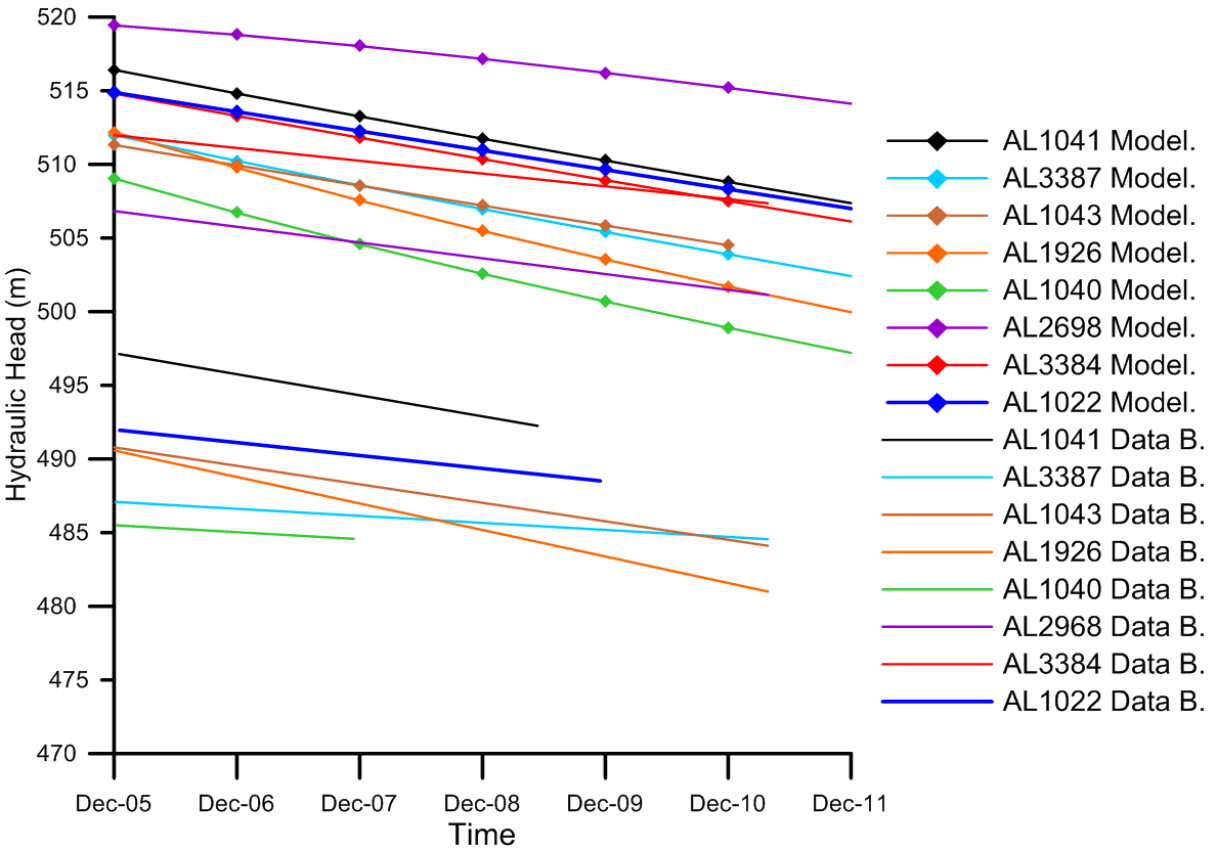

Figure 37: Hydraulic head at the monitoring wells based on data records (Data B.) compared with FEFLOW modeled hydraulic head at the same wells (Model.)

Table 13: The differences between modeled and measured drawdown at selected wells in the studied basin.

Well Name	Mean annual drawdown from 2001 till 2010 (m)	Modeled mean annual drawdown from Jan. 2001 to Dec. 2010 (m)
AL 1041	0.89	1.51
AL 1040	0.51	2.02
AL 1043	0.56	1.36
AL 1926	1.51	2.09
AL 2698	0.95	0.85
AL 3384	0.88	1.46
AL 1022	0.85	1.31
AL 3387	0.48	1.62

To achieve this it was necessary to transform the previous 1st kind boundary conditions to equivalent nodal sources (in FEFLOW® nomenclature "4th kind" boundary condition). The final initial head distribution of the model, representing December 31st, 2010, is shown in Fig. 38. All modeled cooling scenarios start in 2011 and run for 10 years.

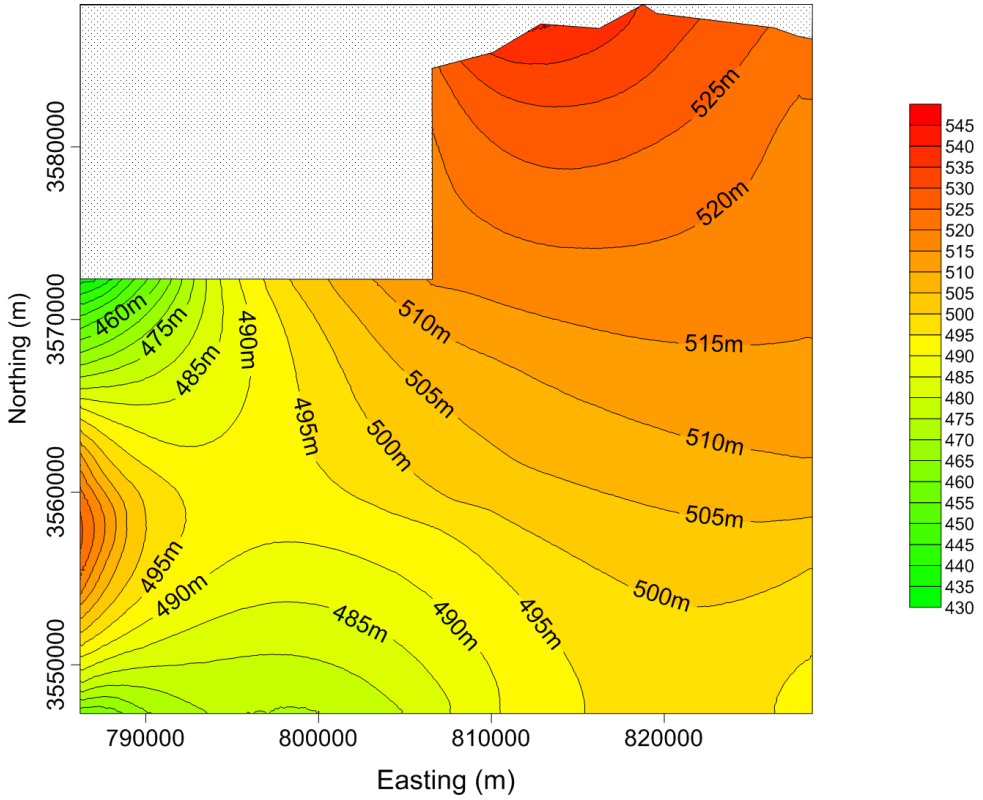

Figure 38: Final head distribution in the model area represents the head distribution in Dec. 31st, 2010 (Coordinates are given in UTM).

3.5. Heat - Initial and Boundary Conditions

Information about the subsurface temperature distribution in the study area is very limited. One survey was conducted in central Jordan (more than 150 km south west the study area) by Swarieh (2005). Thus, an initial quasi steady state temperature distribution was computed. For this computation a surface temperature of 19 °C was set as 1st kind boundary condition on top of the model. A basal heat flow rate of 95 m·W·m^{-2}, according to the global heat flow data base (Pollack, et al., 1993), set as 2nd kind boundary condition at the bottom of the model. The thermal conductivity of the subsurface is previously given in Table 4. To bring this temperature distribution into equilibrium with the pumping activities a transient heat transport model from 1998 till 2010 is computed, starting with the quasi steady state result (Fig. 38). The temperature distribution at the end of this run (Fig. 39) is then used as initial and boundary condition for the scenario runs. In the latter simulations the bottom 2nd kind (Neumann) boundary condition is replaced with an equivalent 1st kind (Dirichlet) boundary condition to improve the stability of the simulation process.

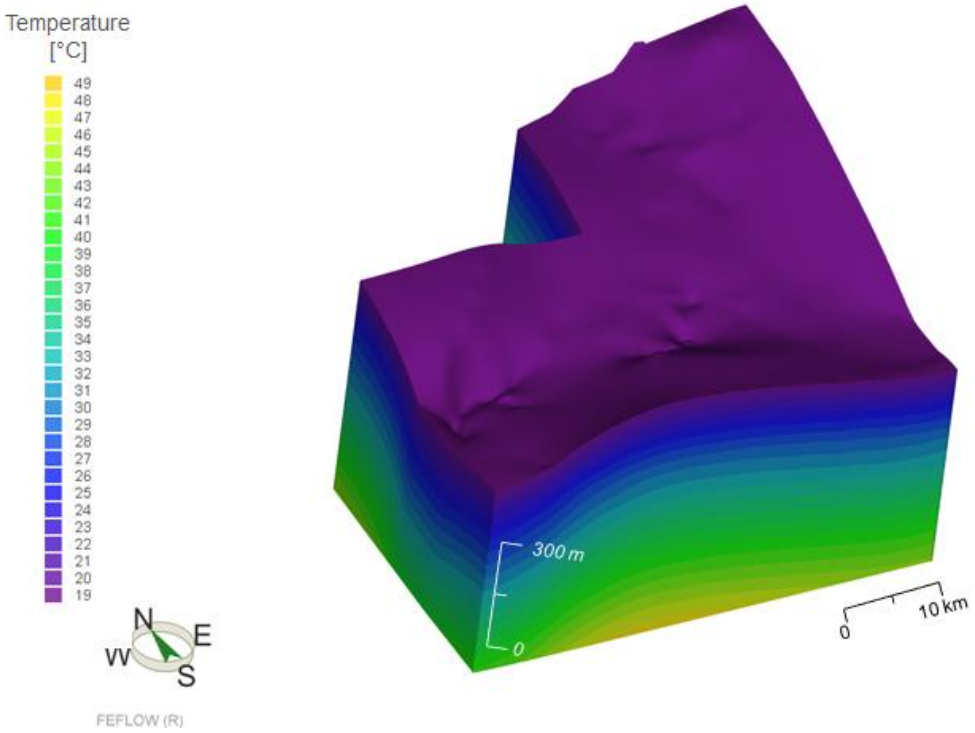

Figure 39: 3D view of the initial temperature distribution

A comparison of the resulting modeled temperature profile with measured temperature logs (Galanis et al., 1981) outside the model area (there are no logs with sufficient depth available inside the model area) shows a good agreement. The modeled profiles were extracted from a box model which has the same thermophysical properties of the investigated rocks with the same thickness at each investigated well (JD013, JD019 and JD022). These wells locations and the correlation between temperature logs in each well with the modeled temperature profile using FEFLOW® are illustrated in Fig. 40. This also shows that the specific heat flow of 95 m·W·m^{-2} at the modeled wells is in good agreement with temperature data observed close to the study area model location. Therefore, the value for the basal specific heat flow is reliable and is not a source for additional major uncertainties.

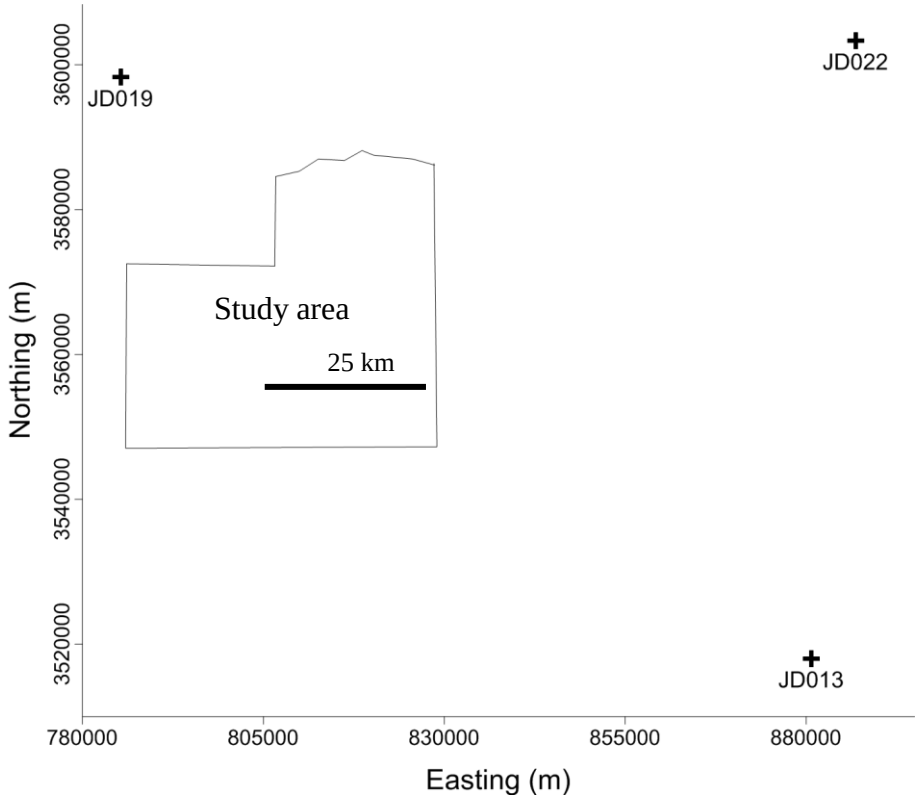
JD019
JD022
JD013
Study area
25 km
Northing (m)
3600000
3580000
3560000
3540000
3520000
780000
805000
830000
855000
880000
Easting (m)

(a)

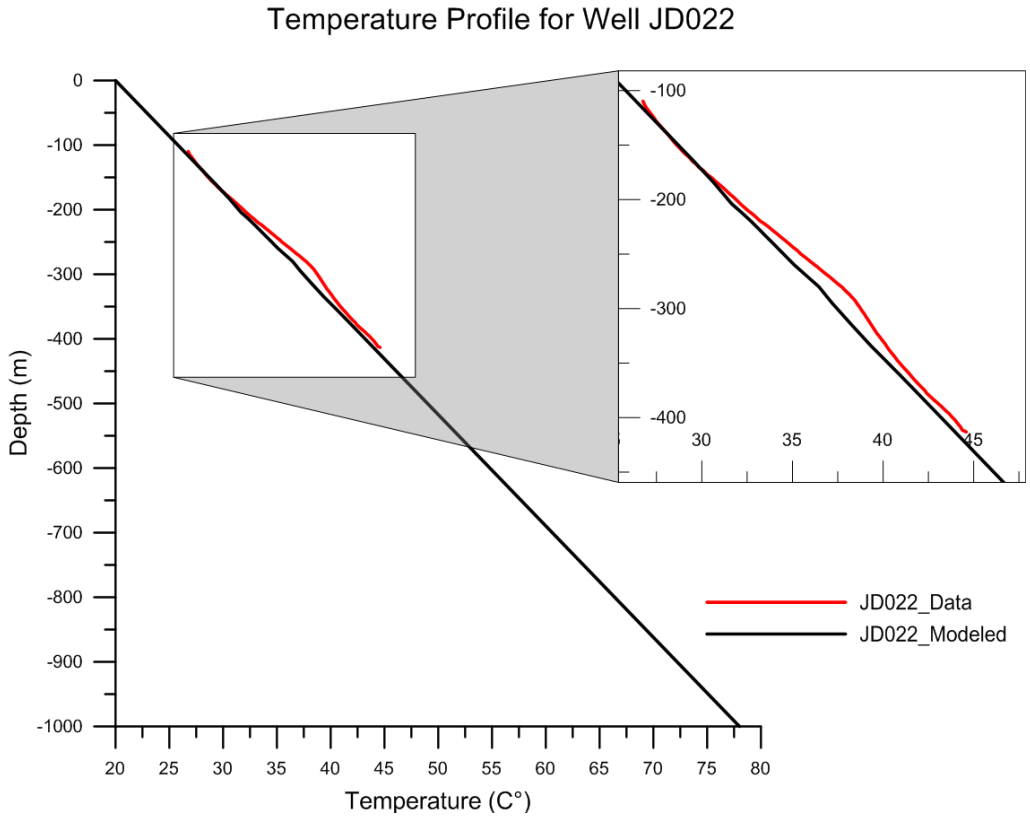
Temperature Profile for Well JD022
Depth (m)
0
-100
-200
-300
-400
-500
-600
-700
-800
-900
-1000
20
25
30
35
40
45
50
55
60
65
70
75
80
Temperature (C°)
JD022_Data
JD022_Modeled

(b)

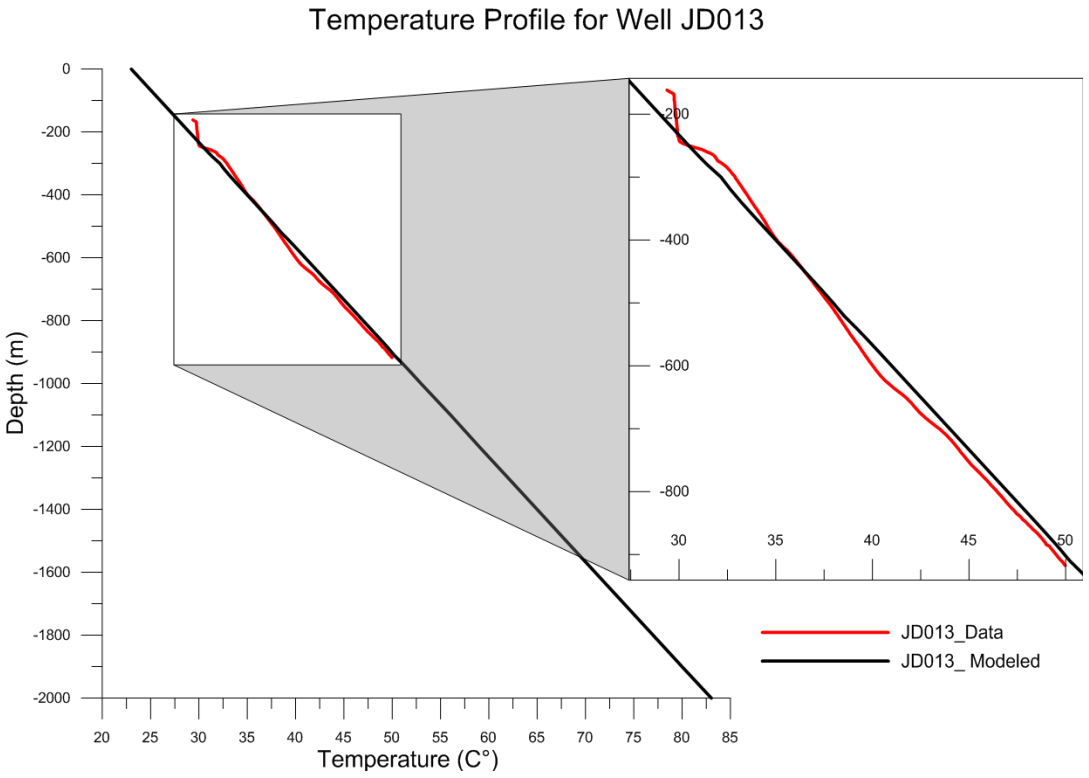

(c)

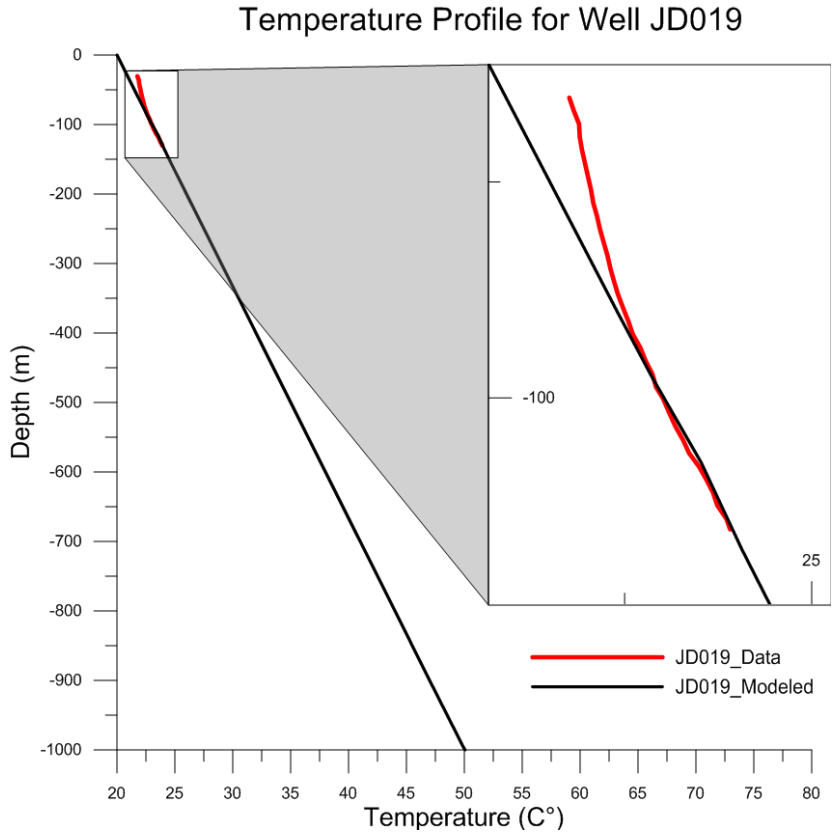

(d)

Figure 40: (a) Locations of the wells used for temperature calibration, (b, c and d) Modeled temperature profiles.

3.6. Setup of the Cooling Scenarios

The extraction of the relatively cool groundwater may be achieved by different arrays of extraction wells, see Fig. 41. For the injection wells the same well geometry is applied.

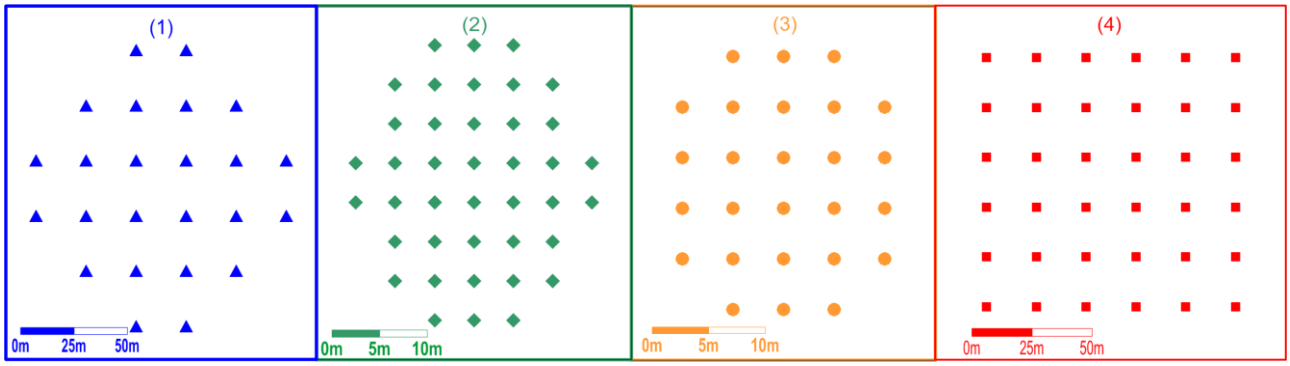

Figure 41: Configuration of the well arrays for the three different cooling scenarios.

For the three scenarios, the groundwater extraction takes out at different depths (Table 14) using multi-level wells. For the simulation of the effect of injecting heated water, a fixed temperature boundary condition is assigned to the injecting wells in scenarios (1), (2) and (3). Scenario (4) will be discussed later in this section.

Each scenario has its individual parameters. Different extraction and injection depths were applied, controlled by hydraulic head, groundwater temperature and aquifer thickness of each case. The total array spacing differs in each scenario, due to the available area for the system's installation (Table 14).

The relative positions of extraction and injection wells are shown in Fig. 42 and the approximate distances are given in Table 14.

Table 14: Scenarios Characteristics

Scenario	Number of Extraction- / Injection Wells	Extraction / Injection Rate ($m^3 d^{-1}$)	Maximum Extraction Depth (m)	Maximum Injection Depth (m)	Injection Temperature (°C)	*Total Wells Spacing (m)	**Distance between Extraction and Injection Arrays (m)
Power Station	24	100	130	25	34	125	1300
Hashemite University	40	200	90	70	28	35	800
Al Hashimiyya City	26	200	40	30	28	25	1700
Refinery	36	100	50	50	dynamic	150	700

*The total spacing between first and the last well in the longest raw of well array as shown in Fig. 41.

** Distance between extraction and injection arrays as indicated in Fig. 42.

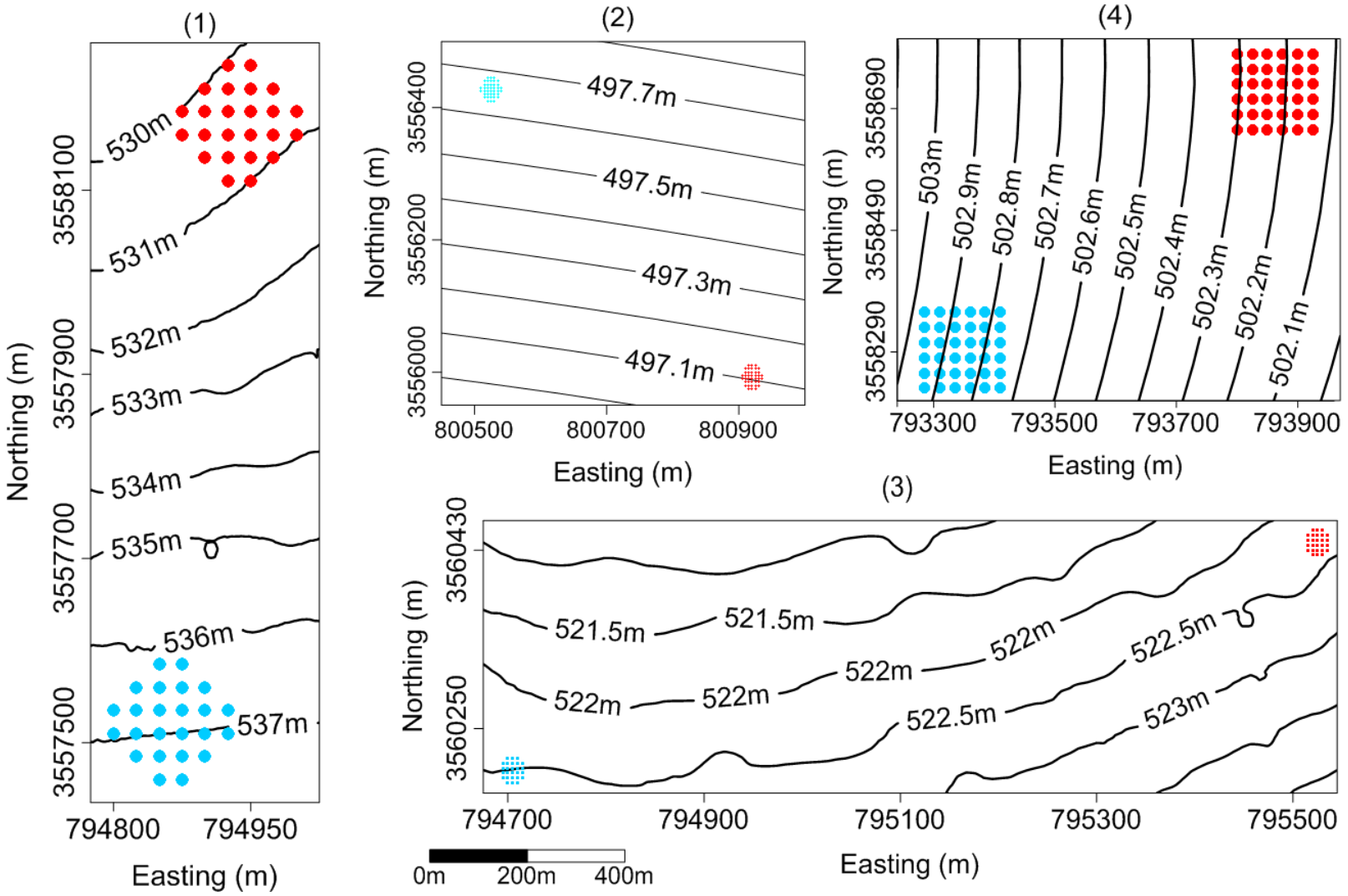

Figure 42: Locations of extraction (blue crosses) and injection (red crosses) arrays (compare with Fig. 31) of scenarios (1), (2), (3) and (4); additionally the groundwater head isolines are given.

In scenario (4) a programmed module was added to the model, using the programmable interface of FEFLOW®. The module simulates an annual reversing of the flow direction, (i.e. extraction and injection are reversed), to allow the subsurface to regenerate thermally. Additionally the module controls the temperature difference between injection and extraction wells according to the cooling load demand in Table 12. This means that the system delivers exactly the requested cooling load by default. However, the respective extraction temperatures may become slightly high for cooling.

Therefore the performance of the system was optimized by coupling with night sky cooling (Dan, 1989; Birtles, et al., 1996; Shaviv, et al., 2001; Dobson, 2005; Artmann, et al., 2008) in an extended setup. This system uses the cool air temperature during the winter nights to cool the water for 8 hours using special tanks and pipes installed on an exposed area (i.e. buildings' roof). This procedure allows heat exchange between the warm water and the air, before re-injecting the water into the ground. This cold-storage approach limits the heating of the subsurface, thus increasing the system's efficiency. The studied different cooling loads for winter are given in Table 12.

3.7. Geothermal System and Well Design

3.7.1 System Design

The use of groundwater for cooling purposes in Jordan began only recently in 2000 (French Environment and Energy Management Agency, 2003 & 2011; MENA-Geothermal, 2007). Despite of Jordan's limited availability of groundwater, this resource can be utilized due to its relatively constant temperature for several cooling technologies. These technologies rely on groundwater acting as a heat transfer medium (heat sink). This is more cost effective and efficient than conventional cooling systems which use non-renewable energy resources. The most common systems installed in Jordan are ground source heat pumps or geothermal systems involving open or closed loop systems. Another system that is utilized in Jordan is the standing water column system (Abu Nada et al., 2008).

The open loop geothermal system which is modeled in this study is presented in this chapter. Its operating principles and design criteria are introduced.

Open loop geothermal systems typically include one or more extraction, supply or discharge wells and one or more injection, recharge, return or diffusion wells. In the described geothermal cooling system, groundwater is withdrawn from the aquifer through the extraction well and pumped to a heat exchange device where it acts as a heat sink for the cooling process (Fig. 43).

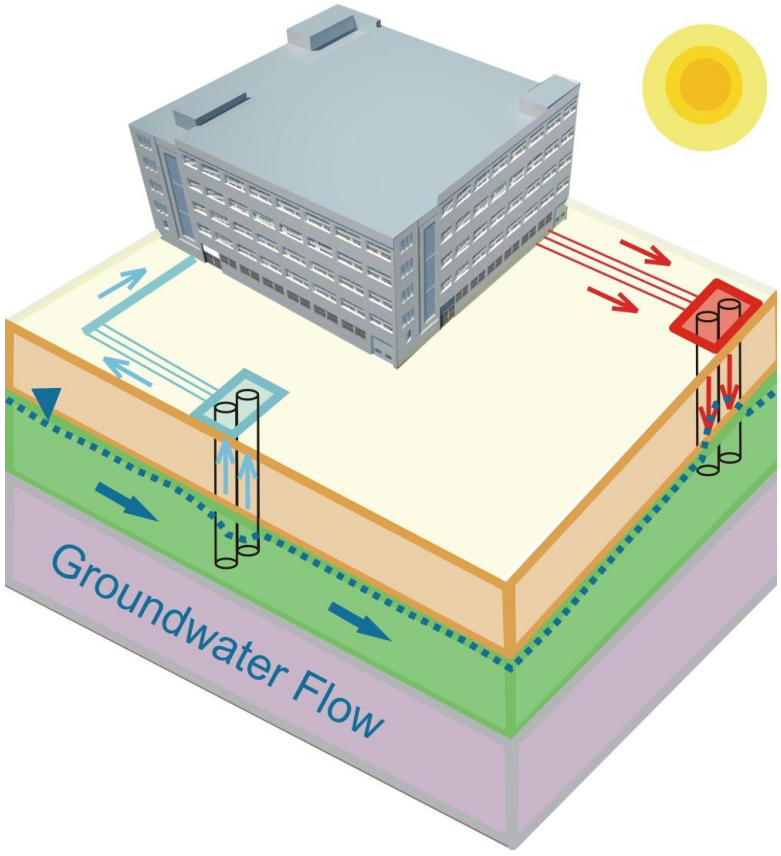

Figure 43: Open loop system

The heat exchanger operates with non-contact and non-consumptive processes between groundwater and the building's internal circulation fluid. Heat is transferred between the two fluids without mixing or physical interaction. After the cold groundwater passes through the heat exchanger device, it returns to the aquifer through the injection well (Fig. 43). In this study the groundwater side of an open loop geothermal well system operates in a fairly simple and straight forward manner. In the investigated scenarios groundwater is pumped from extraction wells penetrating basalts and limestone at different depths (Table 14) and recharged through injection wells (for each scenario extraction and injection wells depth and numbers of these well see Table 14). This system can be utilized for large and small scale applications; therefore, this study considers four different scenarios (applications). The wells used for these systems require the same design as water supply wells (Fig. 44).

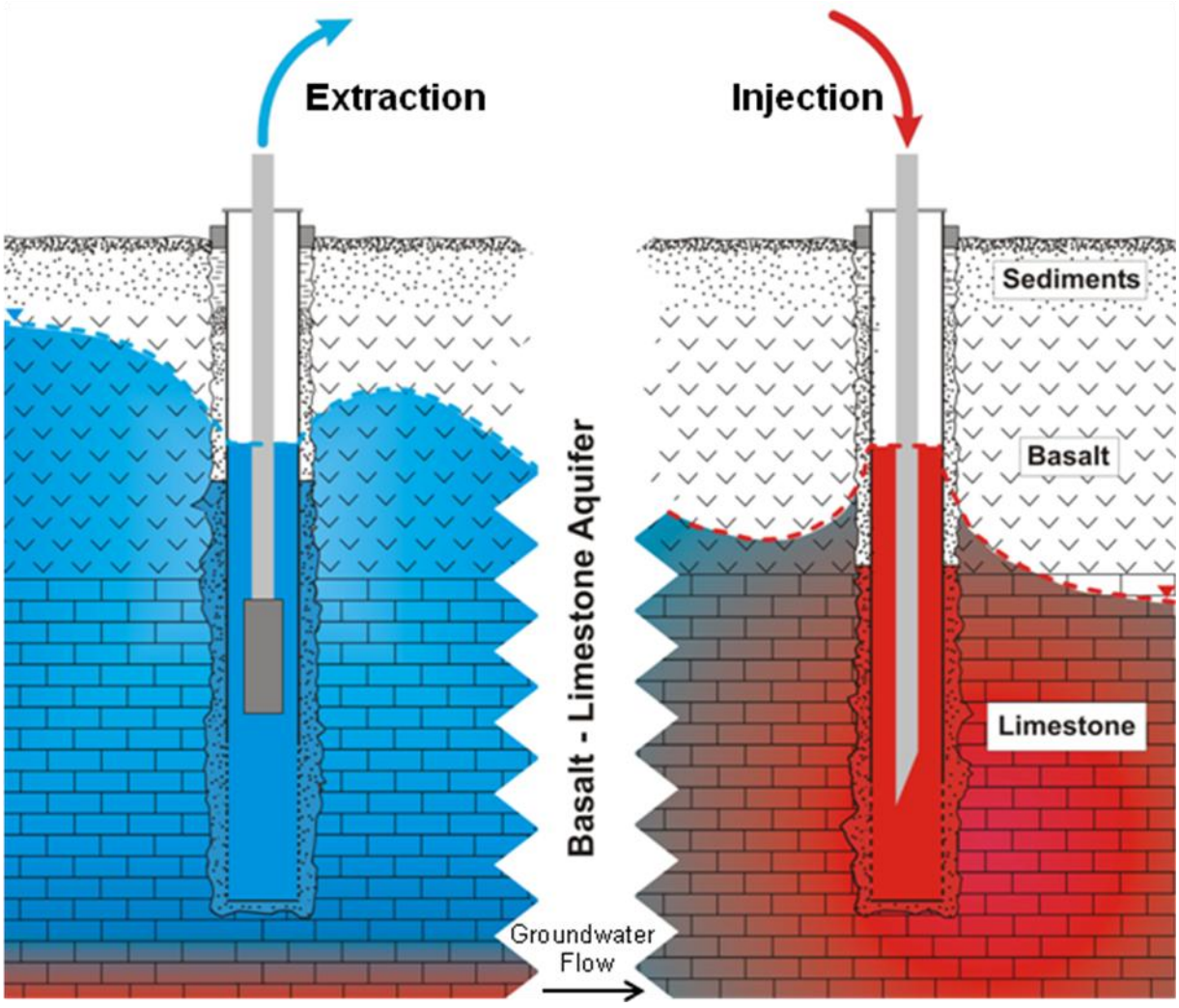

Figure 44: Geothermal well design for open loop system, modified after (Sass, 2012)

Aquifer hydrogeology plays a major role in the design of an open loop geothermal system. The significant amount of published data and the limited available groundwater data bank of the

Ministry of Water and Irrigation on the Amman Zarqa Basin are used. This data presents a preliminary screening tool to determine the applicability of using this geothermal system for the investigated scenarios. The significant parameters which are needed to evaluate an open loop geothermal system include: groundwater depth, hydraulic conductivity, specific yield, specific capacity and the aquifer type and characteristics (sections 1.4.3, 2.2, 2.4 and 2.5).

The importance of groundwater well depths for the system design comes from: (1) the effects of recharge head developed in the injection wells and (2) the well casing and the pump size used in the extraction wells. A greater depth of the injection wells allows larger recharge head to be developed in the injection wells casing. In igneous rocks (crystalline) the optimum depth of a well is determined largely by geologic factors; fractures and joints permeability and by economic factors. In general, wells in crystalline rocks should be less than 180 m deep, normally between 50 m to 60 m (Davis & Turk, 1964). In general, as the depth of groundwater is shallower, especially in semi-confined aquifers such as the studied Amman Zarqa Basin, open loop geothermal systems are less and less desirable (Boyce & Doreen Fitzsimmons, 2003). However, the injection wells should be installed at an appropriate depth shallow enough to prevent water table rise over the acceptable level. Thus higher flow rate systems require deeper injection wells to ensure that water diffusion is achieved through gravity (Boyce & Doreen Fitzsimmons, 2003). Furthermore, the deeper the extraction well, the larger the power and size of the pumping unit required. In this study different extraction and injection depths are considered (Table 14). Two parameters were regarded to determine the extraction and injection depths; groundwater table (static and dynamic) with annual aquifer drawdown and the flow rate demand. Scenario 2 has the deepest injection well because of the highest flow rate. Pumping (flow) rates for the studied systems, from 100 $m^3 \cdot d^{-1}$ to 200 $m^3 \cdot d^{-1}$, depend on the cooling load demand and the scale of each application (Table 12). Extraction wells in scenario 1 have the lowest hydraulic head. Therefore the depth of extraction wells exceeds 130 m to satisfy the demanded flow rate in this scenario. However, the increase of well depth i.e. scenario 1 and 2, causes an increase of the systems complexity along with the operational costs. The aquifer complexity at the different scenario locations analog with the system's scale play an important role for groundwater and heat flow between the respective extraction and injection well arrays. For instance; scenario 2 and scenario 4 require a more detailed control and monitoring methodology due to the larger system size than scenarios 1 and 3.

The investigated basaltic aquifer and the Limestone aquifer bellow have relatively low porosity. The fractured hydraulic conductivity which characterizes the shallow basaltic aquifer of Amman Zarqa Basin is very important for open loop geothermal systems. These basalts can provide and accept water more readily than the massive volcanics (Boyce & Doreen Fitzsimmons, 2003). Since fracturing decreases with depth, there will be a depth beyond which the drilling cost will outweigh the prospect of significantly increasing the well yield (Misstear, et al.,2006). The underlying micritic limestone's hydraulic conductivity is also fracture and karst controlled. As the hydraulic conductivity is the main indicator of the aquifer's ability to transmit water, the better performing or more efficient systems have higher hydraulic conductivities associated with them.

The fractured hydraulic conductivity was calculated as a boundary condition for each scenario using cubic law (Snow, 1965). This includes fracture density, spacing, roughness and width into

the calculation of hydraulic conductivity. This value is then implemented into the FEFLOW® model. However, the fracture orientation, stress field, fracture length, fracture displacement and filling material should be considered separately for each well design. These parameters were not taken into account in this study.

The specific capacity is a basic measurement of a well efficiency. Specific capacity is controlled by several variables such as well diameter; well screen length, gravel pack size, aquifer type and aquifer characteristics (Driscoll, 1989). Specific capacity is a good indication of the amount of extractable or injectable water from or into an aquifer (Boyce & Doreen Fitzsimmons, 2003). The higher the value of this capacity, the better the well productivity and well efficiency (Driscoll, 1986). In this study it is assumed that most wells, which are constructed in the same aquifer, are correctly and similarly designed. The specific capacity during the design phase can be assumed to be characteristic for the whole aquifer. Specific capacity for the Amman Zarqa Basin, under the limited data availability from pumping tests, ranges from 54.5 $m^3 \cdot d \cdot m^{-1}$ to 66.6 $m^3 \cdot d \cdot m^{-1}$.

In the studied cooling systems the groundwater is withdrawn through the extraction well, generally using a submersible pump. After the groundwater is withdrawn from an extraction well it will be pumped through a larger piping system where it will pass through various control devices, monitoring equipment, instrumentation and then a heat exchanger before being re-injected to the ground.

To prevent the system of partially draining on shut down, an inline check valve, either integral to the submersible pump or installed in the discharge column, is required. This also helps to minimize the air entering the system. In the discussed system where each system comprises multiple extraction and injection wells, a gate valve can be used to isolate one of the wells during maintenance procedures, thus allowing the remaining wells to continue operating. At the well heads air relief and vacuum breaker valves need to be installed to reduce the air in the system in order to avoid many problems air can cause for the system itself. Also, a strainer will remove coarse particulate matter and prevent it from reaching the pumps. A throttling valve can be used to control the flow from the extraction well by increasing or decreasing the amount of the back pressure the pumping unit is working against. This will increase the pump's efficiency.

The most critical aspect of the geothermal system design is the geothermal wells. Since the wells are the key to utilizing the groundwater in the system, sizing and location are very important. For well design all aquifer parameters such as permeability, porosity, hydraulic conductivity, transmissivity, storativity, aquifer thickness, groundwater depth and flow direction are required (Driscoll, 1989; Misstear et al, 2006 and Sterrett, 2007). Obviously, conducting actual field tests is the preferred and most accurate method to obtain these parameters, but is often economically infeasible, especially for smaller projects. In this study due to this reason most of the aquifer parameters are collected from literature and obtained from the limited data available through the files of the Ministry of Water and Irrigation archive and database.

The flow rate of geothermal water was calculated considering an acceptable temperature difference between extraction and injection and the cooling load for each of the four scenarios investigated in this work (Eq. 8). In addition, higher temperature differences require larger distances between extraction and injection wells to avoid the possibility of thermal breakthrough.

Scenario 4 has the highest temperature difference (10 °C) between extracted and injected water. The limited area available around the location of scenario 4 (Refinery) is the determining factor in reducing the separation distance between the extraction and injection arrays to 700 m (Fig. 45). The dynamic operation system is required in this scenario to limit the closeness effect of excessive heating of the system between the extraction and injection arrays. Scenario 3 has a medium temperature difference of 9 °C between extracted and injected water. Due to the large availability of space this system has the highest separation distance between extraction and injection arrays of 1700 m (Fig. 45). To satisfy the cooling demand of 2.2 MW in this scenario a higher flow rate for each well of 200 $m^3 \cdot d^{-1}$ was defined.

Scenario 2 has a medium temperature difference of 9 °C between extracted and injected water and the well arrays are limited by a relatively short separation distance between extraction and injection arrays of 800 m (Fig. 45). Therefore, a high flow rate of 200 $m^3 \cdot d^{-1}$ in each well was defined to satisfy the highest cooling demand of 3.5 MW of the four studied scenarios.

The first scenario showed to be the most appropriate for the installation of such a geothermal systems due to its characteristics and conditions. This scenario has the lowest temperature differences of 8 °C between extracted and injected water. In addition, it has a relatively high separation distance between extraction and injection arrays of 1300 m (Fig. 45). The flow rate in each well of 100 $m^3 \cdot d^{-1}$ satisfies the cooling demand of 0.93 MW for the cooling in this scenario.

(a) Scenario 1

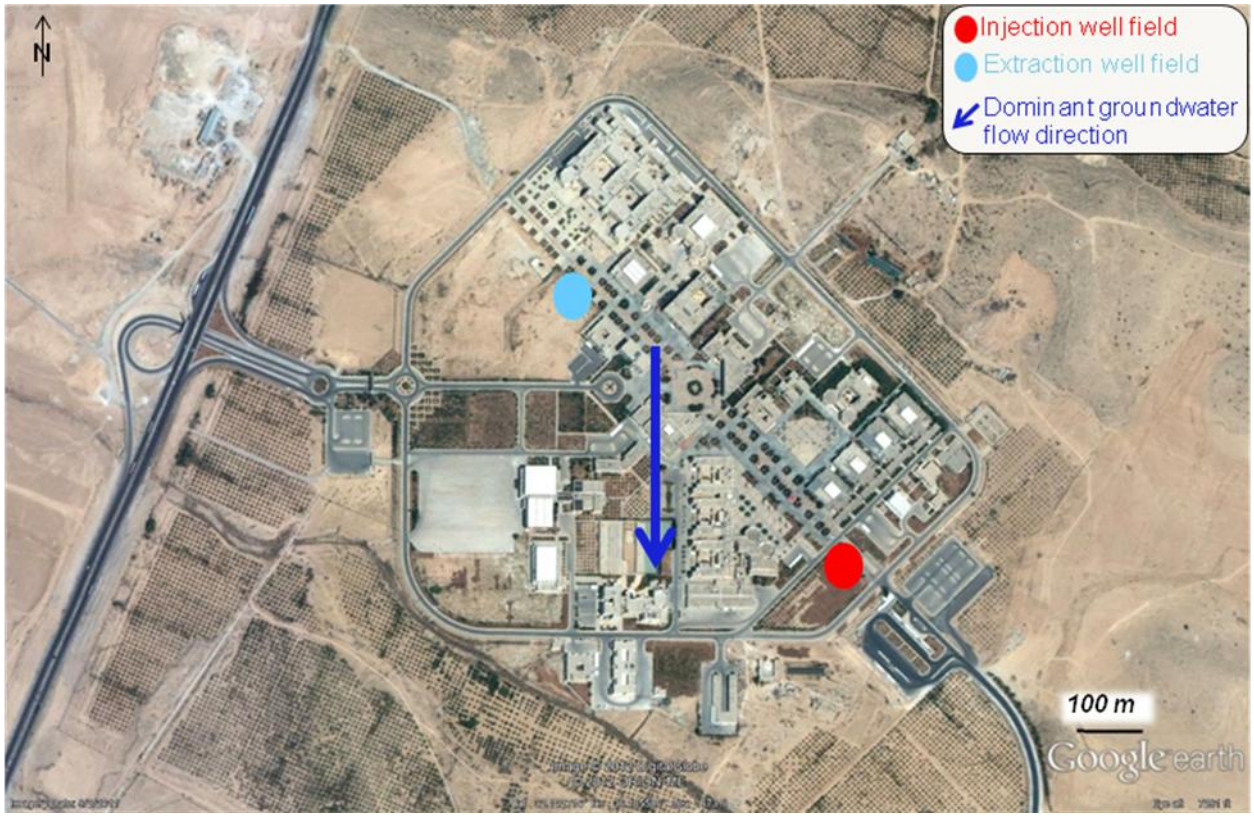

(b) Scenario 2

(c) Scenario 3

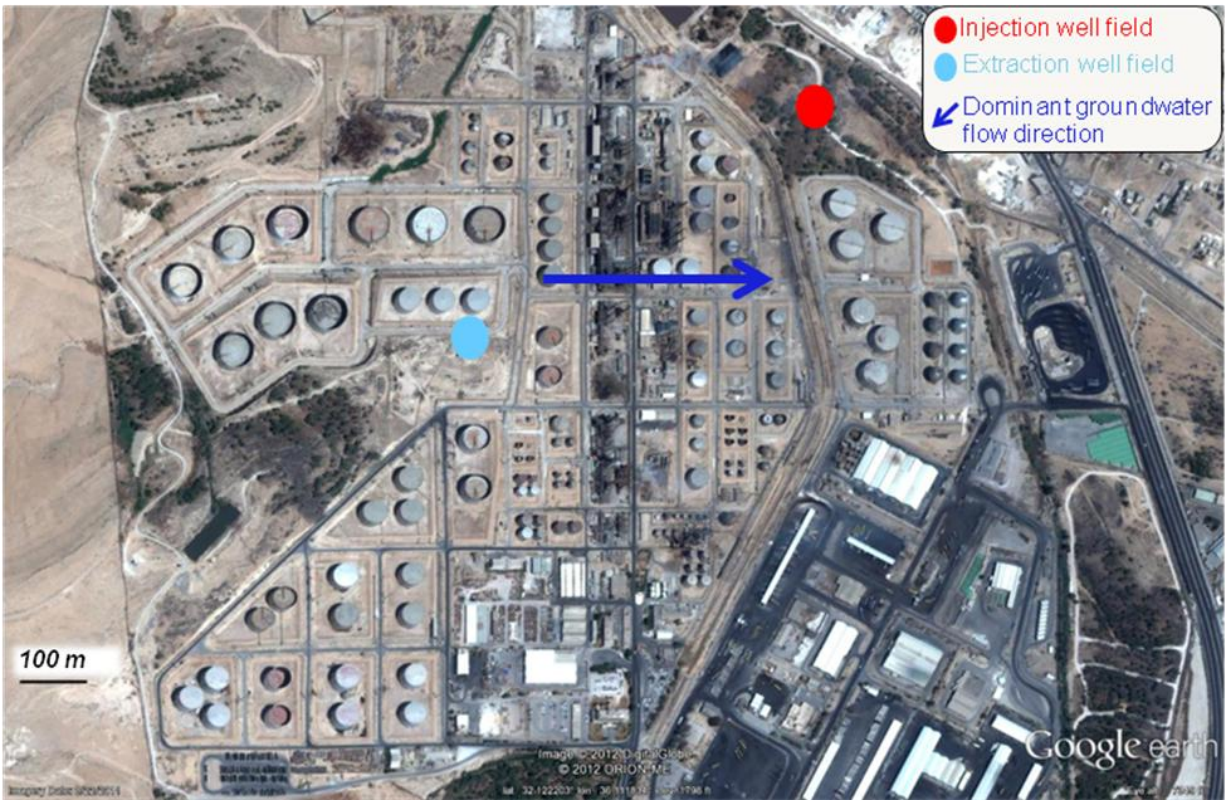

(d) Scenario 4

Figure 45: Extraction and injection well arrays according to the areal extend of infrastructures in the four investigated scenarios.

Extraction wells are placed as far away as possible from the injection wells to reduce the potential effect of thermal breakthrough. The spacing between each two wells within the extraction well arrays is chosen as far apart as is economically feasible to limit the effects of drawdown in the extraction wells as well as to avoid any negative effects which may arise from the closeness of the injection wells: i.e. faster heating of the aquifer or increase of the potentiometric surface to a level that the dominant mechanism shifts to forced injection rather than gravity diffusion. This effect may create higher backpressure in the extraction system and simultaneously cause lower flow rate and lower the system's efficiency. The interference effects between wells in a well array can be estimated using the principle of superposition (Mistear et al., 2006).

$$S_w = \frac{q}{2\pi T_s} \ln \frac{r_e^{\,3}}{r_w \times r_1 \times r_2} \qquad (11)$$

Where, S_w is the equilibrium drawdown in a well of radius r_w; q is the pumping rate in this well and in two other wells located at distances r_1 and r_2 from this well; r_e is the radius of influence of each of the pumping wells; and T_s is the aquifer transmisivity.

In this study FEFLOW groundwater modeling was conducted to accurately predict the rates of extraction and well location and spacing for the four investigated scenarios. The model predicts moderate to high potential for each simulated scenario (Chapter 4).

3.7.2. Well Design

The geothermal wells in the each scenario have to be designed as a typical groundwater supply well after the flow rate and well locations are determined (Fig 34). A sequence of steps and calculations needs to be conducted to design a geothermal well for each respective scenario (Misstear et al., 2006). In this chapter an exemplary evaluation of the first scenario, which has the highest expected potential, regarding its well system design aspects is conducted. Scenario 1 has the deepest extraction wells and the shallowest injection well between the four scenarios (Table 14). It has a medium temperature difference between extracted and injected water of 8 °C (compared to 10 °C in scenario 4 and 9 °C as in scenarios 2 and 3). It has an acceptable well spacing (resulted from system simulation) and a relatively large distance separating the extraction and injection well arrays (Fig. 42). It has the lowest number of extraction and injection wells; 24 wells in each array with 25 m spacing between each two wells. For extraction and injection well field geometry see Fig. 41.

Pump size determination

Determining the required pump size depends on three characteristics; pressure, friction and the required flow rate of the system. Pressure is the driving force which moves the fluid inside the system. Friction along to confining walls of pipes and tubes is responsible for slowing down fluid molecules (Chaurette, 2008). Flow rate is the water volume that is displaced per unit time (Driscoll, 1989). At a given pressure the flow rate is controlled by friction which depends on the length and diameter of the pipes. The pump used in this system is a submersible pump with a variable flow rate depending on the system pressure and due to the reduced flow caused by the temperature dependent increase of viscosity (Sterrett, 2007). In such a pump three factors must considered; friction, static head and fluid viscosity.

First step for dimensioning the pump is to determine the required flow rate which is 100 m^3 d^{-1} in scenario 1. The second step is to determine the static head considering the distance between the pumping level and the discharge pipe end height. In this case the static head equals 110 m as the groundwater table is 130 m bellow. To determine the friction head loss, the fluid velocity is assumed to be 3 m s^{-1}. A friction loss of 0.14 m m^{-1} is assumed (Boyce & Doreen Fitzsimmons, 2003). The friction head can then be calculated as 110 x 0.095 = 10.45 m. There is additional friction loss in the fittings, an assumption of 30 % of the pipe friction head loss can be made here. The fittings friction head loss here equals 10.45 x 0.3 = 3.14 m. The total head is the sum of the static head and the friction head as 110 + 15.4 + 4.62 = 123.6 ≈ 124 m. The last step is selecting the pump using the previous specifications of total head and required flow rate as well as the suitability to the application. Installation of a solar powered pump in this geothermal installation seems to be an interesting option (Abu-Aligah, 2011). Model SP 8A-25NE water pump from Grundfos catalogue is the most suitable pump to fit into the investigated system (Grundfos, 2012). This pump can be coupled with a solar panel (Abu-Aligah, 2011). 4.0 inch diameter and 1.5 inch outlet are the suggested dimensions of the submersible pump for this system. Discharge through this 1.5'' outlet pipe can be calculated using the Jean Lois Poiseuille formula

$$q = \frac{\pi \rho_w g r_i^4 \Delta h}{8 \mu \Delta l} \tag{12}$$

Where q is the discharge, Δl is the length of the tube; r_i is the radius of the tube; Δh is the head difference between two ends of the pipe; μ is the dynamic viscosity of the fluid; ρ_w is the water density and g is the gravity acceleration.

Well pipe diameter and casing diameter

Well pipe diameter will be 200 mm (8 inch) as follows:

Well pipe diameter = pump diameter + 0.1 m (13)

The importance of casing diameter of the well is caused by its influence on the drilling costs, which depend on the type of drilling equipment used (Driscoll, 1989). Two requirements must be satisfied when choosing the casing diameter: (1) casing must be large enough to accommodate the pump for efficient operation and sufficient clearance for installation, (2) the casing diameter must be sufficient to limit the up-hole velocity to less than 1.5 m s^{-1} (Driscoll, 1989).

The outer well casing should be used as a permanent part of the installation. The suggested multi-cased wells should be installed in the shallowest part of the well for the depth of the recent sediments. As the sediments have variable drill-ability, a permanent stand-up (outer well casing) is preferable. The casing must be free of any interior and exterior protective coatings and must be steam cleaned or washed under high-pressure using approved water immediately before installation. The type of material and wall thickness of the casing must be adequate to withstand the installation process. The ends of each casing section should be either flush-threaded or beveled for welding (Driscoll, 1989).

Different casing sizes are required depending on the types of the sediments encountered at the drill site and the purpose of the well. Also, the diameter of all casings in multi-cased wells

should be sized so that a minimum of 2 inches of annular space is maintained between the surface casing and the borehole. In the investigated well 8 inch diameter well screen is required with 10 inch borehole diameter resulting in a 1 inch annular gap. As the casing diameter should be twice the nominal size of the pump diameter, or at least one nominal size larger than the pump bowls, here the minimum nominal casing diameter should not be less than 9 in (Sterrett, 2007).

Determining the casing depth and specifications of the material weights and connections is vital to the well life and integrity and to the success and safety of the well drilling process (Hole, 2008). The outer casing string is necessary for the drilling operation and the inner strings are required for production process. The minimum two concentric casing strings which are more completely cemented must be steel from a technical and legal sense for a geothermal well (Hole, 2008). The 40 (STD) steel pipe is satisfied with the geothermal wells in this system requirements. Thus an Inconel 600 (Nickel, Cobalt, Chromium and Iron composition) casing is preferable in such a geothermal application due to its strong resistance to stress-corrosion cracking (Sterrett, 2007). The maximum pressure estimated in the well is about 500 psi. The columnar pressure was calculated as hydrostatic pressure and equals 200 psi.

Well screen

One of the most important proposes of well screening is to retain grains and filter pack material through stabilizing the aquifer. This is controlled by the screen slots size and gravel pack degradation (Driscoll, 1989; Sterrett, 2007).

To calculate the well screen open filter area (screening area) the critical velocity needed to be calculated using Sichardt formula as follows (Sass, 2012):

$$v_{crit} = \frac{\sqrt{k_f}}{15} \tag{14}$$

Where v_{crit} is the critical velocity of groundwater penetrating into the well screen filter, k_f is the effective hydraulic conductivity.

The discharge equation Sichardt formula for well intake capacity at equilibrium conditions which was derived by various investigators (Slichter, 1899; Turneaure & Russell, 1901; and Thiem, 1906) is used. The equation assumes a two dimensional radial flow towards the well and the vertical extent of the well is ignored. This equation relates well discharge to the drawdown, and all dynamic conditions at the well and in the ground are assumed to be in equilibrium.

The maximum well intake capacity q_f can be calculated from Sichardt formula which is used to characterize the investigated well is as follows (Sass, 2012),

$$q_f = 2\pi \cdot r_p \cdot Th \cdot v_{crit} \tag{15}$$

Where r_p is effective well pipe radius, Th is the aquifer thickness

The equation of the actual well intake capacity q_a is calculated using the Dupuit formula as follows (Sass, 2012)

$$q_a = 2\pi \cdot k_f \cdot Th \cdot \frac{H_s - h_w}{\ln\left(R/r_w\right)}$$

(16)

Where H_s is static head measured from bottom of the aquifer, h_w depth of water in the well while pumping and R is the range approximation from Sichardt formula as (Sass, 2012):

$$R = 3000 \cdot S_w \cdot \sqrt{k_f} \tag{17}$$

Where S_w is the drawdown in the well during pumping.

The results of applying different drawdown values is used to interpret the optimum drawdown (S_w) and optimum water depth in the well during pumping (h_w) using the intersection point method (Bieske, 1998).

Then the required opening area (A_o) can be calculated through Darcy law as follows:

$$A_o = q_f / v_{crit} \tag{18}$$

Here a 100 $m^3 \cdot d^{-1}$ of maximum well intake was assumed in Eq. 10 from the cooling load demand calculations. As the designed wells are shallow and have small diameter the polyethylene high density (PE-HD) screen filter is preferred because of its low environmental effects, ease of handling and low costs (personal discussion with Prof. Dr. Ingo Sass). PE-HD is a flexible material available in a wide variety of sizes from 0.5 inch to 42 inch diameter. To date, PE-HD material has seen little application in direct-use geothermal systems. As the maximum temperature of the investigated system is 38 °C this material seems to be suitable from its operating temperature limits. Stüwa catalogue was used to define the screen type of PE-Filter/ Vollwandrohre – SDR 11 (Stüwa, 2012). PE-HD Filter specifications were then used to specify the open area percentage. For the 8 inch pipe diameter a 3.51 % open area is required and 1 mm slot size seems to be appropriate.

Screen slot size can be defined from the open area A using the manufacturer's catalogue for different screen materials as follows;

$$A = \left[\frac{sl}{(sl + w)} \right] \times 100 \tag{19}$$

Where sl is the slot size and w is the wrap-wire face width.

The total screen area can be later calculated from the open area percentage and the screen open area (A_o). Where

$$A_o = A \times A_T \tag{20}$$

Screen length (L_s) can be calculated from the total screen area (A_T) as follows:

$$A_T = 2\pi r_w \cdot L_s \tag{21}$$

Where L_s is the screen length.

The screen length was calculated to be 17 m with 1 mm slot size and 3.51% open area. The cone of depression of the designed well is shown in Figs. 46.

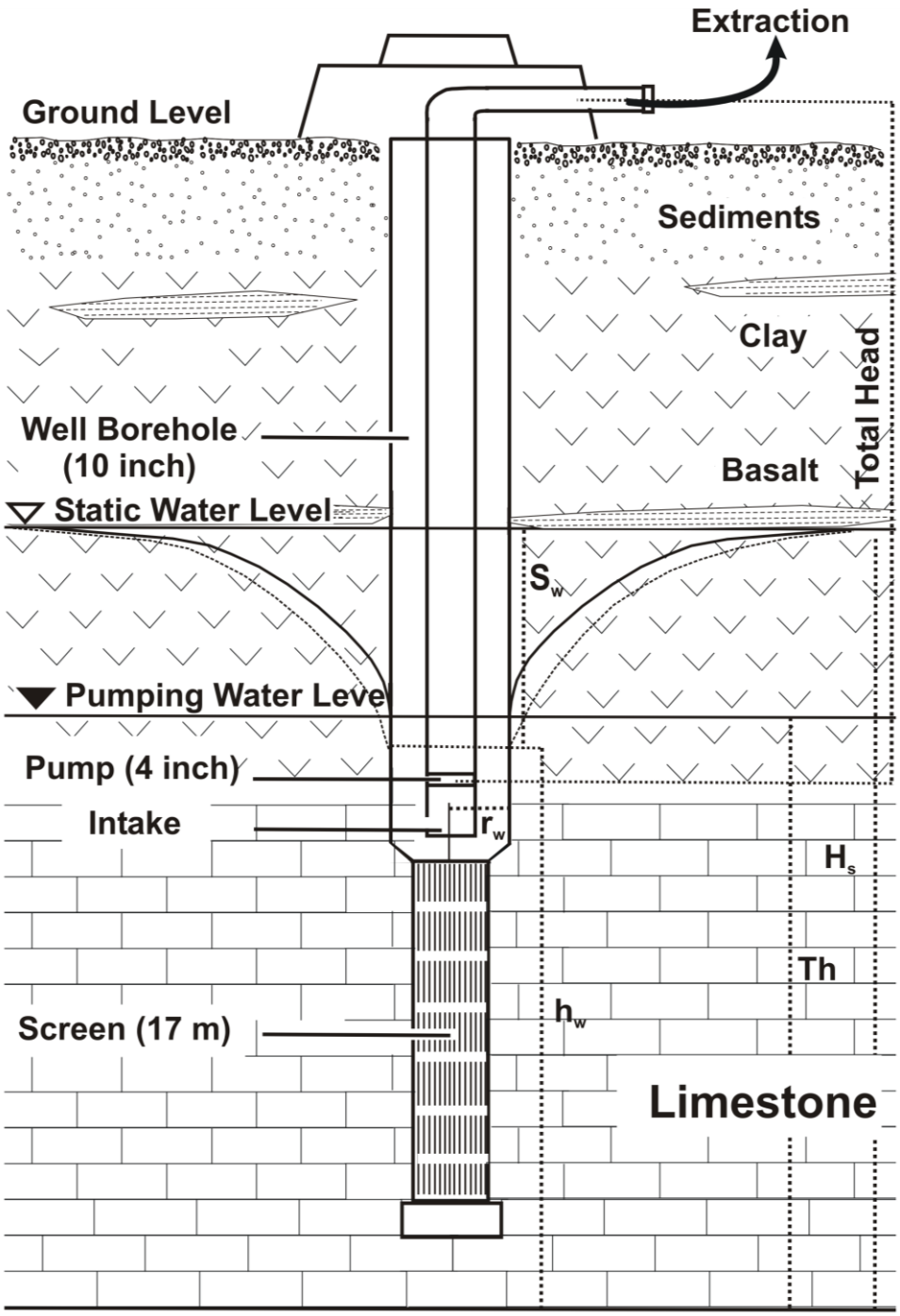

Figure 46: Cone of depression of the extraction well in scenario 1.

Gravel pack

Gravel pack is used to prevent fine-grained material from entering the well during pumping and to stabilize the formation while causing minimal impairment to well productivity (Driscoll, 1989). It is used to fill the annular space (Fig. 47). In addition, the gravel used as gravel-pack must come from a clean source and should be thoroughly washed before being placed in the well. Fining upward grain size gravel pack should be applied in the designed wells where it should end up with cement grout in the casing strings at the surface (Fig. 47). The

recommended gravel pack grain size (for 0.3 mm screen opening) for this well design may range from 8.0 mm to 1.0 mm.

Cementing

Grouting (cementing) is one of the most well design parameter which will not discussed here in detail. Cementing involves filling the annular space between casing and the drilled hole with suitable slurry of cement (Driscoll, 1989). In the investigated geothermal system design where the basalts are overlain by recent loose and unconsolidated sediments the grout should extend from the land surface down to the basalt interface (Sterrett, 2007). An industrial cement type which normally used in this dry region could satisfy the grouting purposes. Well design is shown in Fig. 47.

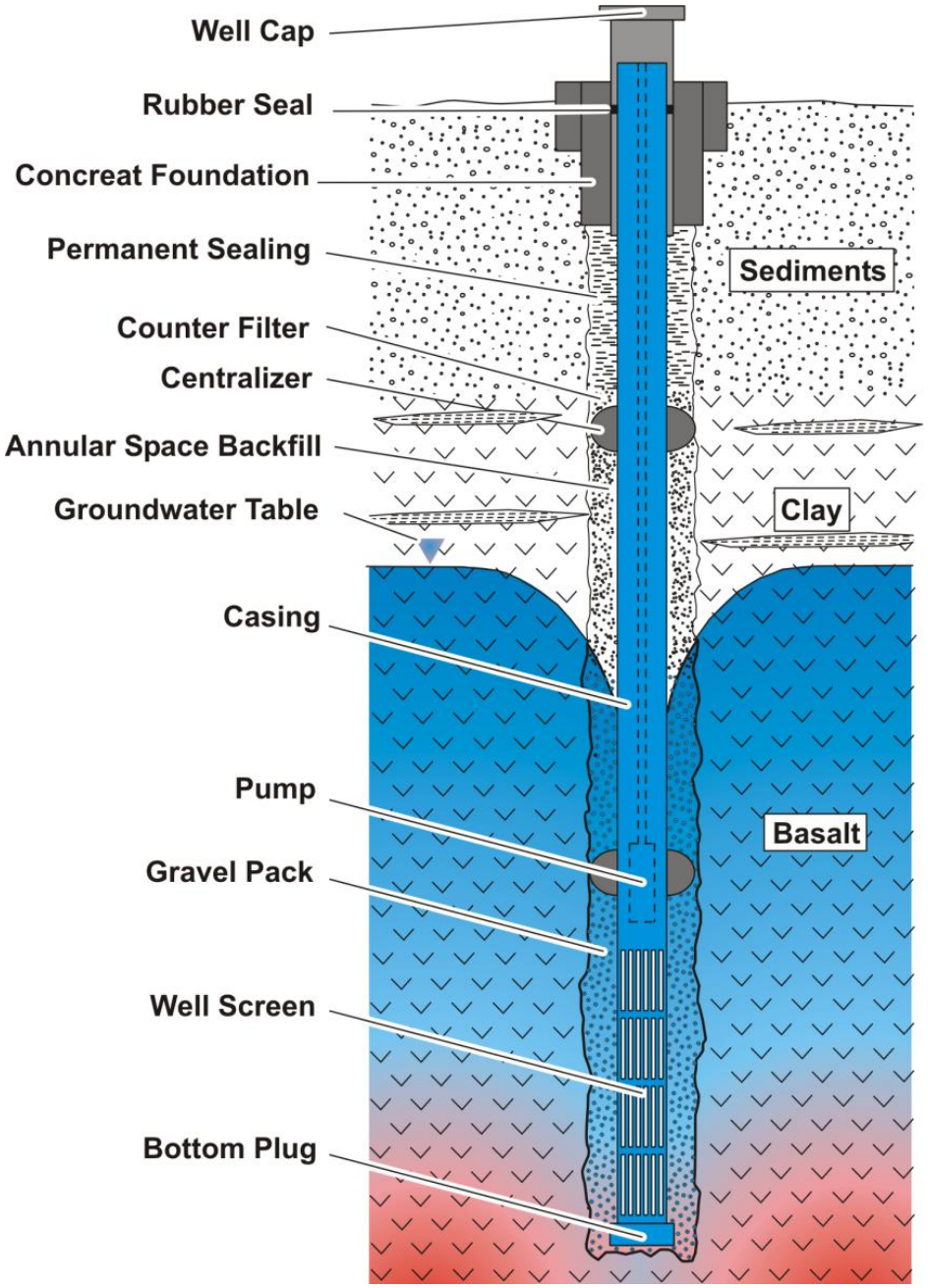

Figure 47: A schematic drawing showing the well design modified after (Sass, 2012).

Drilling Method

For the studied system the recommended drilling method could be any rotary drilling method for the basaltic rocks. But auger drilling should be used for the upper unconsolidated sediments.

Another method which could be applied is downhole Hammer Air Lift drilling, where the drilling progress can be increased in this case. This method is widely used for drilling shallow wells (10 – 400 m) depending on compressor capabilities (Sass, 2012). This technology is relatively cheap and easier to implement than rotary drilling. There are certain benefits associated with this drilling type such as its high rate of penetration, ease of implementation, and increased borehole stability (Thompson, 2010). In this case a permanent casing should be installed first as discussed above. The required depths of the wells also influence the appropriate method. In any case, an initial exploratory well should be drilled to gain better insights into the aquifer conditions.

4. Results

4.1. 4.1. Cooling Scenarios

. Scenario 1, 2 and 3

Temperature differences between extraction and injection wells were derived from the FEFLOW® simulation model.

The cooling load progression (Eq. 8) for a 10 year simulation period for scenarios 1, 2 and 3 is shown in Figs. 48, 49 and 50 respectively.

In scenario 1 the obtained cooling load of approximately 7 KW (0.007 MW in Fig. 48) slightly increases with time. This slight increase, with reference to Eq. 8, is due to the decrease of the computed extracted water temperature of about 1 °C (Fig. 52) over a 10 year period. In scenario 2 the cooling load increases by approximately 0.05 MW (Fig. 49) due to a 0.2 °C decrease in extracted water temperature (Fig. 53) over a 10 year period. The cooling load of scenario 3 decreases by 0.05 MW (Fig. 50) over time, due the increase of the extracted water temperature of 0.3 °C (Fig. 54). The seasonal (summer / winter) operation controls the cooling load variations in scenarios 2 and 3 very well, where the system is shut down in winter. A comparison between the first three scenarios cooling load is depicted in Fig. 51. It is clear that the second scenario has the highest cooling load where the first one has the lowest.

Figs. 52, 53 and 54 show the temperatures at the extraction wells in scenario 1, 2 and 3 respectively. Due to the different locations and therefore differences regarding lithology, groundwater level and hydraulic situation, the results of the modeled cooling load and of the water temperature at the extraction wells each show an individual trend. Scenario 1 (Fig. 52) and 2 (Fig. 53) show a decrease in the extracted water temperature. This is due to the higher vertical hydraulic conductivity at the well locations of scenarios 1 and 2 compared to the lower vertical hydraulic conductivity at the location of scenario 3. However, based on the hydrologic situation this result is reasonable as slightly cooler water from overlying layers is pumped.

In scenario 3 (Fig. 44) the temperature increases because the ground temperature around the array of extraction wells increases with time due to the heat dissipated by re-injected water. This thermal short-circuit is due to the effect of the distance between extraction and injection well arrays together with the parallel oriented groundwater flow-field (Fig. 42). Furthermore, this scenario has the smallest well spacing distance of 25 m compared with the other two scenarios spacing distance of 125 m and 35 m for scenarios 1 and 2 respectively. However, the setup of well spacing was limited due to existing structures in each scenario area (section 3.7).

The average temperature for each scenario is illustrated in Fig. 55. It is evident that each scenario shows its own temperature stability and constancy through the simulation time period. This may increase the system’s potential and durability due to small variations in extracted water temperature over time.

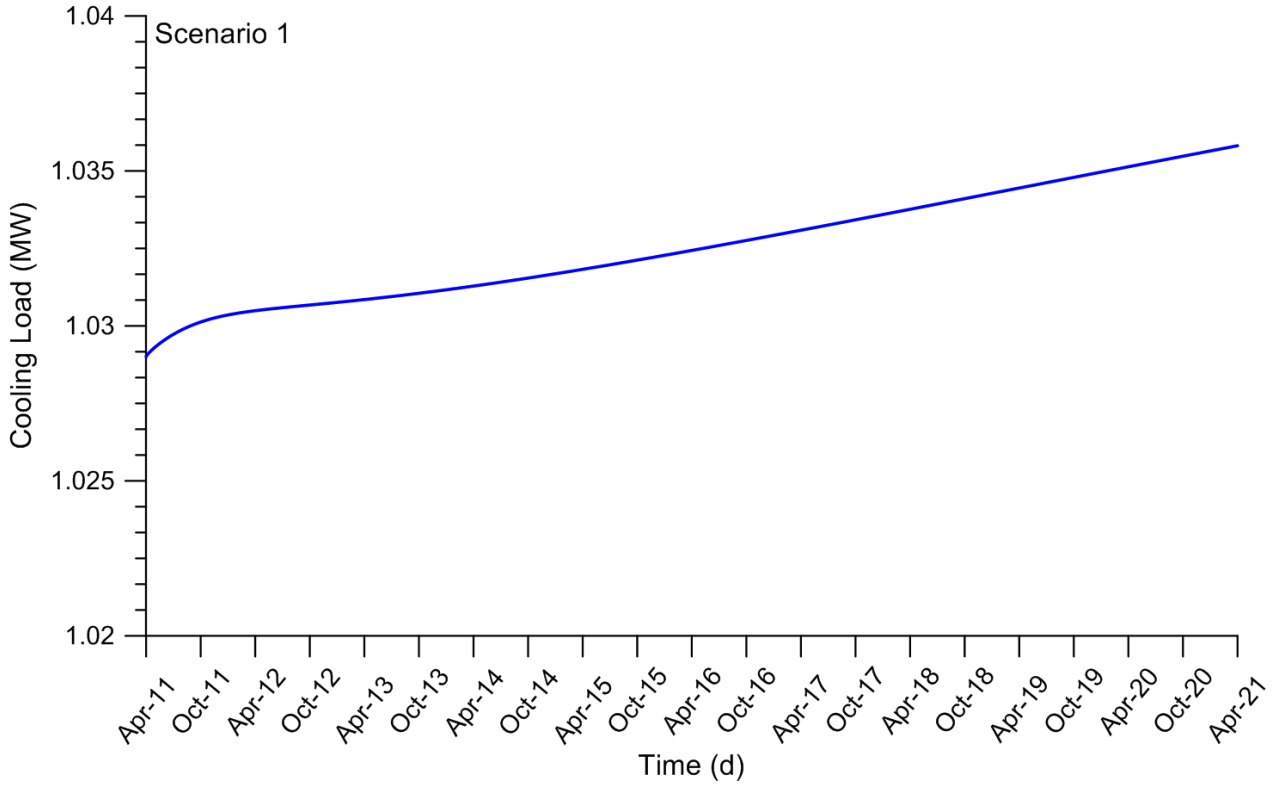

Figure 48: Cooling load for scenario 1.

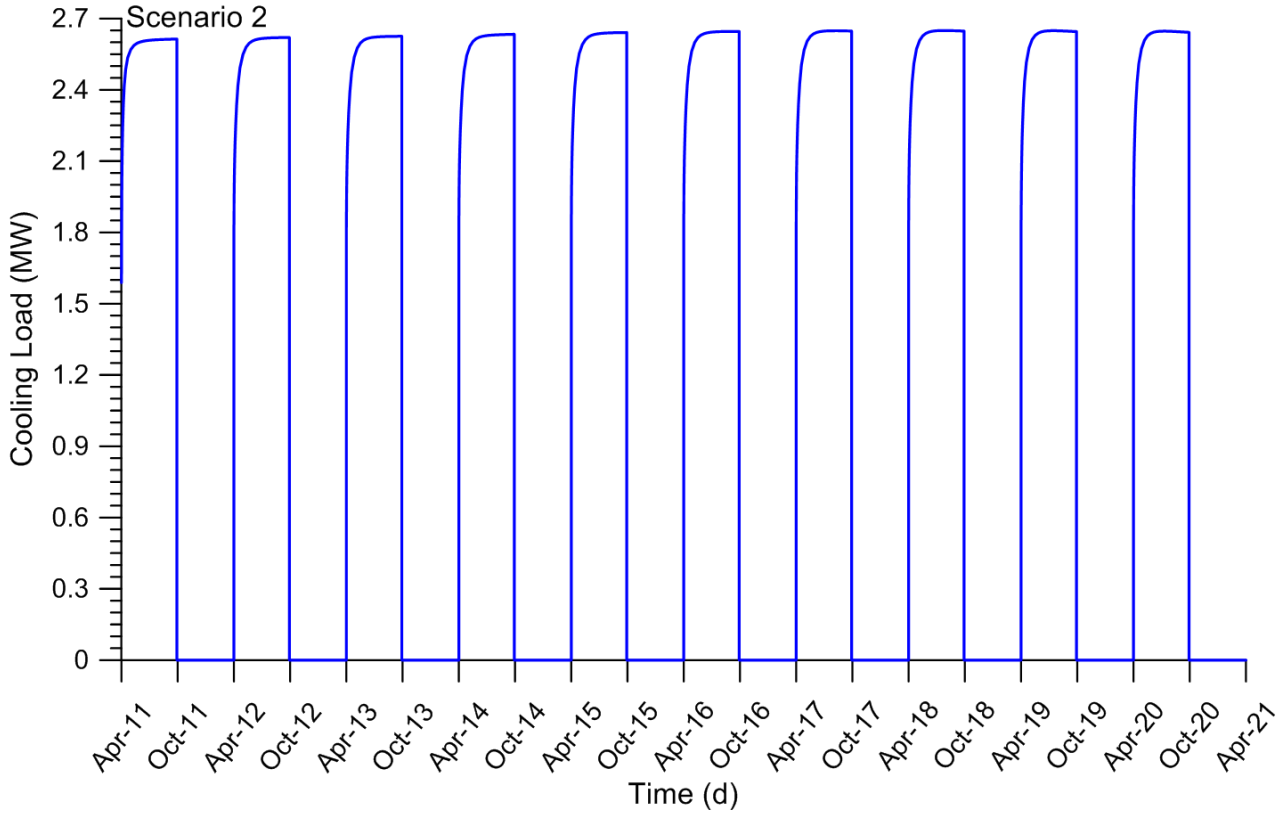

Figure 49: Cooling load for scenario 2.

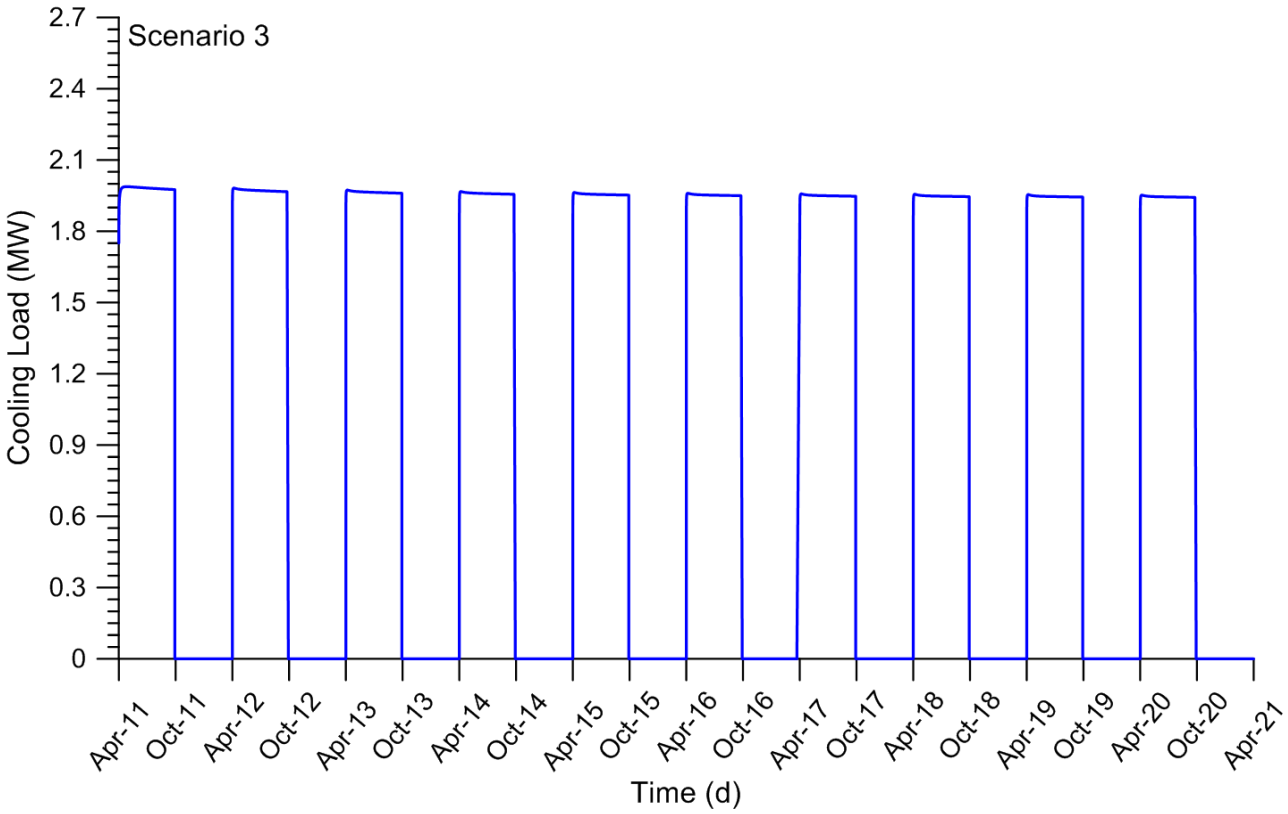

Figure 50: Cooling load for scenario 3.

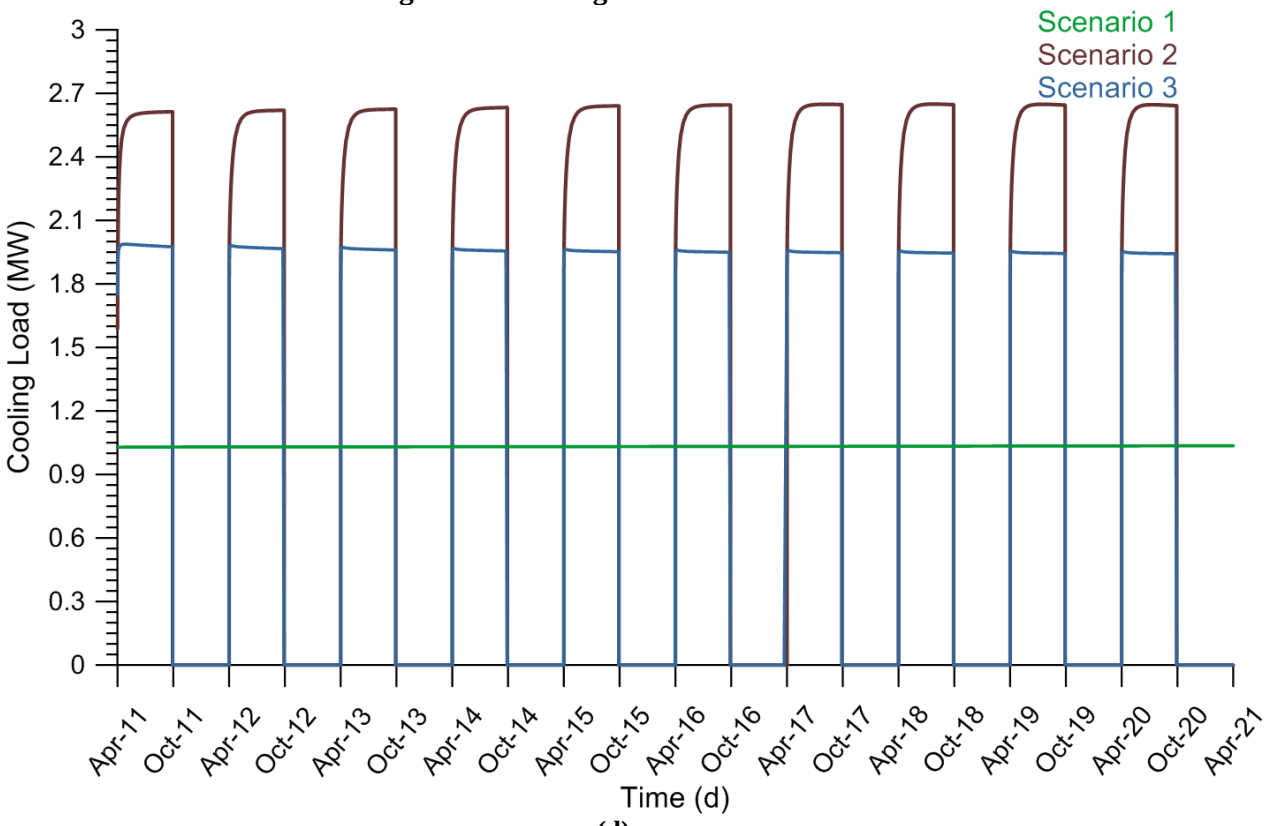

(d)

Figure 51: Cooling load for the three scenarios.

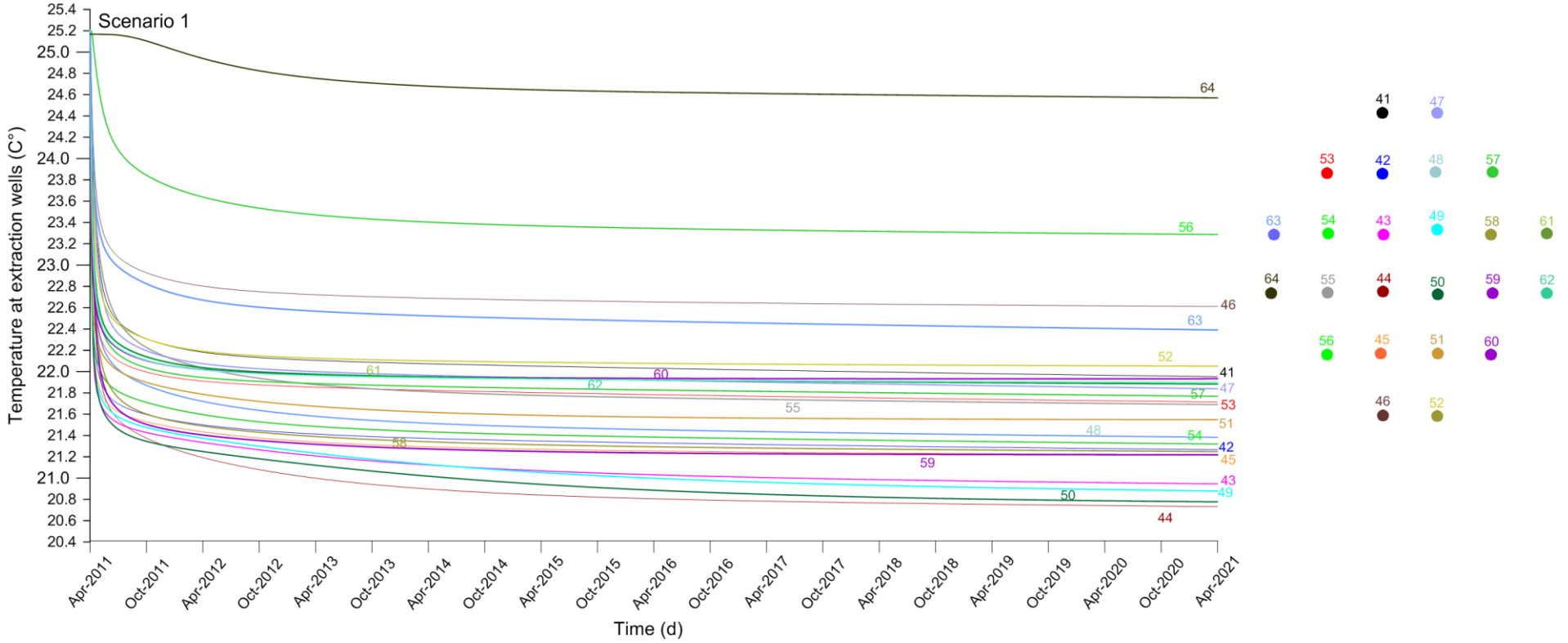

Figure 52: Groundwater temperature at extraction wells in scenario 1.

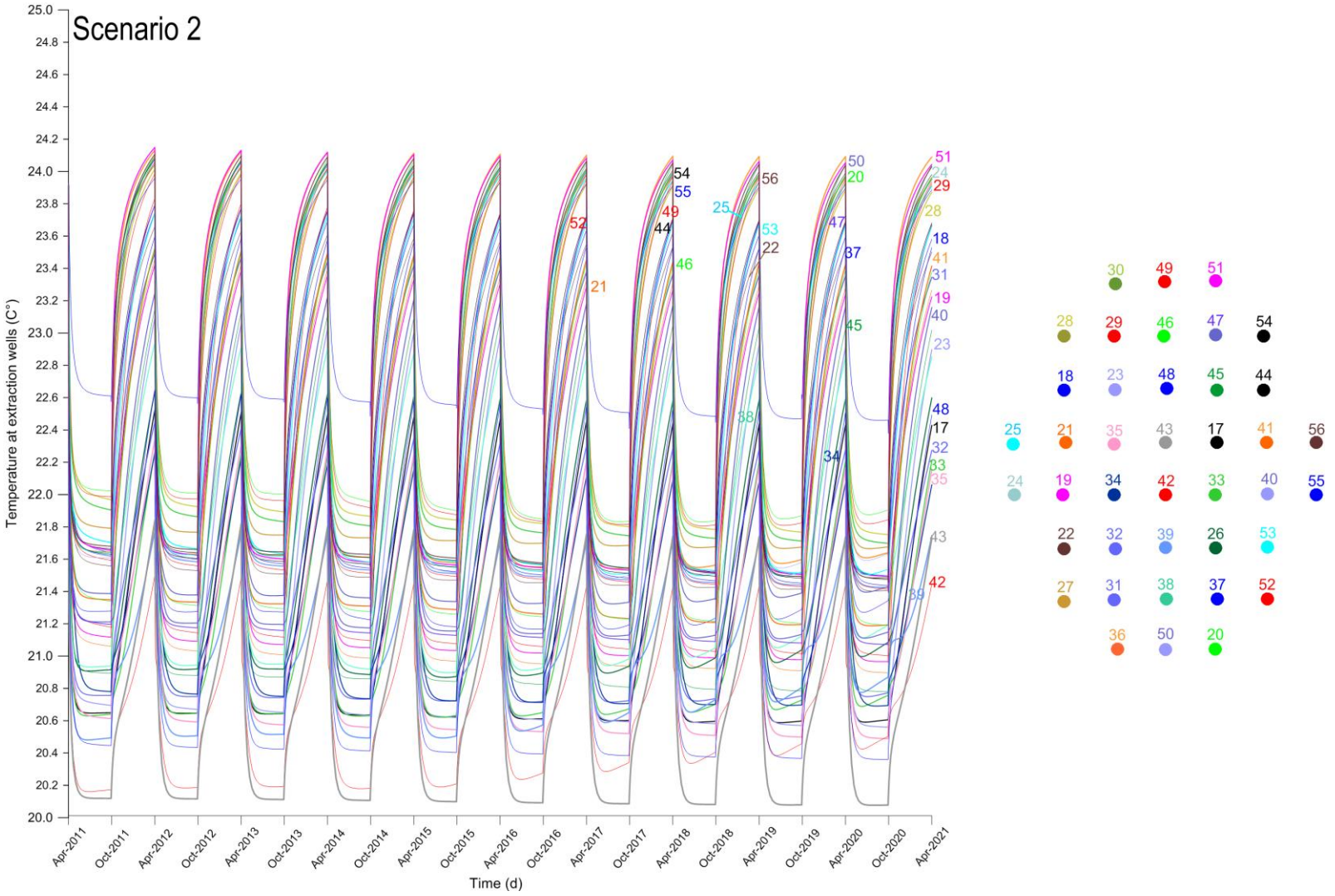

Figure 53: Groundwater temperature at extraction wells in scenario 2.

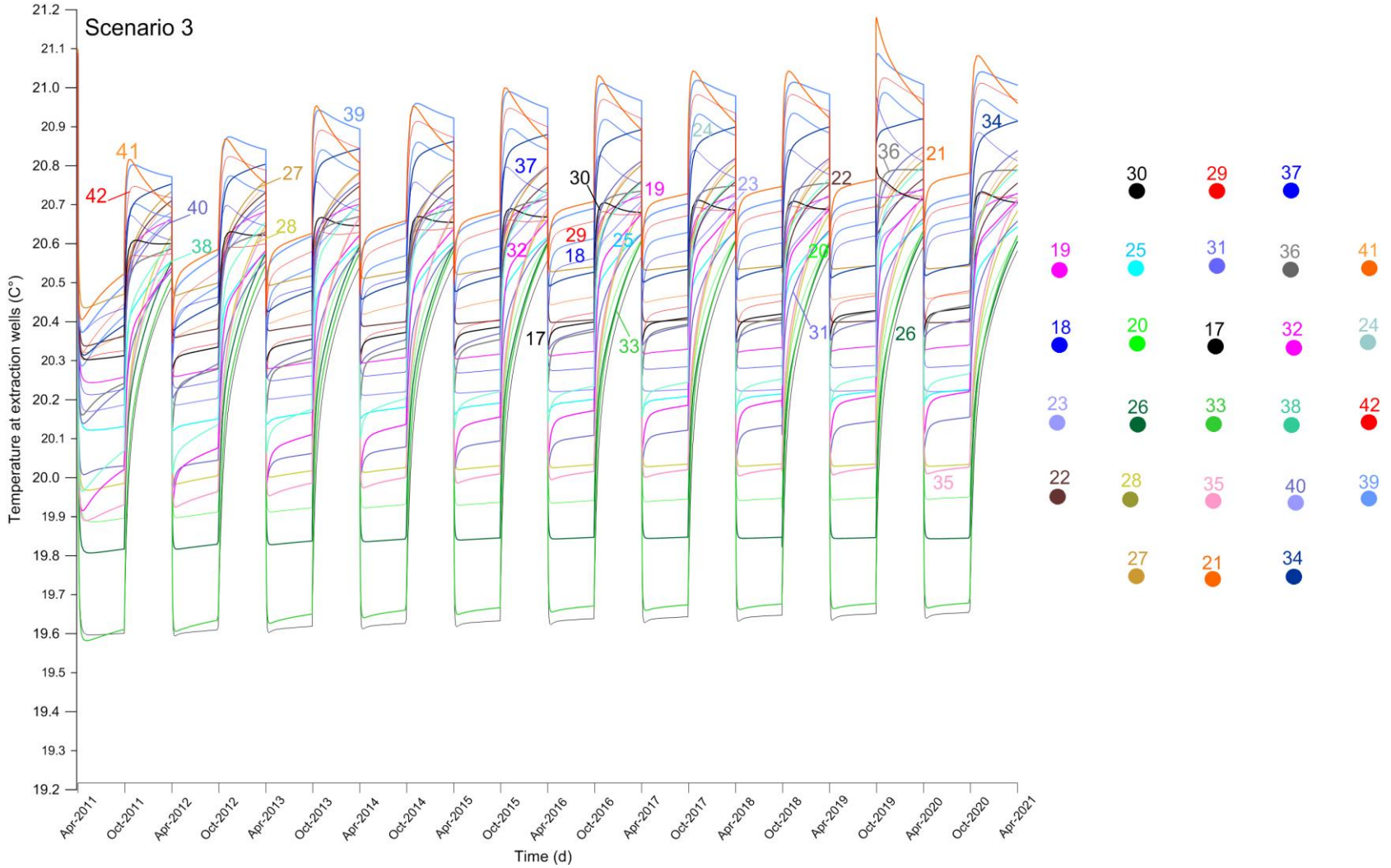

Figure 54: Groundwater temperature at extraction wells in scenario 3.

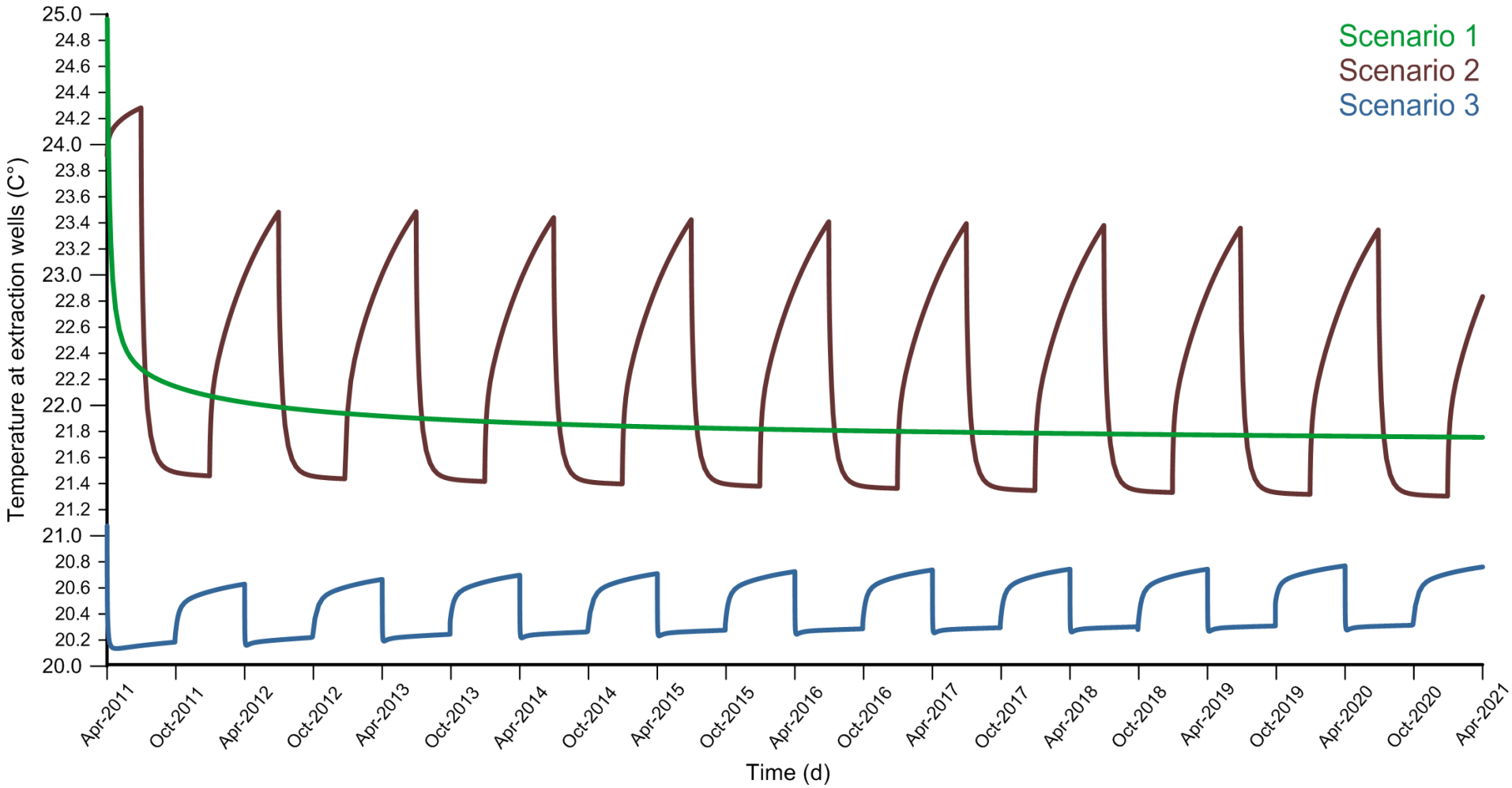

Figure 55: Average groundwater temperature at extraction wells for scenario 1, 2 and 3.

Modeled temperature isolines around extraction and injection wells after simulating 10 years of operation for scenarios 1, 2 and 3 are illustrated in Figs. 56, 57 and 58 respectively. It is evident that the temperature of extracted water is highly dependent on the separating distance between extraction and injection well arrays flow direction (Fig. 42) and well spacing at each array (Table 14). Scenario 1 has the largest separation distance between extraction and injection arrays of about 1,300 m with 25 m spacing between each two successive wells. The required water temperature, which is needed to fulfill the cooling load in this scenario (Table 12), is 22 °C. The actual extracted water temperature from the system at the end of the simulation is expected to be between 23 °C to 25 °C. Of all first three scenarios, this is the smallest temperature difference (Fig. 56) of about 2 to 3 °C between simulated extracted water temperature and the required extracted water temperature.

Scenario 2 has the smallest separation distance, between extraction and injection arrays, among the first three scenarios. This distance which limited here by the space availability (see system design) is approximately 800 m. Well spacing between each two successive wells is 10 m. In addition, the 20 m difference in depth between extraction and injection wells influences the temperature distribution around the extraction array. All these pre-defined factors cause the warm front propagating from the injection array reach the extraction wells. The required water temperature in this scenario is 19 °C. The simulated extracted water temperature from the system at the end of the simulation is expected to be 24 °C .Therefore; this scenario has the highest temperature difference (Fig. 57) of about 5 °C between simulated extracted water temperature and the required extracted temperature between the first three scenarios. This difference lowers the system's potential to fulfill the cooling demand. Therefore a coupled system, i.e. geothermal installation supplemented by a photovoltaic unit, may be required to increase the potential of the cooling system in scenario 2.

The modeled temperature distribution around the extraction wells of scenario 3 (Fig. 58) is directly influenced by the direction of groundwater flow and the limited well spacing (Table 14). In this scenario flow direction has the highest impact on the modeled temperature distribution. The best system installation possible due to space limitations at the site, arranges the injection and extraction well arrays at the same hydraulic head. Space limitations at the location prevent the injection array to be located downstream of the extraction wells, as in the other two scenarios. This, along with the differences in depth between injection and extraction wells (Table 14), avoids contact between the warm front and the extraction array. In this scenario the required water temperature is 19 °C and the simulated extracted water temperature from the system at the end of the simulation period is expected to be between 20 °C to 21 °C. Therefore, scenario 3 has the lowest temperature differences of 1 °C to 2 °C between the simulated extracted water temperature and the required extracted water temperature. The initial results were reported by Al-Zyoud et al. 2012d.

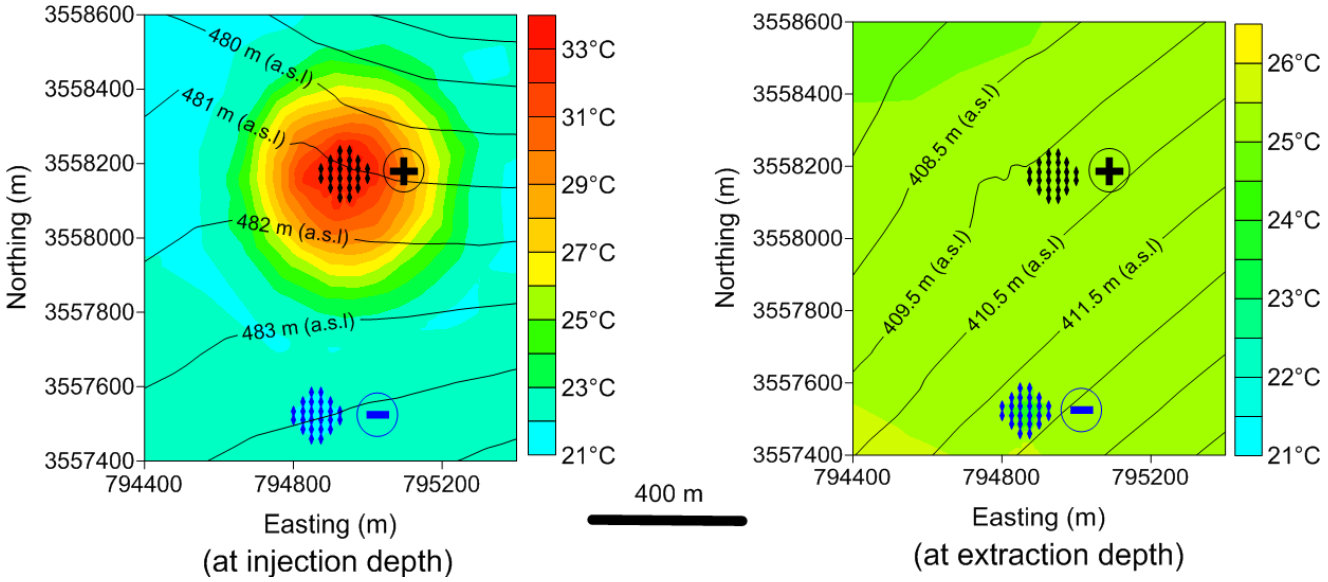

Figure 56: Heat distribution around extraction and injection wells after 10 years of simulation for scenario 1. Black arrays (+) are injection wells and dark blue arrays (-) are the extraction wells.

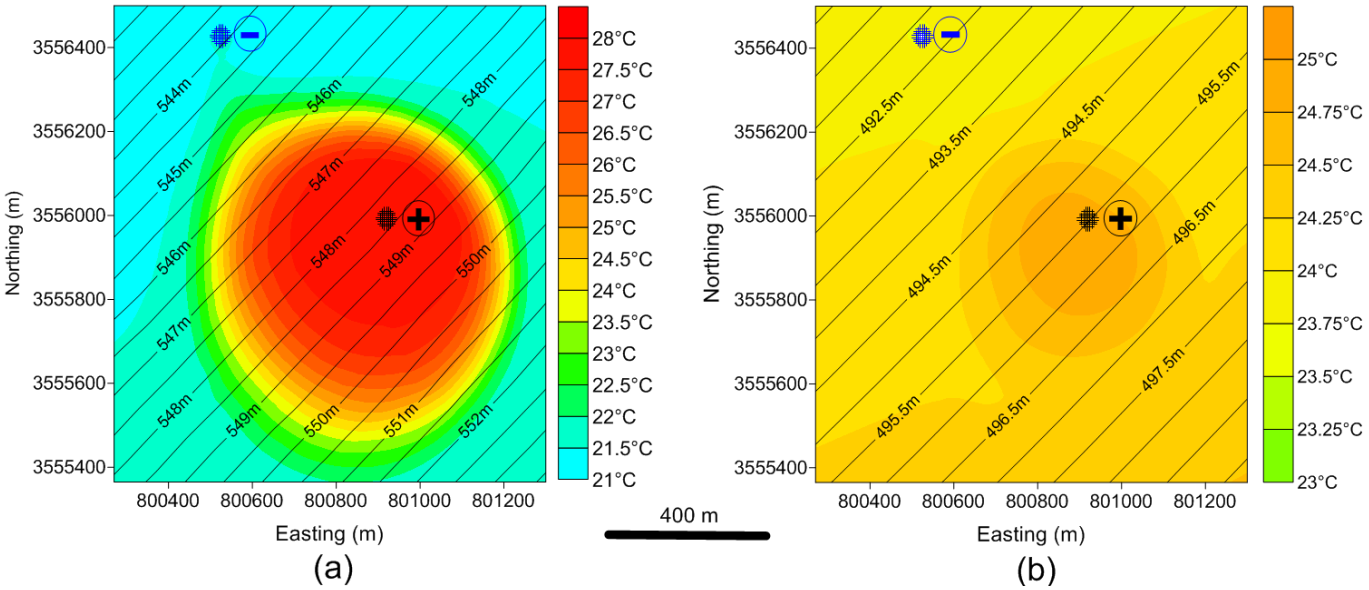

Figure 57: Heat distribution around extraction and injection wells after 10 years of simulation for scenario 2. Black arrays (+) are injection wells and dark blue arrays (-) are the extraction wells.

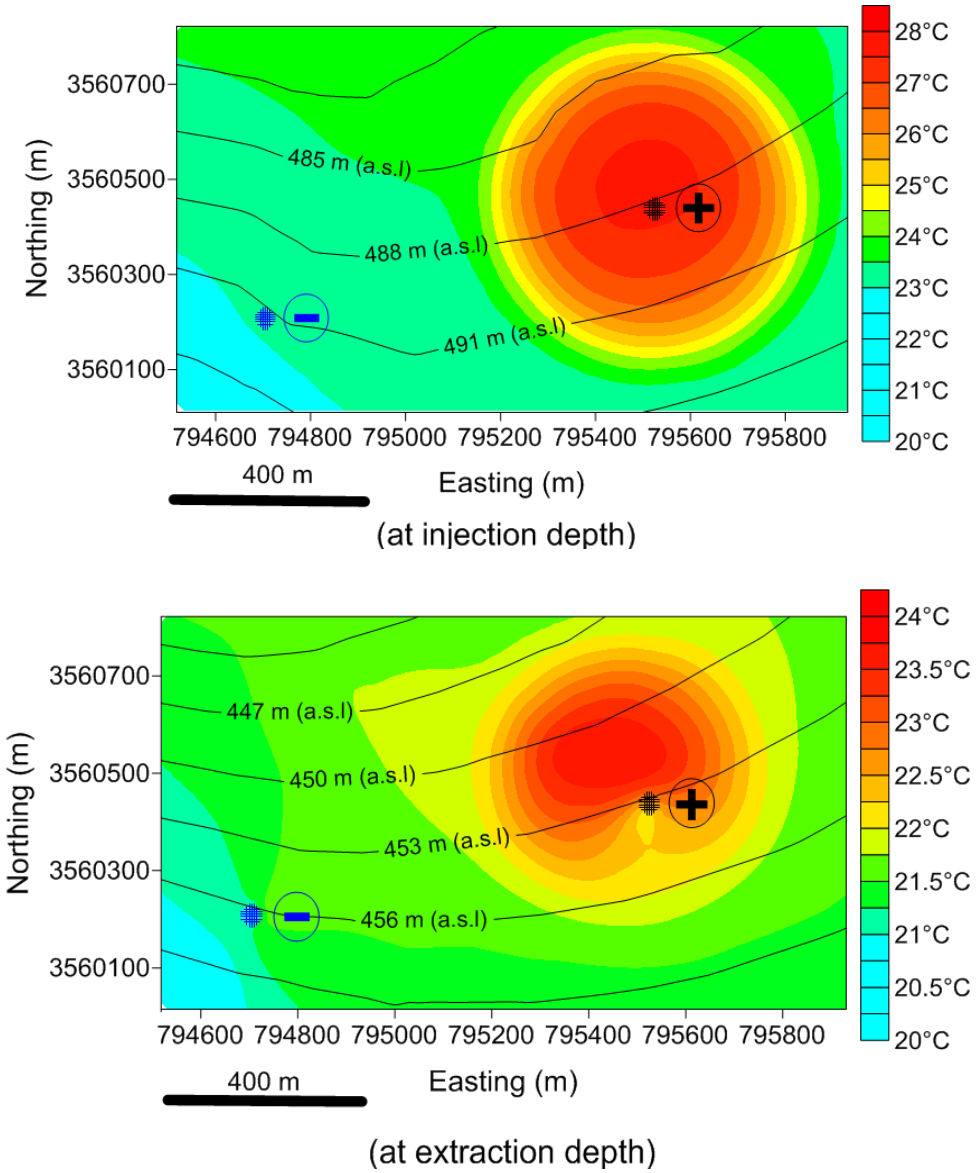

Figure 58: Heat distribution around extraction and injection wells after 10 years of simulation for scenario 3. Black arrays (+) are injection wells and dark blue arrays (-) are the extraction wells.

4.1.2. Scenario 4

Scenario 4 is more dynamically modeled than the previous ones. Here a programmed module is forcing the system to deliver the required cooling load. However, it has to be monitored if the achieved temperatures are still within a reasonable range. Technically the requested cooling load is obtained by assigning a temperature difference of 10 °C to the extracted water before simulation, which gives exactly the requested amount of 1.75 MW cooling load. To allow the subsurface to regenerate, injection and extraction arrays are reversed after every year (Fig. 59). During winter the requested cooling load is halved.

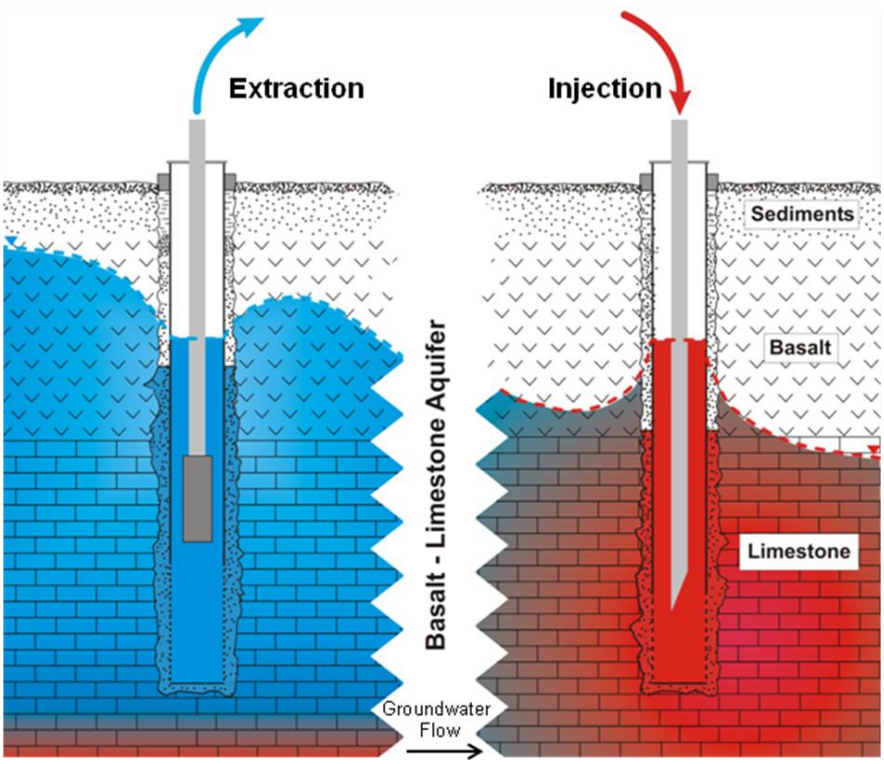

First year operation

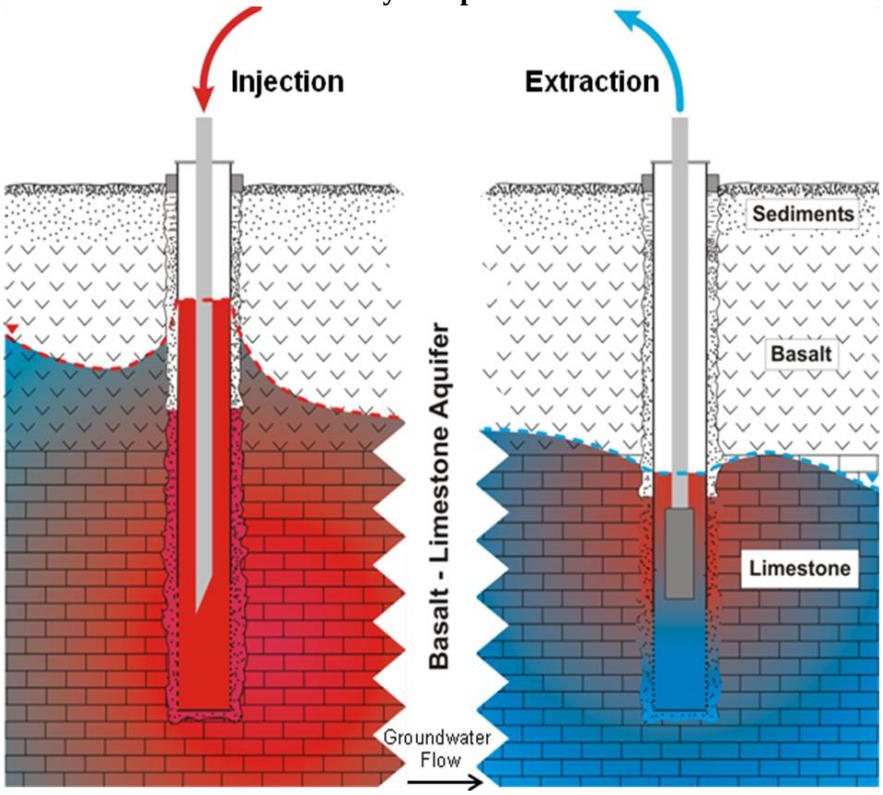

Second year operation

Figure 59: Alternating operation.

To improve this scenario the same setup is computed with an additional night sky cooling, each night of the second half of the year – representing winter time. Technically this is

achieved by injecting the water with 11 °C for 8 hours each night. In the remaining time the original dynamic cooling is simulated.

The resulting temperature distributions for year first, second, fifth, ninth and last, with and without night sky cooling respectively, are depicted in Fig. 60. (a) to (e). Fig. 60 shows the temperature evolution over 10 years for scenario 4, at the extraction array at 25 m depth. As expected, the variation of the temperature at the extraction wells is quite low because the warm water front does not reach the extraction wells position until the end of the simulation and the extracted temperature remains within the required range of 23 °C in winter and 33 °C in summer. Deeper injection wells of 50 m avoid the warm front to reach the extraction wells. The temperature rising in the center of the extraction wells array, however, appears to be much stronger. Hence, the closer the location of the extraction and injection arrays, the more important modeling studies become in terms of investigating the long-term behavior of such geothermal system installations.

In the first year of operation the extracted water has mainly the regular background groundwater temperature. In the following years the temperature at the extraction wells is raised. This is due to the previous operational mode when hot water was injected at the same position.

For this scenario maximum summer requested temperature is approximately 36 °C and 34 °C at the end of winter. Extraction temperatures are between 23 °C - 31 °C. Especially the additional night sky cooling improves the overall performance substantially by reducing the maximum subsurface temperatures at the end of summer to approximately 33 °C and only 28 °C at the end of winter. Extraction temperatures are between 22 °C - 25 °C.

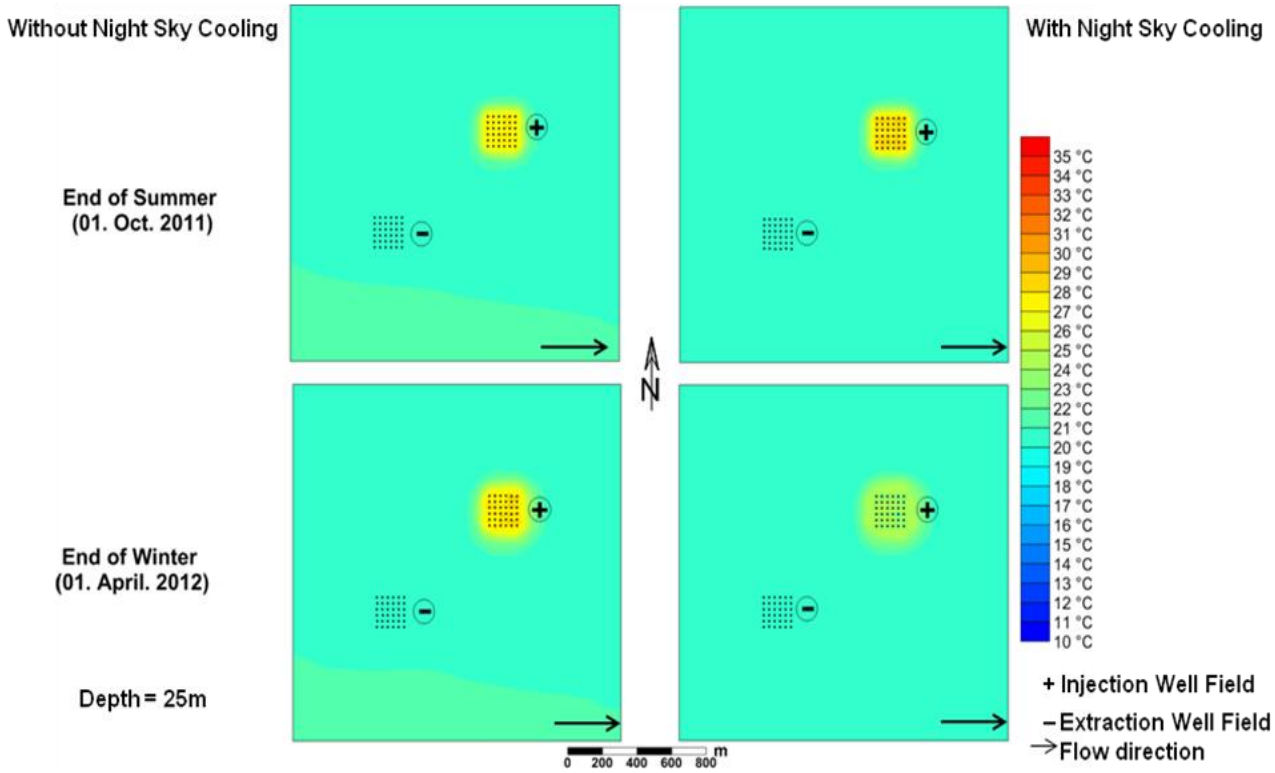
Without Night Sky Cooling
With Night Sky Cooling
End of Summer
(01. Oct. 2011)
End of Winter
(01. April. 2012)
Depth = 25m
N
35 °C
34 °C
33 °C
32 °C
31 °C
30 °C
29 °C
28 °C
27 °C
26 °C
25 °C
24 °C
23 °C
22 °C
21 °C
20 °C
19 °C
18 °C
17 °C
16 °C
15 °C
14 °C
13 °C
12 °C
11 °C
10 °C
+ Injection Well Field
– Extraction Well Field
Flow direction
0 200 400 600 800 m

(a)

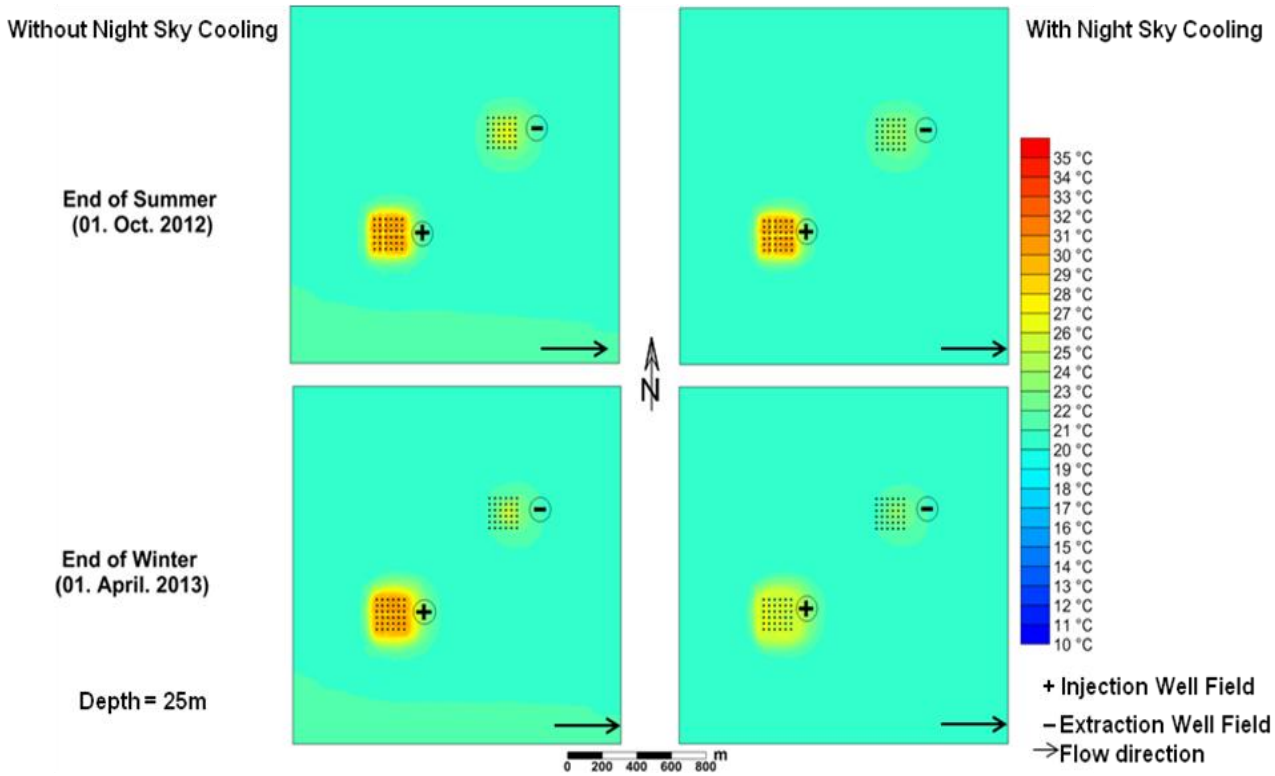
Without Night Sky Cooling
With Night Sky Cooling
End of Summer
(01. Oct. 2012)
End of Winter
(01. April. 2013)
Depth = 25m
N
35 °C
34 °C
33 °C
32 °C
31 °C
30 °C
29 °C
28 °C
27 °C
26 °C
25 °C
24 °C
23 °C
22 °C
21 °C
20 °C
19 °C
18 °C
17 °C
16 °C
15 °C
14 °C
13 °C
12 °C
11 °C
10 °C
+ Injection Well Field
– Extraction Well Field
Flow direction
0 200 400 600 800 m

(b)

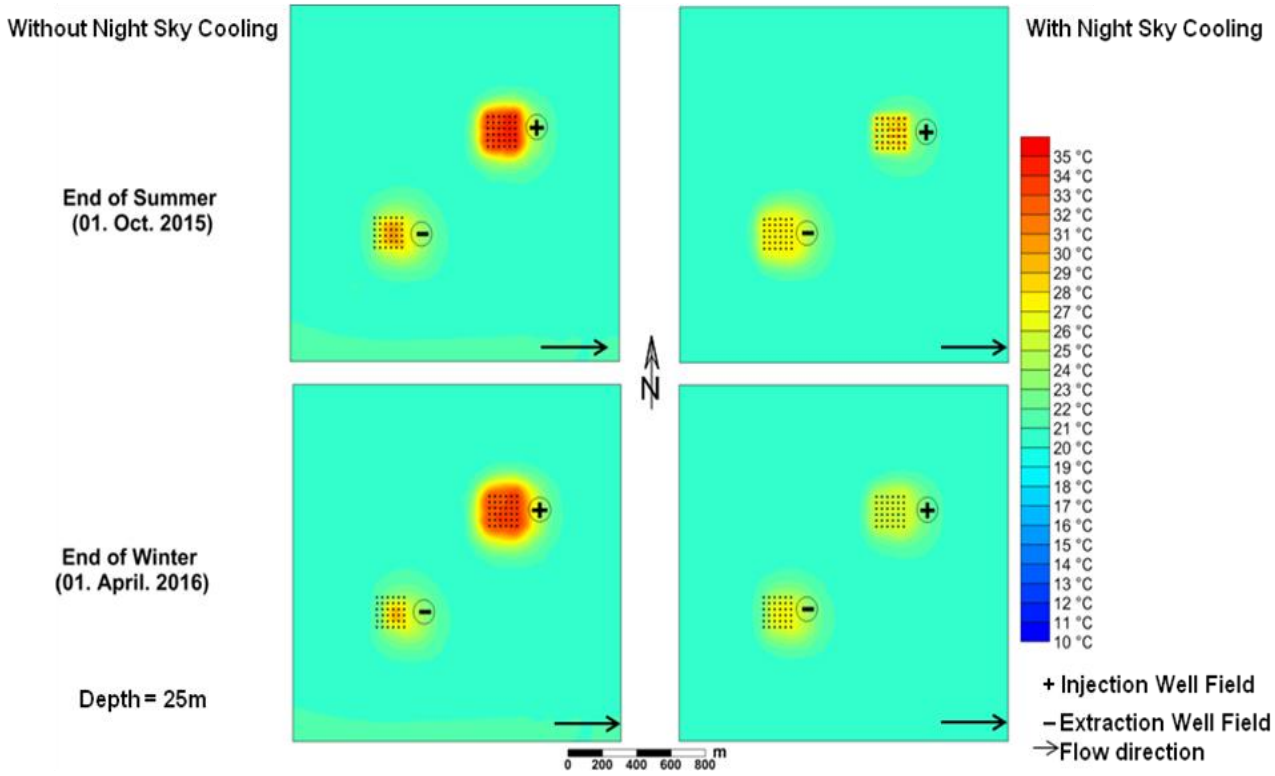
Without Night Sky Cooling
With Night Sky Cooling
End of Summer
(01. Oct. 2015)
End of Winter
(01. April. 2016)
Depth = 25m
N
35 °C
34 °C
33 °C
32 °C
31 °C
30 °C
29 °C
28 °C
27 °C
26 °C
25 °C
24 °C
23 °C
22 °C
21 °C
20 °C
19 °C
18 °C
17 °C
16 °C
15 °C
14 °C
13 °C
12 °C
11 °C
10 °C
0 200 400 600 800 m
+ Injection Well Field
– Extraction Well Field
→Flow direction

(c)

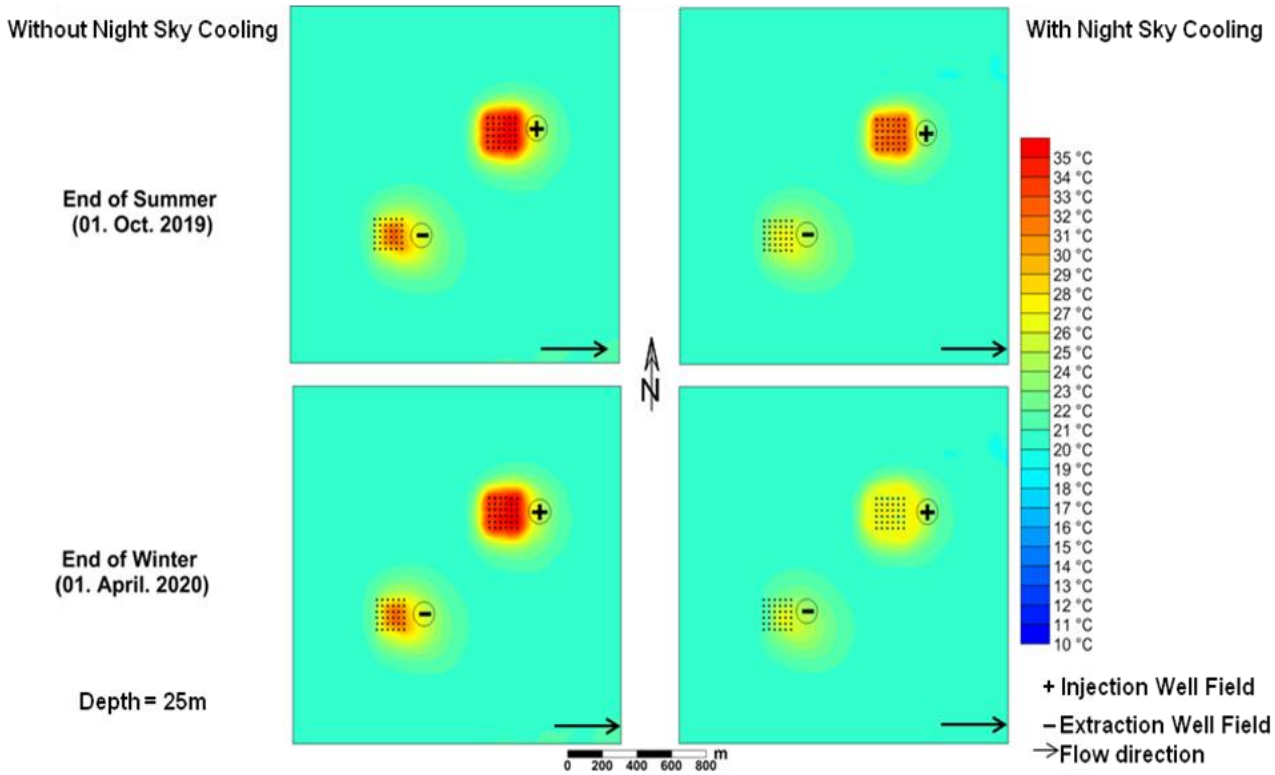
Without Night Sky Cooling
With Night Sky Cooling
End of Summer
(01. Oct. 2019)
End of Winter
(01. April. 2020)
Depth = 25m
N
35 °C
34 °C
33 °C
32 °C
31 °C
30 °C
29 °C
28 °C
27 °C
26 °C
25 °C
24 °C
23 °C
22 °C
21 °C
20 °C
19 °C
18 °C
17 °C
16 °C
15 °C
14 °C
13 °C
12 °C
11 °C
10 °C
0 200 400 600 800 m
+ Injection Well Field
– Extraction Well Field
→Flow direction

(d)

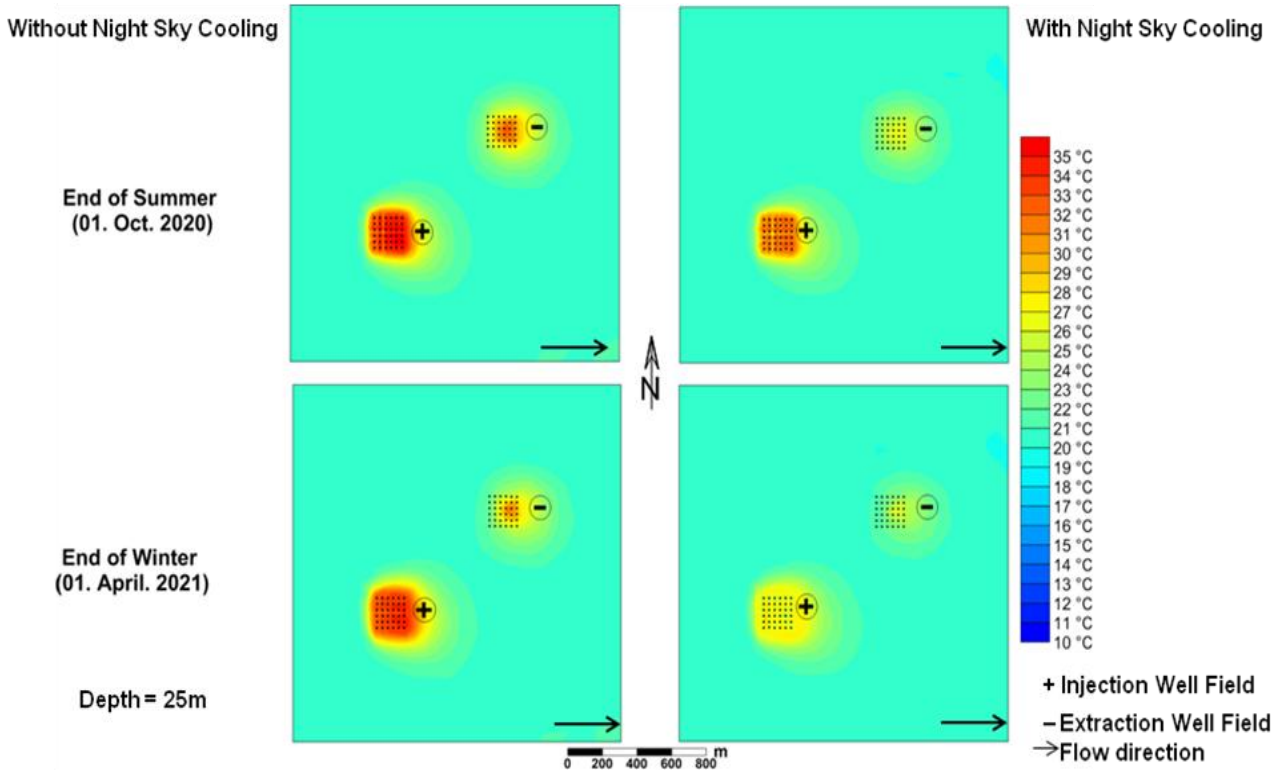

(e)

Figure 60: Temperature distributions of scenario (4) in a depth of approximately 25 m below the surface. The location is according to Figs.33 and 42. (a) the first year, (b) the second year, (c) the fifth year, (d) the ninth year and (e) the last year of simulation.

4.2. Cooling Performance of the Scenarios

Despite the relatively high surface temperatures the cooling system approach presented here satisfies the actual cooling load demands in all cases. The results of the temperature distribution isolines show, under predefined uncertainty, that thermal and hydrological data are valuable for the planning of the utilization of geothermal resources. Large- scale 3D simulation is also crucial for designing shallow geothermal installations. Due to the heterogeneity of the subsurface, the aquifer geometry, and the thermophysical properties, temperature may be deviated from the actual geothermal reservoir temperature. The results of the modeled temperature distribution around the extraction wells can be evaluated to define each scenario performance.

The cooling performance (δ) for each scenario can be calculated based on:

$$\delta = \frac{Qm}{Qd} \cdot 100 \tag{11}$$

Where Q_m is the modeled cooling load and Q_d is the cooling load demand.

The cooling performance of the studied scenarios are given in Table 15 and Fig. 61.

Table 15: Calculated cooling system performance.

Scenario	Performance(%)
1. Power Station	99.5
2. Hashemite University	65
3. Al Hashimiyya City	87
4. Jordan Refinery	by default 100

In scenarios 1 and 3 sufficient cooling loads can be achieved due to different system characteristics; i.e. separation distance, extraction depth, well spacing, demand cooling load…etc (sections 3.7 and 4.1). However, there are several viable options to increase the cooling load of scenario 2, too. Especially the application of so called night sky cooling, as in scenario 4, could increase the overall potential substantially. Another option would be to use electric energy (e.g. by photovoltaic) and to couple heat pumps to the system. Such combined solar and geothermal systems for heating and cooling were previously discussed (Karagiorgas et al., 2003). A third option could be the seasonal heat (cool) storage. Novo et al. (2010) reviewed most studies and results obtained in this particular area. In addition, Paksoy et al. (2000) coupled the solar energy with the seasonal thermal heat storage for heating and cooling utilization.

The result of scenario 4 shows how a dynamic management of the cooling system, by reversing the flow directions annually, can improve the efficiency (for details see section 4.1.2). The temperature increase in the subsurface stays within a reasonable range. Therefore, the system's potential is increased by using this dynamic model and forced to be full efficient for geothermal cooling utilization.

The performance of the other locations in the map view in Fig. 61 are estimated from the results of the first three scenarios. These estimations depend on different pre-defined criteria for each site i.e. groundwater depth, flow direction, hydraulic gradient, cooling load demand

and system scale. For example, Ad Dhulail village (Fig. 61) which has a medium performance has a very deep groundwater table which will affect the extracted water temperature and therefore the system's potential. In contrast, some western villages such as As Shuknah and Umm es Sulayh have higher performance due to very shallow ground water table and a relatively small installation scale.

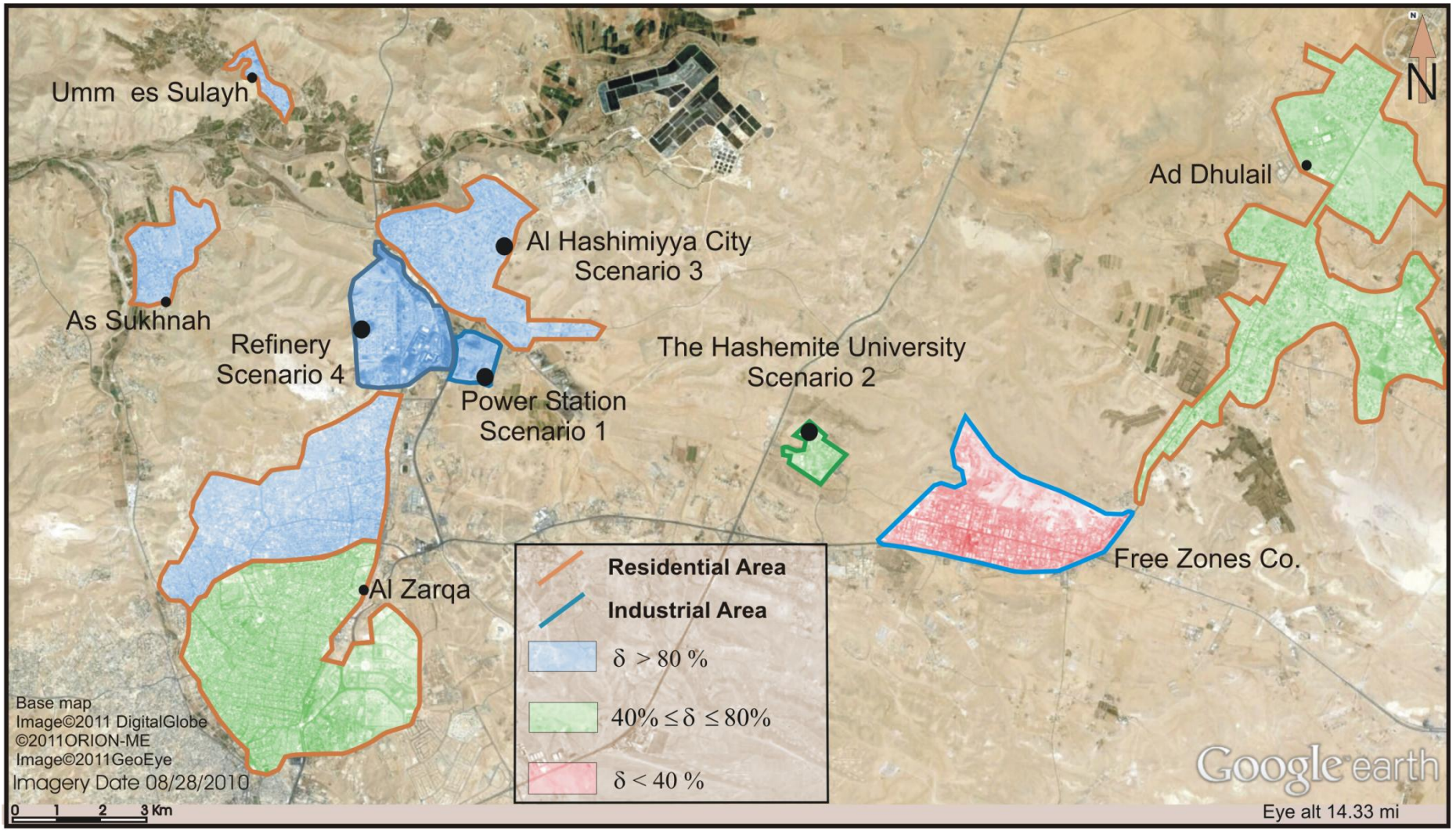

Figure 61: Geothermal cooling potential derived from the results of the numerical modeling (positions are according to Fig. 33).

4.3. Economic and Environmental Feasibility

It is clear that the geothermal systems are one of the most environmentally-sound forms of energy systems available today. There is no other energy system protecting both the local and global environment regarding air emissions, water quality and land use as geothermal energy systems. Compared with the conventional systems used in Jordan, the studied systems in this work if implemented widely are expected to save 520 MWh of electricity consumption for cooling per year (Table 16). Compared with a conventional system of similar size, this geothermal system is expected to reduce CO_2 emissions by 470 tons annually. This estimation is based on a comparison with other newly commissioned systems in Jordan (French Environment and Energy Management Agency, 2003 & 2011 and MENA Geothermal, 2007).

Table 16: Expected annual electricity and CO_2 emission reductions by implementing the geothermal cooling systems.

Scenario	Annual Reduction of CO_2 Emissions (Tons)	Annual Electricity Savings (MWh)
Al Hussein Power Station	94	111
Hashemite University	58	98
Al Hashemiyyia City	45	88
Refinery – Summer	182	215
Refinery – Winter	91	107

In the four geothermal cooling systems, 7.384 $MW \cdot a^{-1}$ will be injected in the system. This system has a mean temperature of 20 °C in summer. This injection is done during approximately 9000 h for scenarios 1 and 4 and 4000 hours for scenarios 2 and 3. During storage approximately 1.88 MW will disappear as storage losses and as a result of this the system temperature will rise by about 2 to 10 °C (scenario1), 2 to 7 °C (scenario 2), 2 to 7 °C (scenario 3), and 3 to 8 °C in different locations (scenario 4).

During summer, approximately 6.864 MW will be required for cooling the four scenarios for the running hours. This will replace the major part of the conventional cooling system and save some 520 MWh of electricity. The electricity needs for pumps in this system will be supplied

from coupled solar panels. It is found that the average COP for cooling systems is 2.4. However, these cooling systems will save oil in the order of 400 m^3a^{-1} during summer.

In winter, a total of 1.8025 MW will be used for cooling the first and fourth scenario during the 9000 running hours. This will replace the whole conventional cooling system and save about 218 MWh of electricity. However, these cooling systems will save oil in the order of 80 m^3a^{-1} during winter.

The environmental benefits from this project will be a reduction in energy consumption as electricity and fuel oil through the replacement of the conventional systems. The savings in fuel oil of 400 m^3a^{-1} in summer and 80 m^3a^{-1} in winter will approximately decrease the CO_2 emissions by 285 $ton \cdot a^{-1}$ in summer and 185 $ton \cdot a^{-1}$ in winter.

5. Conclusions and Outlook

This study has demonstrated the feasibility of shallow geothermal cooling systems to provide the cooling needs of four selected applications; (1) Power station, (2) the Hashemite University, (3) 100 houses in Al Hashimiyya city and (4) the Refinery of Jordan. Realization of the studies scenarios will avoid local CO_2 emissions associated with fuel burning. The hydrogeological characteristics of the reservoir support the four exploitation scenarios that were investigated. Each scenario is designed with an individual pattern of groundwater extraction and injection.

The scope of the study is to estimate the potential of shallow geothermal systems and numerically simulate their response to 10 years of operation, utilizing their cooling potential. 3D simulation using FEFLOW® is very valuable in designing these shallow geothermal installations. Additionally, a 3-D structural model based on field mapping and literature using GOCAD® was created and implemented in the final numerical model. The results of this study present, for the first time, a numerical model for geothermal cooling in Jordan and specifically in the north eastern basaltic desert. The results of the reservoir simulation models are encouraging, as the resulting potential is moderate to high.

The results of this study have to be viewed considering a number of constraints. First of all, the calibration of the models depends on rather sparse hydraulic head and temperature data. This makes it difficult to quantify the absolute uncertainty in both temperature and hydraulic head values. However, field measurements, laboratory measurements, log interpretations, and pumping tests provide an acceptable complementary basis.

Other approximations include the assumption of isotropic and homogeneous permeability and thermal conductivity as well as neglecting the stress field and fracture characteristics at depth. Furthermore, permeability and thermal conductivity data were obtained from existing core sample sparsely collected from outcrops. This encouraged a study on the statistical variation of the thermophysical properties of the reservoir. Thus, the heterogeneity of certain geological units in the 3D domain will be reflected when considering the spatial distribution of thermal conductivity and permeability. This allows a reliable quantification of the uncertainty of the temperature and hydraulic head evolution at the extraction wells. Thereby, this investigation shows an acceptable reliability if all initial conditions are initially satisfied.

This study indicates that the shallow basaltic aquifer in northeastern Jordan could provide the thermal energy required by cooling systems, under pre-defined uncertainties, without causing a significant negative environmental impact. Geothermal installations therefore represent a viable alternative to cooling systems that rely on non-renewable resources. The results may also be included in a future assessment of potential environmental impacts of such systems. The value to the community provided by sustainable and environmentally sound open loop geothermal energy systems should be given a much higher priority when future decisions regarding cooling systems are made in Jordan.

Much effort needs to be focused on the development and application of geothermal systems in Jordan. There are a lot of investigations that need to be done for future study in order to further broaden the applicability of open loop geothermal installations; (1) the chemical and microbiological effects on the groundwater along with the impact of temperature on the ground system have to be investigated in more detail. The temperature increase should be evaluated regarding its effect on groundwater quality, before exploration commences. The influence of

the cooling system on the underground temperature should also be monitored during exploitation, whether the temperature increase of the reservoir is acceptable without endangering the groundwater biochemistry. The temperature increase may cause degasification in the groundwater. (2) Cheaper drilling technology for wells is desirable. This would lower the initial cost and improve the life-cycle performance of the geothermal system. (3) Exploration sites must be chosen according to other important surface and subsurface administrative limitations and circumstances: e.g. heritage protected locations, groundwater protection areas, drinking water, spa zones and areas of vegetation. (4)The simulated models should be further validated by measured field data. To evaluate their accuracy and applicability for engineering practices a comprehensive comparison routinely applied is needed.

References

Abdulagatova, Z., Abdulagatov, I. & Emirov, V., 2009. Effect of Temperature and Pressure on the Thermal Conductivity of Sandstone. *Int. J. Rock Mech. Min. Sci.*, Volume 46, p. 1055–1071.

Abu Qudaira, M., 2004. *The Geology of Zarqa Area, Bulletin 58.* Amman: Natural Resources Authority.

Abu Sharar, T. & Rimawi, O., 1993. Water Chemistry of the Dhuleil Aquifer (Jordan) as Influenced by Long Term Pumping. *Journal of Hydrology,* Volume 149, pp. 49-66.

Abu-Ajamieh, M., 1980. *The Geothermal Resources of Zarqa Ma'in and Zara,* Amman: Natral Resources Authority.

Abu-Aligah, 2011. Design of Photovoltaic Water Pumping System and Compare it with Diesel Powered Pump. *Jordan Journal of Mechanical and Industrial Engineering,* 5(3), pp. 273-280.

Abu-Hamatteh, Z., Al-Zughoul, K. & Al-Jufout, S., 2011. Potential Geothermal Energy Utilization in Jordan: Possible Electrical Power Generation. *Int. J. of Thermal and Environmental Engineering,* 3(1), pp. 9-14.

Abu-Nada, E. et al., 2008. Modeling of a Geothermal Standing Column Well. *International Journal of Energy Research,* 32(4), pp. 306-314.

Akbar Jordan, 2010. *Akbar Jordan, eMarketing Jo, in arabic.* [Online] Available at: http://www.akhbar-jo.com
[Accessed 03 06 2011].

Al Mahamid, J., 2005. *Integration of Water Resources of the Upper Aquifer in Amman – Zarqa Basin Based on Mathematical Modeling and GIS, Jordan,* Freiberg: Freiberg Online Geology.

Al-Dabbas, M., 2009. The Simulation of Performance of Seasonal Heat Storage Coupled to Solar-Assisted Heat Pump in Jordan. *Applied Solar Energy,* 45(2), pp. 83-92.

Al-Dabbas, M., 2011. Achievement of Geothermal Energy Using Ground Heat Exchanger in Ma'in. *Journal of Mechanical Science and Technology,* 25(8), pp. 2013-2023.

Al-Kharabsheh, A. & Al-Mahamid, J., 2002. Optimizing Pumping Rates of Hallabat-Khalidiya Wellfield using Finite-Difference Model: a Case Study for Evaluating Over Pumped Aquifers in Arid Areas (Jordan). *Journal of Arid Environments,* 52(2), pp. 259-267.

Al-Kharabsheh, A. & Al-Malabeh, A., 2002. *Water Harvesting in Wadi Al-Maghyer, Azraq Basin-Jordan and its Environmental Impacts.* Amman, Proceeding of Congress in Urban Developments in Arid region & Associated Problems, 3, 97-106.

Allen, D., 1988. *Prlimiminary Evaluation of the Geothermal Potential of Jordan Recommendations for Future Studies,* Keyworth, UK: BGS, 34p.

Al-Malabeh, A. et al., 2002. Geochemical and mineralogical related magnetic characteristics of the Tertiary – Quaternary (Um Al-Qutein) Basaltic flows from the basaltic field of Hara El-Jabban, Northeast Jordan.. *Physica B: P,* 321(1-4), pp. 396-403.

Al-Malabeh, A., 1993. *The Volcanolgy , Mineralogy and Geochemistry of Selected Pyroclastic Cones from NE – Jordan and their Evolution for Possible Industrial Applications, PhD thesis.* Erlangen: Erlangen University.

Al-Malabeh, A., 2011. New subdivision of Jordanian Harrat: A spatial and Temporal distribution and their source regions. *Earth Science and Engineering,* Volume 1, (in press).

Al-Malabeh, A. & Kempe, S., 2009. Petrolithology of the Permian Melaphyre lavas. Darmstadt, Germany. *N. Jb. Geol. Paläont. Abh,* 252(2), pp. 129-143.

Al-Mashagbah, A., 2010. *Computer (Geostatistical, GIS, Remote Sensing) and Isotopes Applications for Modeling the Spatial and Temporal Variations of the Environmental Pollutannts in the Amman - Zarqa Basin (Basalt area), PhD Thesis.* Amman: University of Jordan.

Al-Weshah, R., 1992. Jordan's Water Resources: Technical Perspective. *Water International,* 17(3), pp. 124-132, doi: 10.1080/02508069208686132..

Al-Zyoud, S., Al-Malabeh, A., Ferreiro Mählmann, R. & Sass, I., 2012c. Predicting thermal conductivity of flood basalts controlled by mineral volume proportion, a case study in north east Jordan. *in prep.*

Al-Zyoud, S., Rühaak, W. & Sass, I., 2012a. Over Exploitation of Groundwater in the Center of Amman Zarqa Basin - Jordan. *Ground Water , in prep.*

Al-Zyoud, S., Rühaak, W. & Sass, I., 2012b. *The Potential of Shallow Groundwater Resources for Cooling Purposes - a Geothermal Case Study in North East Jordan.* Stanford, CA, USA, Stanford University.

Al-Zyoud, S., Rühaak, W. & Sass, I., 2012d. Dynamic numerical modeling of the usage of groundwater for cooling in north east Jordan - a geothermal case study. *Renewable Energy,* p. in press.

Al-Zyoud, S. & Sass, I., 2010. *Thermophysical Properties of Flood Basalts as Prospective Geothermal Reservoirs: Case Study Harrat Al Shaam, Jordan.* Berlin, 18. Tagung für Ingenieurgeologie.

Anderson, M., 2005. Heat as a Ground Water Tracer. *Ground Water,* 43(6), p. 951–968.

Artmann, N., Manz, H. & Heiselberg, P., 2008. Parameter Study on Performance of Building Cooling by Night-Time Ventilation. *Renewable Energy,* Volume 33, pp. 2589- 2598.

Bani-Domi, M., 2005. Trend Analysis of Temperature and Precipitation in Jordan. *Umm Al-Qura University Journal of Educational , Social Sciences & Humanities,* 17(1), pp. 15-36.

Barberi, F. et al., 1979. Recent basaltic volcanism of Jordan and its implication on geod ynamic history of Dead sea shear zone. *Inter. Symp. Geody. Evol. of the Afro-Arabian Rift System,* pp. 667-687.

Bear, J., 1972. *Dynamics of Fluids in Porous Media.* New York, NY: American Elsevir Publishing Co., 761p.

Bär, K, 2012. Untersuchung der tiefengeothermischen Potenziale von Hessen, PhD thesis, 2012.

Bender, F., 1974. *Geology of Jordan.* Hannover: Natural Resources Authority and German Geological Mission in Jordan, 196 p.

Bieske, E., 1988. *Bohrbrunnen.* München: Oldenbourg Verlag.

Birch F and Clark H (1940) The thermal conductivity of rocks and its dependence upon temperature and composition. American Journal of Science. 238:529-558.

Birtles, A., Kolokotroni, M. & Perera, M., 1996. Night Cooling and Ventilation Design for Office-Type Building. *WREC,* pp. 259- 263.

Blöcher, M. Z. G. et al., 2010. 3D Numerical Modeling of Hydrothermal Processes During the Lifetime of a Deep Geothermal Reservoir. *Geofluid,* Volume 10, pp. 406-421.

Boyce, P. & Doreen Fitzsimmons, P., 2003. *Open Loop Geothermal Well Systems on Long Island.* New York,, The 10th Conference on Geology of Long Island and Metropolitan New York, April 1-13.

Camp, V. and Roobol, M. (1989): "The Arabian continental alkali province : part I , Evaluation of Harrat Rahat , kingdom of Saudi Arabia" – Geol .Soc .Am . Bull, 101: 71-95.

Cebrià, J.M., Lopez-Ruiz, J., 1995. Alkali basalts and leucitites in an extensional intracontinental plate setting: the late Cenozoic Calatrava volcanic province (central Spain). Lithos 35, 27–46.

Chaurette, J., 2008. *Cintrifugal Pump System Tuturial.* .:http://www.lightmypump.com/tutorial2.htm#energy_and_head.

Chayes, F (1956) Petrographic Modal Analysis. John Wiley and Sons, Inc., New York.

Clauser, C., 1992. Permeability of crystalline rocks. *EOS transactions American Geophysical Union,* 73(21), pp. 237-238.

Clauser, C. & Huenges, E., 1995. Thermal Conductivity of Rocks and Minerals. In: T. J. Ah¬rens (ed), Rock Physics and Phase Relations - a Handbook of Physical Constants. *AGU Reference Shelf, American Geophysical Union, Washington,* Volume 3, pp. 105-126.

Coombs, D. S. 1963. Trends and affinities of basaltic magmas and pyroxene as illustrated on the diopside-olivine-silica diagram.—Mineral Soc. Am., Spec. Paper, 1: 227-250.

Dan, P. C. C., 1989. The Cooling of Water Flowing Over an Inclined Surface Exposed to the Night Sky. *Solar and Wind Technology,* 6 (1), pp. 41-50.

Davis, S. & Turk, L., 1964. Optimum Depth of Wells in Crystalline Rocks. *Ground Water,* Volume 2, pp. 6-11.

Department of Statistics, 2010. *Department of Statistics, Jordan in Figures.* [Online] Available at: http://www.dos.gov.jo/dos_home_e/main/linked-html/jordan_no.htm [Accessed 23 February 2012].

DHI-WASY, 2012. *What is FEFLOW?.* [Online] Available at: http://www.feflow.info/ [Accessed 05 03 2012].

Di. Paola, G., 1981. *Mission report on Visit to the Geothermal Project JOR/76/004 in the Hashemite Kingdom of Jordan from 30 November to 4 December 1981,* New York: UN/DTCD.

Diabat, A., 2004. *Structural Map of Jordan, Unpublished report,* Amman: Natural Resources Authority.

Diabat, A. & Masri, A., 2002. *Structural Framework of Central Jordan - Geothermal Project of Central Jordan,* Amman: Mapping Div., Geol. Directorate. Natural Resources Authority.

Diersch, H.-J., 2005. *FEFLOW Finite Element Subsurface Flow and Transport Simulation System," Reference Manual, WASY.* Berlin: Institute of Water Resources Planning and Systems Research, p.292.

Diersch, H.-J.et al., 2011a. Finite Element Modeling of Borehole Heat Exchanger Systems: Part 1. Fundamentals. *Computers and Geosceinces,* 37(8), pp. 1122-1135.

Diersch, H.-J.et al., 2011b. Finite element modeling of borehole heat exchanger systems: Part 2. Numerical simulation. *Computers and Geosciences,* 37(8), p. 1136–1147.

Diersch, H.-J., Rühaak, W., Schätzl, P. & Renz, A., 2008. *A New Method for Modelling Geothermal Heat Exchangers in Shallow Aquifer Systems.* Graz, Proc. of Conf. on Numerische Grund Wasser Modellierung (GWM).

Dobson, R., 2005. Thermal Modelling of a Night Sky Radiation Cooling System. *Journal of Energy in Southern Africa,* 16(2), pp. 20-31.

Dottridge, J. & Abu Jaber, N., 1999. Groundwater Resources and Quality in Northeastern Jordan: Safe Yield and Sustainability. *Appl. Geography,* Volume 19, pp. 313-323.

Downes, H., Seghedi, I., Szakaćs, A., Dobosi, G., James, D.E., Vaselli, O., Rigby, I.J., Ingram, G.A., Rex, D. and Pećskay, Z., 1995.Petrology and geochemistry of the late Tertiary/Quaternaryn mafic alkaline volcanism in Romania. Lithos 35, 65-81.

Driscoll, F.G. 1986. Ground Water and Wells, 2nd edition. Johnson Division, St. Paul, Minnesota, 1089 pp.

Eicker, U. & Vorschulze, C., 2009. Potential of Geothermal Heat Exchangers for Office Building Climatisation. *Renewable Energy,* Volume 34, pp. 1126-1133.

El Sayed, A. M. A., 2011. Thermophysical Study of Sandstone Reservoir Rocks. *J. of Petrol Sci. and Engineering,* Volume 76, pp. 138-147.

El-Naqa, A., Al-Momani, M., Kilani, S. & Hammouri, N., 2007. Groundwater Deterioration of Shallow Groundwater Aquifers Due to Overexploitation in Northeast Jordan. *Clean,* 35(2), pp. 156-166.

Fardous, A., Mudabber, M., Jitan, M. & Badwan, R., 2004. *Jordan National Report - Harnessing Salty Water to Enhance Sustainable Livelihoods of the Rural Poor in Four Countries in West Asia and North Africa: Egypt, Jordan, Syria and Tunisia* , Amman: Ministry of Agriculture / National Center for Agricultur Research and Technology Transfere.

Florides, G., Christodoulides, P. & Pouloupatis, P., 2012. An Analysis of Heat Flow Through a Borehole Heat Exchanger Validated Model. *Applied Energy,* Volume 92, pp. 523-533.

Floyd, P.A. and Winchester, J.A. 1975.Magma type and tectonic setting discrimination using immobile elements. Earth and Planetary Science Letters ; 27:211-218.

Franzson, H., Guðlaugsson, S. Þ. & Friðleifsson, G., 2001. *Petrophysical Properties of Icelandic Rocks.* Trondheim, Norway, Proceedings of the 6th Nordic Symposium on Petrophysics.

Freiwan, M. & Kadioglu, M., 2007. Spatial and Temporal Analysis of Climatological Data in Jordan. *International Journal of Climatology,* Volume 28, pp. 521-535.

French Environment and Energy Managaement Agency, A., 2003. *ADEME.* [Online]
Available at: http://www2.ademe.fr/servlet/getDoc?id=11433&m=3&cid=96
[Accessed 16 03 2012].

French Environment and Energy Managaement Agency, M., 2011. *A tool for companies and office activities: the "Carbon Inventory" of ADEME.* [Online]
Available at: http://www.manicore.com/anglais/missions_a/carbon_inventory.html
[Accessed 16 03 2012].

Fuchs, H. U., 2010. *The Dynamics of Heat; a unified approach to thermodynamics and heat transfer.* 2nd ed. New York: Springer Science + Business Media, LLD.

Galanis, S., Sass, J., Munroe, R. & Abu-Ajamieh, M., 1986. *Heat Flow at Zarqa Ma'in and Zara and a Geothermal Reconnaissance of Jordan,* s.l.: U.S. Geol. Survey.

Garaibeh, A., 2008. *Heat Source Study and Geothermal Reservoir Assessment for the Zarqa Ma'in - Dab'a Area, Central Jordan,* Orkustofnun, Iceland: Geothermal Training Programme.

Goggin, D., 1988. *Geologically Sensible Modelling of the Spatial Distribution of Permeability in Eolian Deposity: Page Sandstone (Jurassic), northern Arizona.* s.l.:University of Texas, Austin, 417p.

Griffiths, C., N.R., B., R., B. & Castillo, D., 1992. Thermal Conductivity Prediction from Petrophysical Data: a Case Study,. *Geological Society, London, Special Publications January 1,* Volume 65, pp. 299-315, DOI: 10.1144/GSL.SP.1992.065.01..

Grundfos, 2012. *Grundfos web caps.* [Online]
Available at: http://net.grundfos.com/Appl/WebCAPS/custom?userid=GWS
[Accessed 02 06 2012].

Hakki, W. & Teimeh, M., 1981. *The Geology of Zarqa Ma'in and Zara Areas, Bulletin,* Amman: Natural Resources Authority.

Hartmann, A., Rath, V. & Clauser, C., 2005. Thermal Conductivity from Core and Well Log Data. *Int. J. Rock Mech. Min. Sci.,* Volume 42, pp. 1042-1055.

Hashin, Z. & Schtrickman, S., 1962. A Variational Approach to the Theory of Effective Magnetic Permeability of Multiphase Materials. *J. Appl. Phys,* Volume 33, pp. 3125-3131.

Hole, H., 2008. *Geothermal Well Design - Casing and Wellhead.* Dubrovnik, Croatia, Petrolum Engineering Summer School.

Horai, K., 1991. Thermal Conductivity of Hawaiian Basalts: a New Interpretation of Robertson and Peck`s Data.. *J., Geophys., Res.,* Volume 96, pp. 4125-4132.

Hughes, C., 1982. *Igneous Petrology.* New York: Elsevier Scientific Pub. Co., 551p.

Hunting technical services Ltd. & partners, S. M. M. &., 1965. *Wadi Dhuleil investigation,* Herts, London: (Unpubl.), Report,.

Hwang, Y. et al., 2009. Cooling Performance of a Vertical Ground-Coupled Heat Pump System Installed in a School Building. *Renewable Energy,* Volume 34, pp. 578-582.

Ibrahim, K., 1993. *The Geological Frame Work for Harrat Ash-Shaam Basaltic, Super Group and Its Volcanotectonic Evolution. Bulletin 25.* Amman: Natural Resources Authority.

Ilani, S. et al., 2001. New KAr Ages of Basalts from the Harrat Ash Shaam Volcanic Field in Jordan: Implications for the Span and Duration of the Upper Mantle Upwelling Beneath the Western Arabian Plate. *Geology,* Volume 29, pp. 171- 174.

İnallı, M. & Esen, H., 2005. Seasonal Cooling Performance of a Ground-Coupled Heat System in a Hot and Dry Climate. *Renewable Energy,* Volume 30, pp. 1711-1424.

International Geothermal Association, I., 2012. [Online]
Available at:
http://www.geothermalenergy.org/205,welcome_to_our_page_with_data_for_jordan.html
[Accessed 07 03 2012].

Irvine, I. & Barger, W., 1971. A gide to the chemical classification of the common volcanic rocks. *Can.J. Earth Sci.,* Volume 8, p. 528_548.

Iturrino, G. et al., 2000. Permeability, Electrical and thermal Properties of Sulfide, Sedimentary, and Basaltic Units from the Bent Hill Area of Middle Valley, Juan de Fuca Ridge. *Zierenberg, R.A., Fouquet, Y., Miller, D.J., and Normark, W.R. (Eds.),* Volume 169, pp. 1-42.

Jaynes, E., 1990. Temperature variation effects on field measured infiltration. *Journal os Soil Science Society of America,* 54(2), pp. 302-312.

Jessop, A., 2008. Models of Thermal Conductivity of Crystalline Rocks. *Int. J. Earth Sci. doi: 10.1007/s00531-007-0214-y.*

Jordan Meteorological Department, J., 2011. *Archive.* Amman: Jordan Meteorological Department.

Kabariti, M., 2005. *Identification of National Energy Policies and Energy Access in Jordan,* Amman: National Energy Research Center / Energy Research Group / Report 52p.

Karagiorgas, M., Mendrinos, D. & C., K., 2003. Solar and Geothermal Heating and Cooling of European Centre for Public Law Building in Greece. *Renewable Energy,* Volume 29, pp. 461-470.

Kerr, P.F., 1977. Optical Mineralogy. 442pp, 416 Fig., 10 Tab; New York.

Kolin, S., Golob, M. & Rajkovic, D., 2002. *Impact of the Heat Power on the unit Geothermal Energy Cost.* Cologne, Germany, World Renewable Energy Congress VII.

Le Maitre, et al., 2002. *Igneous Rocks: A Classification and Glossary of Terms.* Cambridge: Cambridge University Press.

Lund, J., Freeston, D. & Boyd, T., 2010. *Direct Utilization of Geothermal Energy 2010 Worldwide Review.* Bali, Indonesia, World Geothermal Congress.

Macdonald, G.A. and Katsura, T., 1964: Chemical composition of Hawaiian lavas: J. Petrol., 5: 82-132.

MacDonald, S. M. a. P., 1965. *East Bank Jordan Water Resources,* Amman - Jordan: Central Water Authority/ unpublished report .

Magri, F., Akar, T., Gemici, U. & Pekdeger, A., 2010. Deep Geothermal Groundwater Flow in the Seferihisar - Balcova area, Turkey: Results from Transient Numerical Simulations of Coupled Fluid Flow and Heat Transport Processes. *Geofluids,* pp. 388-405, doi:10.1111/j.1468-8123.2009.00267.x.

Margane, A., Hobler, M., ALmomani, M. & Subah, A., 2002. Contributions to the Hydrogeology of Northern and Central Jordan. *Geologisches Jahrbuch, C,* Volume 68, p. 52.

Marinelli, G., 1977. *Report on the Possibility of Developing Geothermal Resources in Jordan,* s.l.: University of Piza.

Mason, M., Al-Muhtaseb, M. & Al-Widyan, M., 2009. The Energy Sector in Jordan - Current Trends and the Potential for Renewable Energy. *Renewable Energy in the Middle East,* pp. 41-54, DOI 10.1007/978-1-4020-9892-5_3.

McNitt, S., 1976. *Geothermal Resources in Jordan- Interpretation of Data Submitted by the Government,* s.l.: UNDP.

MENA-Geothermal, 2007. *MENA Geothermal.* [Online]
Available at:
http://www.menageothermal.com/University%20of%20Madaba%20in%20Jordan.htm
[Accessed 10 03 2012].

Mertoglu, K., Ozbek, T. & Kara, H. K. N., 2000. Present Situation of Geothermal Energy in the World and in Turkey. *Turkish J Geothermal,* Volume 2, pp. 13-17.

Micromeritics, 2012. *Combining Skeletal and Envelope Volume Measurement..* [Online] Available at: http://www.micromeritics.com/Pressroom/Press-Release-List/Combining-Skeletal-and-Envelope-Volume-Measurements-to-Determine-Total-Pore-Vol
[Accessed 01 04 2012].

Mielke, P., Bignall, G. & Sass, I., 2010. *Permeability and Thermal Conductivity Measurements of Near Surface Units at the Wairakei Geothermal Field. New Zealand.* Bali, Indonesia, World Geothermal Congress 2010.

Minisrty of Energy and Mineral Resources, M., 2008. *Annual Report.* Amman: MEMR, 64p.

Ministry of Energy and Mineral Resources, M., 2010a. *Annual Report.* Amman: MEMR, 68p.

Ministry of Energy and Mineral Resources, M., 2010b. *Archive files and personal communications.* Amman.

Ministry of Water and Irrigation, M., 2000. *Outline Hydrogeology of the Amman – Zarqa Basin,* Amman: Ministry of Water and Irrigation, MWI.

Ministry of Water and Irrigation, M., 2010. *Personal Commun ications and Internal Files.* Amman: MWI.

Misstear, B., D., B. & Clark, L., 2006. *Water Wells and Boreholes.* Chichester, England: John Wiley & Sons.

Moffat, D., 1988. *A volcano tectonic analysis of the Cenozoic continental basalts of northern Jordan: implications for hydrocarbon prospectivity in the block B area.,* Swanson, UK: Unpubl. Report Unirersity college of Swanson. UK, 73p., 40Fig.,2 Tab..

Morimoto, N., Fabries, J., Ferguson, A. K., Ginzburg, I. V., Ross, M., Seifert, F. A., Zussman, J., Aoki, K. and Gottardi, G., 1988. Nomenclature of pyroxene. –Mineral. Petrol., 39: 55-76, 7 Fig., 5Tab., Wien.

Mottaghy, D., Pechnig, R. & Vogt, C., 2011. The Geothermal Project Den Haag: 3D Numerical Models for Temperature Prediction and Reservoir Simulation. *Geothermics,* Volume 40, pp. 199-210.

Mouty, M., Delaloye, M. Fontigrie , D., Piskin, O. & Wagner, J. (1992): The volcanic activity in Syria and Lebanon between Jurrassic and Actual,……Schweiz Mineral. Petrol. Mitt. 72:91-105,13Fig., 3Tab. ,Zurich.

Myslil, V., 1988. *The Evaluation of Geothermal Potential of Jordan,* Amman: Natural Resources Authority, NRA, 43p.

Nam, Y. & Ooka, R., 2010. Numerical Simulation of Ground Heat and Water Transfer for Groundwater Heat Pump System Based on Real-Scale Experiment. *Energy and Buildings,* Volume 42, pp. 69-75.

Nam, Y. & Ooka, R., 2011. Development of Potential Map for Groundwater Heat Pump Systems and The Application to Tokyo. *Energy and Buildings,* Volume 43, pp. 677-685.

National Capacity Self Assessment for Global Environmental Management, N., 2006. *An Environmental Profile of Jordan,* Amman: NCSA Project.

National Environment Strategy for Jordan, 1991. *National Environment Strategy for Jordan, A Resource Book of Information and Guidelines for Action,* Amman: Al Kutba.

Neilson, M.J. & Brockman , G.F. 1977. The error associated with point-counting, *American Mineralogist,* Volume 62, pages 1238-1244.

Nockolds, S. R. (1954) Average composition of some igneous rocks. Bull Geol Soc Am,65, 1007-1032.

Norton Rose, G., 2010. *Norton Rose.* [Online]

Available at: http://www.nortonrose.com/knowledge/publications/62385/renewable-energy-in-jordan

[Accessed 06 March 2012].

Novo, A., Bayon, J., Castro-Frensco, D. & Rodriguez-Hernandez, J., 2010. Review of Seasonal Heat Storage in Large Basins: Water Tanks and Gravel-Water Pits. *Applied Energy,* Volume 87, pp. 390- 397.

O'Sullivan, M., Pruess, K. & Lippmann, M., 2001. State of the Art of Geothermal Reservoir Simulation. *Geothermics,* Volume 30, pp. 395 - 429.

Paksoy, H. et al., 2000. Heating and Cooling of a Hospital Using Solar energy Coupled with Seasonal thermal Energy Storage in an Aquifer. *Renewable Energy,* Volume 19, pp. 117-122.

Pasquale, V., Gola, G., Chiozzi, P. & Verdoya, M., 2011. Thermophysical Properties of the Po Basin Rocks. *Geophys. J. Int.,* Volume 186, pp. 69-81.

Pasquale, V. et al., 1997. Thermophysical Properties of the Lipari Lavas (Southern Tyrrhenian). *Annali Di Geophysica,* Volume 6, pp. 1493-1503.

Pearce, J.A., 1975, Basalt geochemistry used to investigate past tectonic environments on Cyprus : Tectonophysics, 25, 41-67.

Petrunin, S., Popov, V. & Ladygin, V., 2001. Thermal properties of basalts from the Bouvet triple junction and their implications for petrophysical characterization. *Physics of the solid earth,* 37(6), pp. 441-451.

Pollack, H., Hurter, S. & Johnson, J., 1993. Heat Flow from the Earth's Interior: Analysis of the Global Data Set. *Reviews of Geophysics,* 31(3), pp. 267-280.

Popov, Y. A. et al., 2003. Interrelations between Thermal Conductivity and Other Physical Properties of Rocks: Experimental Data. *Pure app. geophys.,* Volume 160, pp. 1137-1161.

Popov, Y. et al., 1999. Characterization of rock thermal conductivity by high- resolution optical scanning. *Geothermics,* 28(2), pp. 253-267.

Rawajfih, Z., Khresat, S. & Buck, B., 2005. Arid Soils of the Badia Region of Northeastern Jordan : Potential Use for Sustainable Agriculture. *Archives of Agronomy and Soil Science,* 51(1), pp. 25-32.

Raymond, L., 2002. *Petrology: The Study of Igneous, Sedimentary, and Metamorphic Rocks.* s.l.:Mcgraw Hill Education. p, 736.

Renz, A., Rühaak, W., Schätul, P. & Diersch, H.-J., 2009. Numerical Modeling of Geothermal Use of Mine Water: Challenges and Examples. *Mine Water Environ. doi:10.1007/s10230-008-0063-3.*

Rimawi, O. & Al – Ansari, N., 1997. *Groundwater Degradation in the Northeastern Part of Mafraq Area, Jordan.* s.l., Freshwater Contamination (Proceedings of Rabat Symposium S4). IAHS Publ. no. 243.

Robertson, E. & Peck, D., 1974. Thermal Conductivity of Vesicular Basalt from Hawaii.. *Geophys Res.*, Volume 79, pp. 4875-4888.

Rorabaugh, M., 1956. *Groundwater in Northeastern Louisville, Kentucky with reference to induced infiltration,* Washington DC: Water Suply Paper 1360-B, USGS.

Rühaak, W., Schätzl, P., Renz, A. & Diersch, H.-J., 2008. *Numerical Modeling of Geothermal Processes: Issues and Examples.* Karlsbad, Czech Republic, Proc. of 10th IMWA Intern. Mine Water Ass..

Russo, S. & Civita, M., 2009. Open-Loop Groundwater Heat Pumps Development for Large Buildings: a Case Study. *Geothermics,* Volume 38, pp. 335-345.

Saffarini, G, Nassir, S., and Abed, A., 1985. A contribution to the petrology and geochemistry of the Quaternary- Neogene basalts of central Jordan, Dirasat, 12: 133-144.

Saggerson, E.P. & L.AS. Williams, 1964. Ngurumanite from southern Kenya and its bearing on the origin of rocks in the northern Tanganyika alkaline district. Iournal of Petrology 5: 40-81

Salameh, E., 2008. Over-Exploitation of Groundwater Resources and their Environmental and Socio-Economic Implications: the Case of Jordan. *Water International,* 33(1), pp. 55 - 68.

Salameh, E., Rimawi, O. & Hamed, K., 1991. Curative Thermal and Mineral Water in Jordan. *Water Resources Center Issue / Jordan University,* Issue 15.

Sass, I., 2012. *Direct and Indirect Use of Geothermal Resources, Wells and Well Design.* Darmstadt: unpublished script.

Sass, J., et al., 1971. Thermal Conductivity of Rocks from Measurements on Fragments and its Application to Heat Flow Determinations. *Journal of Geophysics,* Volume 76, pp. 3391-3401.

Saudi, A., 1999. *The Geochemistry of Thermal Fluid in the Geothermal Field Near Alia Airport in Jordan and Selfoss Geothermal Field, S-Iceland, report no.:13,* s.l.: The United Nations University, 354p.

Saudi, A. & Swarieh, A., 2005. *Geothermal Energy Resources in Jordan, Country Update Report.* Antalya, Turkey, World Geothermal Congress 2005.

Saudi, A. et al., 2004. *Thermal Fluids in Central Jordan,* Amman: Natural Resources Authority, 125p.

Schäfer, R., 2010. *Hydrogeologische und hydrothermal Untersuchungen der Thermalquellen Jordaniens (Hydrogeological and Hydrothermal Investigation of the Thermal Springs of Jordan), B.SC. (unoublished).* Darmdtadt: Technische Universität Darmstadt , 77p.

Schäfer, R. & Sass, I., 2012. The Thermal Waters of Jordan. *in prep.*.

Schwarzer, R. A., and Rogers, J. J. W., 1974, A worldwide comparison of alkali olivine basalts and their differentiation trends: Earth and Planet. Sci. Letters, v. 23, p. 286-296.

Sharqawy, M. et al., 2009. First in Situ Determination of the Ground Thermal Conductivity for Borehole Heat Exchanger Applications in Saudi Arabia. *Renewable Energy,* Volume 34, pp. 2218-2223.

Shaviv, A., Yezioro, A. & Capeluto, I., 2001. Thermal Mass and Night Ventilation as Passive Cooling Design Strategy. *Renewable Energy,* Volume 24, pp. 445-452.

Shaw, D., 1970. Trace Element Fractionation during anatexis. *Geochim et Cosmochim. Acta,* 34(2), pp. 237-243.

Singh, T., Sinha, S. & Singh, V., 2007. Prediction of Thermal Conductivity of Rock through Physic-Mechanical Properties. *Building and Environment,* 42(1), pp. 146-155.
Slichter, C., 1899. *Theoretical Investigation of the Motion of Ground wWter,* Washington D.C.: 19th Annual Report, U.S. Geological Survey.
Smadi, A., 2000. *The Geology of Mafraq Area, Bulletin 48.* Amman: Natural Resources Authority.
Snow, D., 1965. *A parallel plate model of fractured permeable media, PhD Thesis.* Berkeley, USA: University of California, 331pp.
Solani, G., Dall'o', G. & Scansani, S., 1998. Simultaneous Application of Different Natural Cooling Technologies to an Experimental Building. *Renewable Energy,* Volume 15, pp. 277-282.
Sterrett, R., 2007. *Groundwater and Wells.* Third Edition ed. New Brington, MN: Johnson screens.
Streckeisen, A., 1967; Classification and nomenclature of igneous rocks; N. Jb. Minerl., Abh., 107, 144-240.
Streckeisen, A. 1979, Classification and nomenclature of volcanic rocks, lamprophyres, carbonatites and melilitic rocks: recommendations and suggestions of the IUGS Subcommission on the Systematics of Igneous Rocks: Geology, v. 7, p. 331–335.
Stüwa, 2012. *Stüwa Brunnenfilter Bohrbedarf.* [Online]
Available at: http://www.stuewa.de/produkte/pe_aqua23.shtml
[Accessed 02 06 2012].
Sunna', B., 2004. *Recommended Approaches to Develop the Direct Utilization of the Geothermal Energy (Hot Water) in Jordan.* Dead Sea, International Water Demand Management Conference, Jordan.
Swarieh, A., 1990. *Hydrogeology of the Wadi Wala Sub-basin and Zarqa-Ma'in Hot Springs, MSc. thesis.* London, 60p: University of London, UK.
Swarieh, A., 1992. *Thermal Boreholes Near Queen Alia Airport,* Amman: Natural Resources Authority, 47p.
Swarieh, A., 2000. *Geothermal Energy Resources in Jordan, Country Update Report.* Kyushu-Tohoku, Japan, Wolrd Geothermal Congress.
Swarieh, A., 2005. *Heat Sources of the Groundwater in the Zara - Zarqa Ma'in - Jiza Area, Central Jordan.* Karlsruhe, Germany: University of Karlsruhe.
Swarieh, A., 2008. *Geothermal Water in Jordan.* Tianjin, China, United Nation University-Geothermal Training Programme.
Swarieh, A. & Massarweh, R., 1993. *Thermal Springs in Wadi Ibn Hammad, Bulletin,* amman: Natural Resources Authority, 32p.
Swarieh, A. & Massarweh, R., 1995. *Geothermal Water in Zara and Zarqa Ma'in Area, Bulletin 8,* Amman: Natural Resources Authority, 36p.
Swarieh, A. & Massarweh, R., 1997. *Geothermal Water in Mukhiebeh and North Shuneh Areas, Bulletin 9,* Amman: Natural Resources Authority, 29p.
Tester, J. et al., 2005. *Sustainable Energy – Choosing Among Options.*. Cambridge, MA: MIT Press.
Thiem, C., 1906. *Hydrologische methoden.* Leibzig, 56p: s.n.
Thompson, M., 2010. *Hydraulic Hammer Drilling Technology to Rplace Air Hammer Drilling in Deep BHE Design.* Akureyri, Iceland: The School of Renewable Energy Science RES.
Trombe, A., Pettit, M. & Bourret, B., 1991. Air Cooling by Earth Tube Heat Exchanger: Experimental Approach. *Renewable Energy,* 1(5/6), pp. 699- 707.

Truesdell, A., 1979. *Final Report on the Chemistry and Geothermal Energy Possibilities of the Zara - Zarqa Ma'in Springs, Jordan,* Ment Park, California: U.S. Geol. Survey.

Turneaure, F. & Russell, H., 1901. *Public Water Supplies.* New York: John Wiley and Sons, 269p.

UNEP, 1997. *World Atlas of Desertification.* Arnold: s.n.

Van Den Boom, G. & Sawwan, O., 1966. *Report on geological and petrological studies of the plateau basalts in NE Jordan,42p,* Amman: Germ. Geol. Missionin.

Wang, J., Carson, J., North, M. & Cleland, D., 2006. A New Approach to Modelling the Effective Thermal Conductivity of Heterogeneous Materials. *Int. J. Heat Mass Transfer,* Volume 49, p. 3075–3083.

Wang, L. et al., 2010. Anisotropic Thermal Conductivity and Permeability of Compacted Expanded Natural Graphite. *Applied thermal Engineering,* 30(13), pp. 1805-1811.

Williams, C. & Anderson, R., 1990. Thermophysical Properties of the Earths` Crust: in Situ Measurements from Continental and Ocean Drilling. *J., Geophys. Res.,* Volume 95, pp. 9209-9236.

Williams, H., Ramini, H. & Alzyoud, M., 1990. *Regional Petrolum Geochemistry of Jordan,* Amman, 66p: Natural Rescources Authority.

Winchester., J.A. and Floyd, P.A., 1977. Geochemical discrimination of different magma series and their differentiation products using immobile elements. Chemical Geology *;20:*325-343.

Winslow, J., 1962. *Effect of stream infiltration on groundwater temperatures near Schenectady,* Washington DC: N.Y. USGS Proffesional paper 450-c.

Zierenberg, R., Fouquet, Y., Miller, D. & Normark, W., 2000. *Permeability, Electrical, and Thermal Properties of Sulfide, Sedimentary, and Basaltic Units from the Bent Hill Area of Middle Valley, Juan de Fuca Ridge.*. Proceedings of the Ocean Drilling Program, Volume 169.

Curriculum Vitae

Sana`a Abdulkareem AL-ZYOUD

Personal:

Surname:	AL-ZYOUD
Full name:	Sana`a Abdulkareem Fayyad
Nationality:	Jordanian
Date of Birth:	03.09.1981
Place of Birth:	Amman – Jordan
Address:	Rheinstrasse, 66 D- 64259 Darmstadt
Contact:	Telephone : 0049 6151 1545227 Telefax : 0049 6151 16-6539
Web:	http://www.geo.tu-darmstadt.de/fg/angeotherm/geotherm_personen/ansprechpartner_details_7360.de.jsp

Academic Qualification

Sept. 1999 – Feb. 2003
B.Sc. (Honor) degree in Department of Earth and Environmental Sciences, Hashemite University, Zarqa, Jordan.

Feb. 2003 – Aug. 2005
M.Sc. degree in Applied Geology Department of Earth and Environmental Sciences, Hashemite University, Zarqa, Jordan.
Thesis Title: Mineralogy, geochemistry and physico-mechanical evaluations of al-Hashimiyya basaltic Rocks- Jordan

Oct. 2008 – Aug. 2012
Dr.Eng. Degree in Engineering Geology and Geothermal Sciences, Technische Universität Darmstadt, Germany
Thesis Title: Geothermal Cooling in Arid Regions: An Investigation of the Jordanian Harrat Aquifer System

Professional Experience

March 2006 – Oct.2006
Science and Geology Teacher in Al-Hashimiyya Secondary School

Oct. 2006 – June 2008
Teaching and Research Assistant in Department of Earth and Environmental Sciences, Hashemite University, Zarqa, Jordan.

April 2009 – Aug. 2012
Teaching Assistant in Institute of Applied Geosciences, Technische Universität Darmstadt, Germany. i.e. Mechanical properties of Rocks and Soils, for TropHEE students (Master of Science (M.Sc.) „Tropical Hydrogeology, Engineering Geology and Environmental Management“. Duties: Assignments, Lectures preparation, Lecturing, Laboratory work and Practical course.

Training Course

June 2003 – Sept. 2003
Training course in Computer Driving – International Computer Driving License (ICDL)

Aug. 2006– Oct. 2006
Training course in Teaching and Communication Skills for Teachers / Ministry of Education- JORDAN

Feb. 2009
Block course in GOCAD (one week)

March 2010
Block course in FEFLOW modeling (one week)

Modeling and Software

1. Finite Element Subsurface Flow and Transport Simulation System (FEFLOW): groundwater level calibration in the studied wells, heat (temperature) calibration in the studied points, flow transport model, heat transport model
2. Geological Objects Computer Aided Design (GOCAD) : 3-D geology model
3. Geographic Information Systems (GIS): 2-D geology model, lithology and topography.
4. Surfer: groundwater data interpretation
5. Grapher: groundwater drawdown modeling

Grants and Awards

1999-2003
Grant from Hashemite University, during B.Sc. study

2003 - 2005
Grant from Hashemite University, during M.Sc. study

2008 - 2012
DAAD Scholarship, PhD in Technische Universität Darmstadt- Germany

Publications

Published peer reviewed papers

Al-Zyoud, S., Rühaak W. & Sass, I. (2012): *The potential of shallow groundwater resources for cooling purposes - a Geothermal case study in north east Jordan. Proceedings, 37th Stanford Geothermal Workshop. Stanford, California.*

Al-Zyoud, S., Rühaak W. & Sass, I. (2012): *Dynamic numerical modeling of the usage of groundwater for cooling in north east Jordan – a geothermal case study.* Renewable Energy (in press).

Published papers

Al-Zyoud & Al-Malabeh (2007); "*Physico-Mechanical Evaluations of Al-Hashimiyya Basaltic Rocks",* 6th International Symposium on Eastern Mediterranean Geology. (April, 2007), Amman, JORDAN.

Al-Malabeh & Al-Zyoud (2007); "*Mineralogy and Geochemistry Evaluations of Al-Hashimiyya Basaltic Rocks, Jordan",* 6th International Symposium on Eastern Mediterranean Geology. (April, 2007), Amman, JORDAN.

Al-Zyoud.S, Al-Malabeh.A. & Sass.I, (2009) "Geothermal and Engineering *Evaluation of Basaltic Rocks in Harrat Al-Shaam, Jordan",* International Conference and Exhibition on Green Energy and Sustainability for Arid Region and Mediterranean Countries ICEGES (Nov. 2009), Amman , Jordan.

Al-Zyoud, S., Al Malabeh, A. & Sass, I. (2009): *Evaluation of physicomechanical properties of basaltic rocks in Harrat Al-Shaam, Jordan.* International Conference and Exhibition on Green Energy & Sustainability for Arid Regions & Mediterranean Countries. Amman, Jordan.

Al-Zyoud, S. & Sass, I. (2011): *Thermophysical properties of flood basalts as prospective geothermal reservoirs: Case study Harrat Al Shaam, Jordan*. 18. Tagung für Ingenieurgeologie – Berlin. 299-300.

Talks

Al-Zyoud, S., Al Malabeh, A. & Sass, I. (2009*): Evaluation of physicomechanical properties of basaltic rocks in Harrat Al-Shaam, Jordan*. International Conference and Exhibition on Green Energy & Sustainability for Arid Regions & Mediterranean Countries. Amman, Jordan.

Al-Zyoud, S., Al Malabeh, A. & Sass, I. (2010): *Evaluation of Geothermal Properties of Basaltic Rocks in Harrat Al-Shaam, Jordan*. First European Geothermal PhD Day EGP D 2010, An Initiative of the EERA Joint Program in Geothermal Energy, Collection of Abstract: p.p.10, Potsdam. (In English)

Al-Zyoud, S. & Sass, I. (2011): *Thermophysical properties of flood basalts as prospective geothermal reservoirs: Case study Harrat Al Shaam, Jordan*. 18. Tagung für Ingenieurgeologie – Berlin. 299-300. (In English)

Poster

Al-Zyoud, S, Al-Malabeh, A., & Sass, I. (2010): *Hydrological Investigations on Harrat Al Shaam basaltic rocks for geothermal utilization, Jordan* - In: GeoDarmstadt2010, Darmstadt. SDGG, 68: 65. (In English)

Submitted articles

Al-Zyoud, S., Al Malabeh, A., Mählmann R. F. & Sass, I. (2012): *Thermal conductivity of flood basalts controls by mineral composition: a prospective geothermal reservoir study on Jordanian Harrat.* (in review - International Journal of Earth Sciences).

Al-Zyoud, S., Rühaak W. & Sass, I. (2012): *Over exploitation of Groundwater in the Centre of Amman Zarqa Basin – Jordan*. (In prep.)